INFLUENCE OF FRP WIDTH-TO-SPACING RATIO ON BOND PERFORMANCE OF EXTERNALLY BONDED FRP SYSTEMS ON ONE WAY CONCRETE SLABS

by

Karthik Narayan Ramanathan

Bachelor of Engineering, Osmania University, 2006

Submitted to the Graduate Faculty of

Swanson School of Engineering in partial fulfillment

of the requirements for the degree of

Master of Science

University of Pittsburgh

2008

UNIVERSITY OF PITTSBURGH

SWANSON SCHOOL OF ENGINEERING

This thesis was presented

by

Karthik Narayan Ramanathan

It was defended on

February 15, 2008

and approved by

Dr. Piervincenzo Rizzo, Assistant Professor,
Department of Civil and Environmental Engineering

Dr. John F. Oyler, Adjunct Associate Professor,
Department of Civil and Environmental Engineering

Dr. Kent A. Harries, Assistant Professor,
William Kepler Whiteford Faculty Fellow,
Department of Civil and Environmental Engineering
Thesis Advisor

INFLUENCE OF FRP WIDTH-TO-SPACING RATIO ON BOND PERFORMANCE OF EXTERNALLY BONDED FRP SYSTEMS ON ONE WAY CONCRETE SLABS

Karthik Narayan Ramanathan, M.S.

University of Pittsburgh, 2008

Debonding of externally bonded fiber reinforced polymer (FRP) composite materials used for repair of reinforced concrete elements is commonly observed and is often the critical limit state for such systems. The FRP geometry, as quantified by the ratio of FRP width-to-substrate width, b_f/b, (or FRP width-to-FRP spacing, b_f/s, for slabs) is expected to affect the ultimate bond performance. Factors accounting for this effect are included in many design guides. An experimental program using concrete slab specimens having identical reinforcement ratios, strengthened with CFRP strips having different b_f/s ratios is reported. The focus of the study is the strain in the CFRP and its eventual debonding. Thinner (lower b_f/s) CFRP strip are observed to have greater strains at a given load level and to have a higher strain at debonding. The effect of the transverse strain gradient in the CFRP – the CFRP "edge effect" – is also investigated.

TABLE OF CONTENTS

LIST OF TABLES

LIST OF FIGURES

ACKNOWLEDGEMENTS

I am extremely happy to record my profound gratitude to Dr. Kent A. Harries for his valuable guidance, sustained interest, keen encouragement and inspiring instruction. Putting to best use of his uncanny persuasive skills and scholarly erudition in tendering timely and valuable advice, he has been instrumental in bringing out this thesis in its present form. I thank him for his excellent teaching over my years at University of Pittsburgh.

I am extremely thankful to Dr. Piervincenzo Rizzo for his encouragement all through the work and for overseeing the experiments in the absence of Dr. Harries. I am grateful for the technical discussions I had with both of them. These discussions were invaluable and part of this work would have been impossible without them. I thank Dr. John F. Oyler for offering many insights while serving on the committee.

The author would like to thank his peers Mr. Sandeep Degala, Mr. Andrew Peck, Ms. Bhavna Sharma, Mr. Jeremy Tartt, Mr. Marcello Cammarata, Mr. Derek Mitch and Mr. Louis Gualtieri for all the help and support. Special thanks to Mrs. Jacki Temple for all the help during the specimen cast.

Finally, I am extremely thankful to my parents, brother and close friends all of whom have been supportive and encouraging throughout my educational endeavors. Special thanks are due to Mr. Sreenivas Sarma, Senior Associate Professor, Chaitanya Bharathi Institute of Technology, Hyderabad, India. His confidence and encouragement made me start this journey. Lastly, special thanks go to Mr. Sandeep Degala for enduring all the concrete dust.

The in-kind contributions of Fyfe Company and Structural Preservation Systems, specifically, Sarah Witt and Tarek Alkhrdaji, respectively is gratefully acknowledged.

NOTATION

Abbreviations

ACI	American Concrete Institute
ASTM	American Society for Testing and Materials
CFRP	carbon fiber reinforced polymer
DWT	draw wire transducers
FRP	fiber reinforced polymer
RC	reinforced concrete

Notation

a	shear span of beam or slab
A_c	concrete cross-sectional area
A_f	FRP cross-sectional area
A_s	Steel reinforcement cross-sectional area
b	width of RC member (tension face)
b_f	width of FRP strip
c_1	empirical factor
C_E	mechanical and environmental exposure coefficient
cov	covariance
d	effective depth, measured from extreme compressive fiber to centroid of

	internal steel tension reinforcement
E	expected value operator (Chapter 6)
E_f	FRP modulus of elasticity
E_s	steel modulus of elasticity
f_c	concrete compressive strength
f_c'	28 day concrete compressive strength
f_{ct}	concrete tensile strength
f_u	ultimate strength of steel reinforcement
f_y	yield strength of steel reinforcement
G_a	adhesive shear modulus
G_f	interfacial fracture energy
h	overall depth of the concrete section
k_b	retrofit geometry parameter (factor accounting for b_f/b in design)
k_c	factor accounting for concrete compaction
k_L	factor accounting $L_b < L_{bmax}$ in design
L	beam clear span length
L_b	provided anchorage bond length
L_{bmax}	effective anchorage bond length
n	number of plies of FRP
P	applied load at midspan
s	FRP spacing in slab systems
t_a	adhesive thickness
t_f	FRP thickness

V	maximum shear force
V_c	shear strength of concrete
α	empirical constant
ε_{fu}	*in situ* rupture strain of FRP
ε_{fub}	strain in FRP at initiation of debonding
κ_m	ACI 440.2R-02 strain reduction factor
σ	standard deviation
ρ_c	compression reinforcement ratio
ρ_t	tension reinforcement ratio
ρ_v	shear reinforcement ratio
$\rho_{equivalent}$	equivalent reinforcement ratio
$\rho_{X,Y}$	correlation coefficient
μ	expected values

This thesis reports all values in US units throughout and reports SI units in a secondary fashion. The following "hard" conversion factors have been used:

1 inch = 25.4 mm

1 kip = 4.448 kN

1 ksi = 6.895 MPa

Reinforcing bar sizes are reported using the designation given in the appropriate reference. A bar designated using a "#" sign (e.g.: #4) refers to the standard inch-pound designation used in the United States where the number refers to the bar diameter in eighths of an inch.

1.0 INTRODUCTION

1.1 INTRODUCTION

Structural retrofitting is a major growth area in civil engineering because the infrastructure is expanding and aging requiring more and more resources to maintain it. Hence, it is imperative to develop inexpensive and efficient retrofitting techniques. Bonding of longitudinal plates to the reinforced concrete member surfaces has been shown to be an economical, efficient and unobtrusive technique. Researchers have tried various materials in several contexts and Fiber Reinforced Polymers (FRP) have established them to be a highly suitable material for flexural retrofit and strengthening of reinforced concrete. Such retrofits are prone to a debonding limit state. Much high quality research has been done around the world on identifying and quantifying these debonding mechanisms. It is proposed that because plated structures exhibit unique forms of failure, they should be treated as a new form of structure altogether (Oehlers 2004).

FRP composite materials have been used in the repair and retrofit of concrete structural elements (Buyukosturk et al. 2004): (1) to increase axial, flexural or shear capacities; (2) to increase ductility for improved seismic performance; (3) to increase stiffness for reduced deflections under service and design loads; (4) to increase the remaining fatigue life; and, (5) to improve durability against environmental effects.

Reinforced concrete (RC) members can be strengthened in flexure by bonding FRP to the tension face of the member. The FRP is applied in the longitudinal direction along the member, parallel to the greatest tensile forces, and is understood to be augmenting the capacity of the existing tension steel reinforcement. FRP strips must be fully bonded to members to engage composite action between the FRP and substrate concrete. The sound concrete is expected to continue to behave in a composite manner with the internal reinforcement. For the strengthening system to work at its greatest efficiency, there should be full composite action between the concrete and FRP, causing the FRP to be fully engaged. This FRP to concrete bond is critical because this is where the stress transfer occurs that engages the FRP.

One of the benefits of using FRP to strengthen a concrete structure is that it is an environmentally durable material. It is non-corrosive and also has a high tensile capacity (8-10 times that of steel). It also has outstanding ratios of stiffness and strength to weight. FRP is lightweight which adds to its ease of handling and application. Extensive training is not required for its installation due to the ease of the application process. However, utmost care should be exercised during the application process to ensure a proper bond in the FRP concrete system. FRP retrofit measures result in a minimum size and weight increase of the members to which they are applied and therefore, has a minimal impact on a member's dead load and aesthetics. Externally bonded FRP composites have been shown to improve a structural member's performance under both monotonic and fatigue loading conditions by increasing ductility, load carrying capacity, and stiffness of the member (Buyukosturk et al. 2004). These results can be achieved whether the member is initially cracked or uncracked.

FRP-reinforced RC beams can fail by the compressive crushing of concrete (before steel reinforcement yields), steel yielding followed by concrete crushing (before FRP rupture), steel

yielding followed by FRP rupture, concrete cover delamination, or FRP debonding at the concrete/FRP interface. Shear failure, resulting from increased flexural capacity is also a concern (Buyukosturk et al. 2004). Concrete crushing, cover delamination, FRP rupture and shear failure are generally brittle failures. Concrete cover delamination and FRP debonding are undesirable failures which don't allow a retrofitted member to reach its full flexural capacity leaving its capacity under-utilized.

Debonding of the FRP can take place in or between any of the systems components. It can occur in the concrete along a weak plane (such as at the level of internal reinforcement or in a thin layer adjacent to the adhesive line (cover delamination)). Debonding failure could also occur at the concrete/adhesive interface (adhesion failure), in the adhesive itself (cohesion failure) or at the adhesive/FRP interface (adhesion failure) (Oehlers 2004). Owing to FRP being a composite material itself, failure could occur within the FRP between the resin and the fibers (interlaminar failure). However, by proper selection of materials for the strengthening system, and proper surface preparation, the weakest part of the system should be in the concrete very near the adhesive line (fib, 2001). This is the only component of the retrofit system over which little control may had – the original substrate concrete.

The FRP-adhesive-concrete region, together termed as the FRP system, is a multi-component laminate system usually subject to mixed mode loading and eventual failure; thus debonding is a complicated phenomenon. FRP plate end debonding is not a consideration in the present work since the FRP will be extended nearly the full length of the beam, ending just short of the supports where the moment in the beam is negligible. Therefore plate end debonding will be mitigated and "midspan debonding" is expected to be the mode of failure in the experiments described in this work. Shear stresses at the concrete/FRP interface control midspan debonding,

although out of plane peeling stresses are recognized to severely cripple the shear capacity of the interface region.

The present study is "explicitly concerned only with soffit plating of simply-supported beams for simplicity in description, although the conclusions are applicable to tension face plating of beams in general" (Smith and Teng 2001). Numerous studies have proposed strain (or stress) limits for FRP with the intent of mitigating debonding failures. Smith and Teng (2001) report that generally these models only show good predictive capacity of the data from which they were derived. Therefore, this study will focus on established consensus guidelines. It will be shown that the available consensus for mitigating debonding failures requires considerable further study. This thesis focuses on a few specific aspects of the work required to improve the understanding and design of bond.

1.2 SCOPE AND OBJECTIVE OF THE THESIS

The present study is continuation of a larger study of factors affecting the bond behavior of externally bonded FRP flexural retrofit measures conducted under the direction of Dr. Harries (Aidoo 2002 and 2004, Quattlebaum 2003, Reeve 2005 and Zorn 2006). The study addresses the effect of the geometry of the CFRP retrofit measures as measured by the ratio of CFRP width to spacing (b_f/b) on the bond behavior of externally bonded CFRP systems on one-way reinforced concrete slabs. This study will also contribute significantly to the existing ACI 440 Bond Task Group Database of similar tests of FRP strengthened systems and will provide modified formulae for predicting the maximum FRP strain to mitigate debonding failure.

1.3 OUTLINE OF THESIS

Chapter 2 of this work provides a detailed discussion of the background material necessary for the study of FRP bond in the context of flexural retrofit and a literature review of relevant material. Chapter 3 reports details of the experimental program conducted in the study. Chapter 4 presents the results of the experimental test program and a discussion of the behavior of each test specimen. The interpretations of and results derived from the experimental data are reported in Chapter 5. Basis for these interpretations is also reported. Chapter 6 reports a discussion of observed debonding behavior and places this in the context of debonding criteria proposed in various national standards and by other researchers. Finally, in Chapter 7 the work is summarized, and recommendations (including those for future work), are presented.

1.4 NOTATION

The terms *retrofit*, *repair*, and *strengthening* are used interchangeably throughout this thesis in association with the application of the FRP to the structural members in question. The author acknowledges that there is a difference in technical meaning of these three terms, however in the context of the present experimental study, these terms are interchangeable. The objective of a specific "real world" application provides the differentiation in the terms. When used in this writing, these three terms refer solely to the process of applying FRP to the specimens in question.

2.0 LITERATURE REVIEW

The application of fiber reinforced polymer (FRP) materials for the repair and rehabilitation of infrastructure is a very broad topic. The scope of this study and literature review addresses the use of carbon fiber reinforced polymer (CFRP) strips that are adhesively bonded to the soffits of reinforced concrete (RC) flexural members to enhance or rehabilitate their flexural performance. While most extant literature discussed the behavior of beam members, the focus of this work is on one way slab behavior. The following sections provide the necessary background providing discussion of the major debonding mechanisms in adhesively bonded plate systems, factors affecting bond behavior and the effects of the retrofit geometry, as expressed by the ratio of FRP width to substrate width (b_f/b) or FRP width to FRP spacing (b_f/s), on the bond characteristics of externally bonded FRP systems.

2.1 FAILURE MODES IN FRP-STRNGTHENED RC STRUCTURES

A number of failure modes for RC flexural members having FRP plates bonded to their soffits are possible and have been reported in the literature (Oehlers 2005, Harries et al. 2006, Teng et al. 2002). A schematic representation of the typical failure modes is shown in Figure 2-1. The failure modes are classified into seven main categories in the figure and are given as:

1. flexural failure by FRP rupture;

2. flexural failure by crushing of compressive concrete;
3. shear failure resulting in critical diagonal crack debonding (CDC);
4. concrete cover separation (PE);
5. plate-end interfacial debonding (PE);
6. intermediate flexural crack-induced interfacial debonding (VAy/Ib); and,
7. intermediate flexural shear-crack induced interfacial debonding (IC).

Collectively, failure modes (4) and (5) are referred to as plate-end (PE) debonding failures, while failure modes (6) and (7) are referred to as intermediate crack-induced (IC) debonding (often referred to as "midspan debonding").

For relatively low ratios of both internal steel and FRP reinforcement, flexural failure will occur by yielding of the tensile steel reinforcement followed by tensile rupture of FRP prior to concrete crushing. This is described by failure mode (1). For higher reinforcement ratios, flexural failure will occur by compressive crushing of concrete before the tensile steel yields and before the FRP ruptures. This mode is described by failure mode (2). While both of these failure modes may be desirable, debonding of the FRP prior to achieving steel yield or concrete crushing may limit such behavior and result in an undesirable brittle failure. Indeed, debonding failures dominate observed experimental behavior reported in the literature (see Section 2.6).

Shear failure is also an undesirable failure mode which may occur in a retrofitted section where the improved flexural capacity exceeds the available shear capacity (Seim et al 2001). This may require additional shear retrofit in order to maintain a flexurally-dominated behavior. This is described as failure mode (3).

2.2 MAJOR DEBONDING MECHANISMS IN ADHESIVELY BONDED PLATES

In general practice, the adhesive used to bond a plate to a concrete substrate is much stronger than the tensile strength of concrete so that debonding or peeling invariably occurs within the cover concrete element[1] (Oehlers 2005, Kotynia and Harries 2006).

Debonding modes have been characterized by Oehlers (2006) as follows: A concrete flexural crack that intercepts a plate will induce shear (Mode II[2]) deformations and stresses at the FRP-concrete interface adjacent the crack. These stresses are easily calculated and associated debonding is referred to as VAy/Ib debonding. If the concrete crack has any shear component (is inclined), an additional peeling stress (Mode I) is induced on the side of the crack having the lower moment (closer to the nearer support of a simply supported span). This is referred to as intermediate crack-induced (IC) debonding. It has been shown that the toughness of the interface with respect to debonding is significantly reduced in the presence of peeling (Mode I) (Wan et al. 2004). Thus, IC debonding dominates behavior and VAy/Ib debonding is not observed in practice.

The formation of a critical diagonal crack (CDC), the type of crack commonly associated with the shear capacity of a beam or slab, induces significant Mode I stressed at the FRP-concrete interface resulting in rapid, brittle debonding.

---

[1] Failure within the FRP or adhesive or cohesive failure in the adhesive layer is rare and an indication of poor quality material or application (Harries 2006). While not uncommon, these failures are easily mitigated through quality control measures and are not considered further in this discussion.

[2] Mode I and Mode II loading refer to the standard fracture mechanics definitions of crack openings in 2 dimensions (Mode III is out-of-plane tearing and is not discussed in this document). **Mode I:** Opening mode where the crack surfaces separate symmetrically with respect to the plane of the crack due to stresses applied normal to the crack plane. **Mode II:** Sliding mode where the crack surfaces glide over one another in opposite directions in the plane of the crack due to in-plane shear.

Finally, the curvature in a flexural member coupled with the kinematic incompatibility at the termination of an FRP plate can also cause the plate to debond from the plate ends (PE) progressing inwards. In this case, Mode I stresses are significant and a function of the moment carried by the member at the plate termination. PE debonding is easily mitigated by extending the plate to a region of very low moment (point of inflection or near the support of a simple span). The nature of IC and PE debonding are illustrated in Figure 2-2.

Intermediate crack-induced debonding of the focus of the present study although CDC debonding is also observed in the experimental study.

2.3 RETROFITTING OF SLABS

Compared to the flexural strengthening of beams, much less work has been done on the flexural strengthening of slabs. Existing research (Karbhari et al. 1999, Tann 2003) suggests that one-way slab systems fail by IC debonding similar to beams. Hence, the behavior seen in RC strengthened beams applies to RC one-way slab systems. While the existing research on flexural strengthening of RC beams is applicable to the flexural strengthening of one-way slabs, there are also some important differences: Slabs are dominated by flexural behavior (more-so than beams) and are therefore prone primarily to intermediate crack-induced (IC) debonding. Slabs are not easily retrofit for shear where it may be required, thus there is an upper limit to the flexural capacity enhancement that may be affected since it remains necessary to have a flexure dominated behavior. Often, to maintain code compliance, very little flexural capacity enhancement is permitted. As a result, slab retrofits with FRP are limited to significantly under-reinforced slabs or to specific unique load cases. There is a lot of uncertainty about the

application of existing debonding strength models developed for beams to one-way slab systems (Teng et al. 2005).

The basic procedure for flexural strengthening of slabs is similar to that of beams. It involves bonding the FRP plates to the tension faces of the slabs. Research has been conducted on slabs having bonded FRP strips covering only a part of the surface (Erki and Heffernan 1995, Karbhari et al. 1999, Karbhari and Seible 2000, Tann 2003, Limam et al. 2003, Tan et al. 2003, Marzouk et al. 2003). Research has also been conducted on FRP sheets covering the entire surface (Arockiasamy et al. 1996, Erki and Heffernan 1995, Shahawy et al. 1996, Karbhari et al. 1999, Karbhari and Seible 2000). FRP sheets covering the entire soffit of the slab make it difficult to assess the quality of bond and perform future inspections of the slab. Additionally, it restricts the free movement of moisture out of the slab, which leads to the degradation of bond (Karbhari et al. 1999).

Zhang et al. 2001 conducted tests on two-way RC slabs subject to a central concentrated load having a steel plate bonded in the central region, beneath the load. The slabs were found to fail by formation of yield lines around the perimeter of the bonded plate and along the diagonal lines of the unstrengthened part of the slab as shown in Figure 2-3. These slabs were bonded with steel plates but slabs bonded with FRP plates are also expected to fail in a similar fashion. This leads to the interesting concept of slab strengthening by modification of yield line pattern or the collapse mechanism. In such an approach, the designer has the option of strengthening any portion of the slab and hence forcing the yield lines away from this strengthened section (Teng et al. 2005). The strength of such strengthened slabs can be predicted by yield line analysis. It is assumed that the part of the RC slab without bonded FRP possesses sufficient ductility to accommodate the yield lines formed.

No literature is available discussing debonding failures in two-way slabs. The experiments conducted by Zhang et al. (2005) on two way slabs bonded with steel plates did not suffer from any debonding failures. Although a thick steel plate was bonded to a small central region, debonding did not occur. This behavior is in contrast to the behavior observed in case of beams, where PE debonding occurs when the bonded plates are terminated sufficiently far away from the supports. Additionally, the bi-directional behavior of two way slabs and the need or associated bi-directional retrofit would appear to mitigate the IC mode of debonding.

Cantilever slabs differ from one-way or two-way simply supported slabs in that the fixed end support in a cantilever slab is subject to the greatest moment (Teng et al. 2005). In such a case, FRP plates or sheets cannot be terminated before the fixed end and they need to be properly anchored. For slabs cantilevered from a wall or large beam, the FRP strips or sheet may be bent onto the wall surface, however this method is found to be extremely ineffective (Teng et al. 2000) since the anchorage to the wall is entirely affected through tensile or peeling stresses and the anchorage is affected by "prying action", making it particularly weak. In this case, the slab fails by debonding of the FRP strips from the wall while the tensile stresses in the FRP strips are still very low.

To achieve sound anchorage, FRP strips need to be inserted into predrilled holes in the wall. However, this method can only be adapted to slabs retrofitted with narrow FRP strips owing to the presence of internal steel reinforcement in the wall. Most tests have been conducted on model wall-supported slabs adopting this anchorage method, with either one or two FRP strips bonded to the slab. This method was extremely effective in all the tests (Teng et al. 2000, Lam and Teng 2001) but may be relatively impractical in practice.

Neale et al. (2005) developed non linear finite element and numerical models to study the debonding phenomenon in RC beams and slabs. There was an excellent agreement between the models developed and the experimental results obtained from a large number of tests conducted by Harajli and Soudki (2003) and Longworth et al. (2004). Neale et al. deduced that with an increase in the width of FRP, relative to the slab width, the ductility of the strengthened slab is reduced. Such a result is analogous to that observed with FRP-retrofit beams, where increased amounts of FRP result in increased capacity but reduced ductility or deformability. Neale et al. also showed the importance of appropriately modeling the FRP/concrete interface if accurate predictions of the behavior of externally FRP-strengthened members are to be obtained.

2.4 FACTORS AFFECTING BOND BEHAVIOR

The following set of parameters has been reported to affect the bond behavior of FRP strengthened RC members (adapted from ACI Committee 440F Task Group on Bond of Externally Bonded FRP, 2006)

1. Concrete tensile strength, f_{ct},
2. Adhesive shear stiffness, $G_a t_a$
3. Effective bond length of FRP, L_{bmax}
4. Specimen scale and size effect
5. Specimen section geometry
6. Specimen loading (Applied shear-to-moment ratio, Constant applied moment or moment gradient, Static or dynamic loading, Monotonic or cyclic (fatigue), creep effects)

7. FRP retrofit geometry, b_f/b
8. Environmental and Mechanical Exposure, C_E
9. Fatigue loading
10. Mixed mode nature of debonding phenomena

The focus of the present work is item (7). Related studies conducted at the University of Pittsburgh have addressed items (2) (O'Neill et al. 2007) and (9) (Harries et al. 2006).

Bond is affected by the ability of the FRP to transfer stresses to the concrete substrate. This stress transfer is affected by the ratio of the FRP plate width (b_f) to the beam width (b), or spacing (s) between the FRP strips in case of slabs. The effect of this ratio is incorporated through k_b factors used in design as discussed in Section 2.5. A detailed discussion of the effects of the b_f/b ratio is given in Section 2.6. The primary objective of this study is the assessment of the influence of the retrofit geometry parameter, k_b on the bond characteristics of externally bonded RC one way slab systems.

2.5 DESIGN OF FRP RETROFITS TO ADDRESS DEBONDING

This section discusses the provisions of various national standards and the recommendations provided by various researchers for the mitigation of IC debonding in FRP strengthened RC flexural members. A summary of these national standards and the recommendations provided by various researchers is given in Table 2-1.

The dimensions of the member to be strengthened and the FRP are relevant to FRP strengthening performance. As stated previously, the FRP width-to-member width ratio (b_f/b) affects how load is distributed between the two materials and how efficiently they are used. When predicting the

maximum allowable load on an FRP strengthened RC beam, many approaches are currently proposed. In all approaches it is important to have an understanding of the concrete/FRP interfacial shear and normal stresses, as these are the causes of debonding failures (Smith and Teng 2000, Neale et al. 2005). It is also important to design with a maximum allowable FRP tensile strain in mind which should be sufficiently low to ensure that debonding will not occur.

2.5.1 ACI 440.2R-07[3]

The ACI Committee 440F Task Group on Bond of Externally Bonded FRP (2006) adopted the format of the Teng et al. (2004) empirical equation (Section 2.5.10) in its generic form to calculate the maximum permitted FRP strain to mitigate debonding failure, ε_{fub}:

$$\varepsilon_{fub} = \alpha \frac{\left(f_c'\right)^{1/x}}{\sqrt{nE_f t_f}} \tag{2.1}$$

where, n, E_f, t_f are the number of plies or layers, the tensile modulus and nominal ply thickness of FRP, respectively, and f_c' is the concrete compressive strength.

After performing a rigorous correlation analysis with an extensive database (Section 2.7), the best fit was found to have $\alpha = 0.083$ (US units) and 0.41 (SI units) and $x = 2$. Thus the above equation takes the form:

$$\begin{aligned} \varepsilon_{fub} &= 0.083\sqrt{\frac{f_c'}{nE_f t_f}} \quad (US\ units) \\ &= 0.41\sqrt{\frac{f_c'}{nE_f t_f}} \quad (SI\ units) \end{aligned} \tag{2.2}$$

[3] As of this writing (January 2008), the revisions to ACI 440.2R-02 reported in this thesis as ACI 440.2R-07 have been approved by Committee 440 and ACI TAC. Publication of ACI 440.2R-08 is expected in the spring of 2008.

Equation 2.2 is based on the 50 percentile. However, ACI 440.2R-07 further recommends that equation 2.2 have an upper limit of $0.9f_{fu}$.

While ACI Committee recognizes the effects of internal steel reinforcement, adhesive layer properties and the FRP width to member width/spacing ratio (b_f/b), the Committee has chosen to not include these it its recommendations at this time due to lack of definitive research and consensus.

2.5.2 ACI 440.2R-02

ACI 440.2R (ACI, 2002) provides an equation for the maximum FRP strain to mitigate debonding failure:

$$\varepsilon_{fub} = \kappa_m \varepsilon_{fu} \tag{2.3}$$

where, ε_{fu} is the FRP design rupture strain and the value of κ_m is:

$$\kappa_m = \begin{cases} \dfrac{1}{60\varepsilon_{fu}}\left(1-\dfrac{nE_f t_f}{2{,}000{,}000}\right) \le 0.90 \ \ for\ nE_f t_f \le 1{,}000{,}000\ lb/in \\ \dfrac{1}{60\varepsilon_{fu}}\left(\dfrac{500{,}000}{nE_f t_f}\right) \le 0.90 \ \ for\ nE_f t_f > 1{,}000{,}000\ lb/in. \end{cases} \quad (US\ units) \tag{2.4}$$

$$\kappa_m = \begin{cases} \dfrac{1}{60\varepsilon_{fu}}\left(1-\dfrac{nE_f t_f}{360{,}000}\right) \le 0.90 \ \ for\ nE_f t_f \le 180{,}000\ N/mm \\ \dfrac{1}{60\varepsilon_{fu}}\left(\dfrac{90{,}000}{nE_f t_f}\right) \le 0.90 \ \ for\ nE_f t_f > 180{,}000\ N/mm \end{cases} \quad (SI\ units) \tag{2.5}$$

where, n, E_f, t_f are the number of plies or layers, the tensile modulus and nominal ply thickness of FRP, respectively. This older ACI equation only considers FRP properties and has been shown to markedly unconservative for design work (Task Group on Bond 2006).

2.5.3 fib Bulletin 14

fib Bulletin 14 *Externally Bonded FRP Reinforcement for RC Structures* (fib 2001) recommends the use of a shear stress-slip relationship to predict debonding failure. It recommends critical bond stress and slip parameters, which have been determined from experimental analysis. Bulletin 14 then gives three approaches to predict debonding failure. The first approach determines the maximum allowable axial load in the FRP and the length required to anchor this load. It also introduces a k_b factor, which accounts for the b_f/b ratio. The second approach determines a critical (unfavorable) crack pattern and the bond (adhesive) stresses this pattern would cause. Bond stresses rise between flexural cracks and these stresses are then transferred to the FRP. This second approach determines the maximum stress the FRP can have transferred to it, and determines an anchorage length differently than the first approach. The first two approaches can be used to derive allowable tensile strain equations for the FRP in order that debonding is mitigated. The third approach is concerned with checking that the concrete can withstand the FRP/concrete interface shear stress resulting from loading. If the interface shear stress is kept below the concrete bond shear strength, then cracks will not develop to cause debonding, and strain in the FRP will cause no concern.

By rewriting the fib relationships, the implied limiting FRP strain based on debonding stress may be obtained. For the first method:

$$\varepsilon_{fub} = \alpha c_1 k_c k_b \sqrt{\frac{f_{ct}}{E_f t_f}} \quad (SI\ units) \tag{2.6}$$

where, α = reduction factor to account for influence of inclined cracks on bond strength;

$\alpha = 0.9$ typically;

$\alpha = 1.0$ for beams having sufficient internal or external shear reinforcement and slabs;

k_c = factor accounting for concrete compaction;

k_c = 1.0 for FRP bonded to concrete faces cast against formwork;

k_c = 0.67 for FRP bonded to concrete faces not cast against formwork;

f_{ct} = tensile strength of concrete;

c_1 = empirical factor determined to be 0.64 for CFRP;

E_f = FRP modulus of elasticity;

t_f = FRP thickness;

$$k_b = 1.06\sqrt{2 - \frac{b_f}{b} \Big/ 1 + \frac{b_f}{400}} \geq 1.0 \quad \text{(b and } b_f \text{ in mm)} \tag{2.7}$$

b = width of beam soffit in mm;

b_f = width of FRP in mm.

For the second method:

$$\varepsilon_{fub} = c_1\sqrt{\frac{\sqrt{f_{ct} f_c'}}{E_f t_f}} \quad (SI\ units) \tag{2.8}$$

where, f_c' = compressive strength of concrete;

c_1 = empirical factor determined to be 0.23 for CFRP.

2.5.4 JSCE Recommendations

The Japan Society of Civil Engineers *Recommendations for Upgrading of Concrete Structures with use of Continuous Fiber Sheets* (JSCE 2001) uses an FRP stress equation which includes an interfacial fracture energy (G_f) term for the FRP/concrete interface. G_f can be determined from experimental results, and therefore, many factors and aspects of design can be accounted for with this approach. The ultimate stress found can then be used to derive the

allowable FRP tensile strain. However, testing and experimentally determined values of G_f are complex and not conducive to the design process.

The FRP limiting strain is given as:

$$\varepsilon_{fub} = \sqrt{\frac{2G_f}{E_f t_f}} \quad (SI\ units) \tag{2.9}$$

where, G_f = interfacial fracture energy between FRP and concrete; taken as 0.5 N/mm in the absence of experimental data;

E_f = FRP modulus of elasticity;

t_f = FRP thickness.

2.5.5 Concrete Society TR55

The UK's Concrete Society *Technical Report 55 – Design Guidance on Strengthening Concrete Structures using Fiber Composite Materials* (Concrete Society, 2000) uses an approach similar to the first approach in Bulletin 14, described in 2.5.3, only with more generalized factors:

$$\varepsilon_{fub} = 0.5 k_b \sqrt{\frac{f_{ct}}{E_f t_f}} \quad (SI\ units) \tag{2.10}$$

where, f_{ct} = tensile strength of concrete;

E_f = FRP modulus of elasticity;

t_f = FRP thickness;

$$k_b = 1.06\sqrt{2 - \frac{b_f}{b} \Big/ 1 + \frac{b_f}{400}} \geq 1.0 \quad (b_f \text{ and } b \text{ in mm}) \tag{2.11}$$

b_f = width of FRP in mm;

b = width of beam soffit in mm.

2.5.6 Italian CNR DT 200

The Italian National Research Council document *Guidelines for Design, Execution and Control of Strengthening Interventions by Means of Fibre-reinforced Composites* (National 2004) prescribes maximum allowable FRP stress to mitigate both plate end debonding and intermediate crack induced debonding (for a typical design case):

$$\varepsilon_{fub} = 0.484\sqrt{\frac{k_b\sqrt{f_c' f_{ct}}}{nE_f t_f}}\ (SI\ units) \tag{2.12}$$

where, f_c' = compressive strength of concrete;

f_{ct} = tensile strength of concrete;

n = number of plies or layers;

E_f = FRP modulus of elasticity;

t_f = FRP thickness;

$$k_b = 1.06\sqrt{2 - \frac{b_f}{b}\Big/1 + \frac{b_f}{400}} \geq 1.0 \tag{2.13}$$

b_f = width of FRP in mm;

b = width of beam soffit in mm.

2.5.7 Chinese CECS-146

As reported by Ye et al. (2005), the new Chinese CECS 146 *Technical Specification for Strengthening Concrete Structure with carbon Fiber Reinforced Polymer Laminate* (China 2003) adopts the following equation for FRP strain at intermediate crack induced debonding:

$$\varepsilon_{fub} = k_b f_{ct}\left(\frac{1}{\sqrt{nE_f t_f}} - \frac{0.2}{L_d}\right) \quad (SI\ units) \tag{2.14}$$

where, f_{ct} = tensile strength of concrete;

n = number of plies or layers;

E_f = FRP modulus of elasticity;

t_f = FRP thickness;

L_d = development length of the FRP in mm;

$$k_b = \sqrt{2.25 - \frac{b_f}{b} \Big/ 1.25 + \frac{b_f}{b}} \tag{2.15}$$

2.5.8 Teng et al. 2001

In their paper *Intermediate Crack Induced Debonding in RC Beams and Slabs*, Teng et al. (2001) propose the following approach to mitigating debonding by limiting the stress in the FRP as follows:

$$\varepsilon_{fub} = \alpha\beta_b\beta_L\sqrt{\frac{\sqrt{f_c'}}{E_p t_p}} \quad (SI\ units) \tag{2.16}$$

where, f_c' = compressive strength of concrete;

E_p = FRP modulus of elasticity;

t_p = FRP thickness;

$$\beta_b = \sqrt{2 - \frac{b_f}{b} \Big/ 1 + \frac{b_f}{b}} \tag{2.17}$$

$$\beta_L = \begin{Bmatrix} 1 & L_b \geq L_e \\ \sin(\pi L / 2L_e) & L_b < L_e \end{Bmatrix} \tag{2.18}$$

L_e is the full anchorage length or effective length of plate in a pull-push test.

$$L_e = \sqrt{\frac{E_p t_p}{\sqrt{f_c'}}} \tag{2.19}$$

The coefficient k_L accounts for the effect of FRP anchorage length, L_b, being shorter than the effective length, L_e.

The coefficient α = 1.1 and 0.72 for simply supported and cantilever beams, respectively.

2.5.9 The Draft Australian Guideline

The provisions for the limiting value of the debonding strain in the Australian Guideline are exactly the same as those recommended by Teng et al. 2001. However, the value of α is taken as 0.4 to account for the 95th percentile for beams.

2.5.10 Teng et al. 2004

In their paper *Recent Research on Intermediate Crack Induced Debonding in FRP Strengthened Beams*, Teng et al. (2004) present a smeared crack approach for finite element simulation of intermediate crack-induced debonding. A design model, based on interfacial stress

distributions determined using the finite element approach and verified with a database of beam tests is presented. In this model, the limiting FRP strain, ε_{fub}, is given as:

$$\varepsilon_{fub} = 0.54 k_b \frac{f_{ct}}{\sqrt{E_f t_f}} \quad (SI\ units) \tag{2.20}$$

where, f_{ct} = tensile strength of concrete;

E_f = FRP modulus of elasticity;

t_f = FRP thickness;

$$k_b = \sqrt{2.25 - \frac{b_f}{b} \Big/ 1.25 + \frac{b_f}{b}} \tag{2.21}$$

2.5.11 Comparisons and Evaluations of Recommendations

Because very low peeling stresses will still have a very significant effect on bond behavior, it is believed that limiting the allowable strain in the FRP is the best way to design FRP retrofit for RC beams.

Each of the different approaches for computing maximum allowable FRP strain to mitigate debonding failures are plotted in Figure 2-4 (Reeve 2005). (The fib method 1 and Concrete Society TR55 method are essentially identical and only the TR55 method is shown or discussed in subsequent section of this work.) In each case, where appropriate, the design strains are plotted using the upper ($b_f/b = 1$; solid lines) and lower bound values ($b_f/b = 0$; dashed lines) of the parameter k_b. The importance of the k_b factor is very clear in the variation it offers the curves plotted in Figure 2-4. It is also noted that all curves fall well below that of the ACI 440.2R-02 curve (bold black curve), which is the current US standard until ACI 440.2R-07 is adopted. Also shown in Figure 2-4 is some debonding data from a series of similar beam tests

(Harries and Kotynia 2006). The important thing to note is the exceptional variability observed and the non-conservative design values resulting from many of the recommendations, particularly that of ACI 440.2R-02 (bold black curve).

Oehlers and Seracino (2004) made a comparison of recommendations for intermediate crack induced debonding resistances (see Table 2-2). The FRP that was used in this comparison had the following properties: E_f = 23200 ksi (160 GPa); f_c' = 4350 psi (35 MPa); t_f = 0.05 in. (1.2 mm) and, unless shown otherwise and b_f/b = 0.5. Oehlers and Seracino evaluated the effective length for the 0.05 in. thick FRP strips as 7.4 in. (187 mm) from Chen and Teng's (2001) model and 7.44 in. (189 mm) from Neubauer and Rostasy's (2002) model which show a good agreement. The characteristic debonding strains shown in column 2 of the Table 2-2 are the strains that would be adopted in design with appropriate reduction factors. It can be seen that even in this case there is good agreement between the Chen and Teng model and that of Neubauer and Rostasy's. However, these strains are found to be significantly less than the strains observed in Oehlers (1999) test but are in good agreement with Oehlers (2002). The characteristic strains of Chen and Teng, Neubauer and Rostasy and the Oehlers tests are well below the recommendations made by the Concrete Society (2000) and German Institute of Construction (2001). Oehlers and Seracino concluded that the variations between the test results illustrate the complexity of the problem and they identified several parameters which must be investigated thoroughly and the models updated.

Monti et al. (2003) developed finite element models to analyze the response of FRP sheets bonded to RC beams in uncracked and cracked concrete zones. The non linear model they developed was then evaluated through correlation studies with experimental tests. In this analytical study, the predicted peak bond strength was found to depend on the b_f/b ratio:

$$\tau_{\max} = 1.8 k_b f_{ctm} \quad (SI\ units) \tag{2.22}$$

where, f_{ctm} is the concrete mean tensile strength;

$$k_b = \sqrt{\frac{1.5\left(2 - \frac{b_f}{b}\right)}{1 + \frac{b_f}{100}}} \quad (b_f \text{ and } b \text{ in } mm) \tag{2.23}$$

2.6 FRP WIDTH TO CONCRETE SUBSTRATE WIDTH/SPACING RATIO

As is clear in the previous sections, the ratio of FRP retrofit width (b_f) to beam soffit width (b) is believed to have a significant impact on the debonding behavior. Approaches to addressing this behavior are driven by the need to develop a factor (identified as k_b) by which to multiply the maximum allowable FRP strain (to set a limit for mitigating debonding).

One effect addressed by a factor associated with b_f/b is the interaction of the stress field in the disturbed region surrounding individual strips or plates when they are placed close together, as shown in Figure 2-5(b). Similarly, placing the plate close to the edge of a concrete element, as in the bottom plate in Figure 2-5(c), will reduce the width of the concrete that may be engaged. There is an additional issue about the width of the concrete element that should be used in calculating the b_f/b ratio when the FRP plate is placed eccentric to the overall width of the concrete element as shown in Figure 2-5(c) (Oehlers and Seracino 2004). The principles used in national standards in determining the effective width of a flexural member allowing for shear lag or the principles used in determining the effective width of a concrete element resisting the

anchorage forces in post tensioned members can be used to determine an appropriate value of b in this case (Oehlers and Bradford 1999).

The k_b factor is a function of beam geometry and in its simplest form:

$$k_b = \sqrt{2 - \frac{b_f}{b} \Big/ 1 + \frac{b_f}{b}} \tag{2.24}$$

represents an assumed 45^o "spreading" of shear stresses away from the edges of the FRP strip. This spreading is of course limited by the edges of the beam. However, this interpretation of the k_b factor may be too simplistic and has been empirically revised by a number of researchers and documents, as shown in Section 2.5. Teng et al. (2004) have proposed an empirically revised formulation:

$$k_b = \sqrt{2.25 - \frac{b_f}{b} \Big/ 1.25 + \frac{b_f}{b}} \tag{2.25}$$

Some European documents, have adopted a variation apparently "normalized" to a 400 mm soffit width (fib 2001, Concrete Society 2000, National 2004):

$$k_b = 1.06\sqrt{2 - \frac{b_f}{b} \Big/ 1 + \frac{b_f}{400}} \geq 1.0 \quad (b_f \text{ and b in mm}) \tag{2.26}$$

Lateral spreading of shear stresses likely contributes to the effect quantified by the parameter k_b. Equally, the confinement provided by the presence of concrete beyond the edges of the FRP strip also likely affects the value of this parameter. Quattlebaum (2003) has hypothesized that the k_b factor may also be calibrated to account for the significant shear lag effect present at shear interfaces involving thin elements (Timoshenko and Goodier (1970)). This effect will be investigated in the present work.

Beyond simple load spreading, the value of k_b is essentially empirical. Values of k_b recommended by various sources have already been listed in Section 2.5 and Table 2-1. The

value of b_f/b necessarily falls between 0 (no retrofit) and 1 (entire soffit width). For practical beam applications b_f/b will likely exceed 0.25. For slabs, a practical lower limit may be b_f/s = 0.10, where s, the spacing between FRP strips, replacing b. Quantifying the effect of b_f/b is the major objective of the present study.

The ACI Committee 440 Task Group on Bond (2006) identified three factors as affecting the k_b factor associated with the b_f/b ratio:

1. Relative stiffness of the FRP system and substrate
2. Non uniform stress distribution across the FRP strips (shear lag effect as quantified by early researchers like Timoshenko and Goodier 1970, Reissner and Thomas 1946, Carter 1958)
3. Confinement or edge effect.

Thomsen et al. (2004) conducted parametric studies on the failure mode of FRP strengthened RC beams using both finite element modeling and experimental procedures. They deduced that the bond stress which plays a central role in the failure of these systems, is directly influenced by the contact area between FRP and concrete and hence the width of FRP. They conducted experiments by varying the width and thickness of FRP plates keeping the area constant. Figure 2-6 shows various plots obtained from their analysis. As expected, the ultimate load increased with the plate width. Little increase was obtained for plates of smaller width due to the internal tension steel not yielding, whereas larger increases were reported in case of larger widths of FRP owing to yield of the internal tension reinforcement. Also, with the increased plate width, the FRP-concrete contact area increases allowing the bond force to build up over a larger area before failure as seen in Figure 2-6(c). However, for extremely wide plates, the plate fails by rupture before the full bond stress develops. This was evident in case of the 12 in. (300 mm) wide plate.

Thomsen et al. also deduced that the steel yield penetration (as shown in Figure 2-6(d)) is greater when wider plates are used leading to a more ductile response.

Chen and Pan (2005) conducted finite element analysis to assess stress distributions in a typical shear test set-up for FRP-to-concrete bond strength. They observed significant differences between the stresses at the middle and edge of the plate as shown in Figure 2-7 (half-width model shown in Figure 2-7). It can be clearly seen from this figure that the stress distribution across the width of the plate is non-uniform. They deduced that this non-uniformity depends on many factors including bond length and width and thickness of the bonded plate. Figure 2-8 shows the analytically determined stress distributions across the width of the FRP plate. It is clearly seen that both normal and shear stress distributions are highly non-uniform. They deduced that the magnitude of the peak compressive stress (located close to the edge of the plate) is not greatly affected by the b_f/b (described by Chen and Pan as w_p/w_c). However, the peak tensile stress was found to increase rapidly up to $w_p/w_c = 0.8$. The peak value of shear stress at the plate edge was also found to be significantly affected by w_p/w_c ratio. This non uniformity was also observed in case when $w_p/w_c = 1.0$ wherein the concrete substrate and bonded FRP plate were of the same width. Chen and Pan attributed the non uniformity in this case to the differences in Poisson's ratio between the constituent materials. Figure 2-9 and Figure 2-10 show the effect of the plate thickness, t_p on the stress distributions over the length of the plate for a constant plate width, w_p. It was seen that both normal and shear stresses increased with an increase in the plate thickness close to the supports. However, at the points of loading, the normal and shear stress was found to decrease with increasing plate thicknesses. This is because in the case of a plate with lesser thickness, bending is more localized near the loading point leading to larger values of stresses when compared to a thicker plate under the same magnitude

of loading. Also, they found that the plate thickness has insignificant effect on the ratio of shear stress at the edge to that at the middle of the plate near the loaded end where this stress is more significant (Figure 2-11). Away from the loaded end the increase of plate thickness slightly reduced this ratio, reflecting the phenomenon that the shear stress distribution becomes more uniform over the bond length as the plate thickness increases.

Oehlers (2005) formulated the fundamental intermediate crack induced debonding resistance as:

$$P_{AIC} = \sqrt{\tau_f \delta_f}\sqrt{L_{per}(EA)_p} \tag{2.27}$$

where, $\tau_f\delta_f$ is twice the area under the idealized τ/δ characteristics (as in Figure 2-12(a));

L_{per} is the length of the failure plane (as in Figure 2-12(b));

$(EA)_p$ is the axial rigidity of the plate which can also include the axial stiffness of the adhesive bonding the plate.

The above equation was further modified with experimental quantification of the $\tau_f\delta_f$ term as:

$$P_{AIC} = 0.78\sqrt{\left(\frac{d_f}{b_f}\right)f_c}\sqrt{L_{per}(EA)_p} \tag{2.28}$$

where, d_f and b_f are the depth and width of the failure plane (as in Figure 2-12(b));

f_c' is the cylinder compressive strength.

The parameter d_f/b_f can be regarded as a confinement factor that allows for an increase in the intermediate crack material characteristics of strength and ductility due to confinement. Essentially, the better the confinement, the better the bond and interlock.

2.6.1 Stress distribution across the FRP strips

From fundamental mechanics, it is a well established fact that wider strips have more uniform stress distribution when compared to narrow strips. This "shear lag" effect results from very large shears, relative to the average shear stress, at the edges of thin elements. This manifestation of the shear lag effect or the transverse stress distribution is explained by Timoshenko and Goodier (1970), Reissner and Thomas (1946) and Carter (1958).

Timoshenko and Goodier and Reissner and Thomas derived expressions for the shear stress distribution across a beam of depth, 2a and width, 2b. The cross-section and the coordinate system adopted are shown in Figure 2-13 and the results are presented in Table 2-3. Timoshenko and Goodier established that for greater values of b/a, the maximum stress is τ_{yz} at the edges of the plate. Values of this stress normalized by the theoretical peak stress 3P/2A (where P and A are the applied load and cross-sectional area) are given in Table 2-3 for a material having Poisons ratio, $\upsilon = 0.25$.

Reissner and Thomas (1946) further established that for extremely wide beams (plates), the component of shear parallel to the face of the plate, τ_{xz} is 35 percent higher than the value reached by the component of transverse shear, τ_{yz}.

$$\lim_{b/a \to \infty} \frac{\tau_{xz}}{\tau_{yz}} = 1.347 \tag{2.29}$$

Carter (1958) developed equations representing the variation of shear stress across the cross-section width of various shapes. It was seen that with increasing values of width to thickness ratio (b/a), the distribution of shear stress was found more and more uniform although expressing large peak shears at their edges.

2.7 ACI 440 BOND TASK GROUP DATABASE

The ACI Committee 440 Task Group on Bond was charged with assessing the existing 440.2R-02 bond equations and determining an appropriate relationship to capture the limits associated with debonding behavior to be incorporated into 440.2R-07. The task group developed an extensive database of experimental tests of flexural members having FRP retrofits which included 282 tests from 42 citable sources. Only 102 of these tests reported sufficient information to be used to assess FRP debonding strains and behavior. Of these 102 tests:

- 18 reported cover delamination (PE) failures.
- 72 reported FRP delamination (IC) failures.
- 12 reported rupture of the FRP.

The range of parameters encompassed by the 72 tests exhibiting IC failure is given in Table 2-4; the database of the 72 test results is given in Appendix-A. A discussion of data derived from this database is presented in Chapter 6.

Table 2-1 Bond provisions as per various National Standards and researchers (SI units).

ACI 440.2R-07	$\varepsilon_{fub} = 0.41\sqrt{\frac{f_c'}{nE_f t_f}}$	
ACI 440.2R-02	$\varepsilon_{fub} = \kappa_m \varepsilon_{fu}$ $\kappa_m = \begin{cases} \frac{1}{60\varepsilon_{fu}}\left(1-\frac{nE_f t_f}{360{,}000}\right) \le 0.90 & for\ nE_f t_f \le 180{,}000\ \text{N/mm} \\ \frac{1}{60\varepsilon_{fu}}\left(\frac{90{,}000}{nE_f t_f}\right) \le 0.90 & for\ nE_f t_f > 180{,}000\ \text{N/mm} \end{cases}$	
fib Bulletin 14 method 1	$\varepsilon_{fub} = \alpha c_1 k_c k_b \sqrt{\frac{f_{ct}}{E_f t_f}}$	$k_b = 1.06\sqrt{2-\frac{b_f}{b}\Big/1+\frac{b_f}{400}} \ge 1.0$ $c_1 = 0.64$ for CFRP
fib Bulletin 14 method 2	$\varepsilon_{fub} = c_1\sqrt{\frac{\sqrt{f_{ct}f_c'}}{E_f t_f}}$	$c_1 = 0.23$ for CFRP
JSCE	$\varepsilon_{fub} = \sqrt{\frac{2G_f}{E_f t_f}}$	G_f = interfacial fracture energy taken as 0.5N/mm in absence of test values
Concrete Society TR 55	$\varepsilon_{fub} = 0.5k_b\sqrt{\frac{f_{ct}}{E_f t_f}}$	$k_b = 1.06\sqrt{2-\frac{b_f}{b}\Big/1+\frac{b_f}{400}} \ge 1.0$
CNR DT 200	$\varepsilon_{fub} = \frac{3.0}{1.2\sqrt{1.6}}\sqrt{\frac{0.06k_b\sqrt{f_c'f_{ct}}}{nE_f t_f}} = 0.484\sqrt{\frac{k_b\sqrt{f_c'f_{ct}}}{nE_f t_f}}$	"certified" application $k_b = 1.06\sqrt{2-\frac{b_f}{b}\Big/1+\frac{b_f}{400}} \ge 1.0$
CECS-146	$\varepsilon_{fub} = k_d f_{ct}\left(\frac{1}{\sqrt{nE_f t_f}}-\frac{0.2}{L_d}\right)$	$k_b = \sqrt{2.25-\frac{b_f}{b}\Big/1.25+\frac{b_f}{b}}$
Teng et al. 2001	$\varepsilon_{fub} = \alpha k_b\sqrt{\frac{\sqrt{f_c'}}{E_f t_f}}$	$\alpha = 1.1$ for beams $\alpha = 0.72$ for cantilever slabs $k_b = \sqrt{2-\frac{b_f}{b}\Big/1+\frac{b_f}{b}}$
Teng et al. 2004	$\varepsilon_{fub} = 0.54k_b\frac{f_{ct}}{\sqrt{E_f t_f}}$	$k_b = \sqrt{2.25-\frac{b_f}{b}\Big/1.25+\frac{b_f}{b}}$
Australia Guideline	appears to recommend Teng et al. (2001) approach with $\alpha = 0.4$ to account for the 95th percentile for beams	

Table 2-2 FRP Intermediate crack induced interfacial debonding resistances (Oehlers and Seracino 2004).

Source	ε_{IC} 95%	ε_{IC} mean	σ_{IC} (MPa) 95%	σ_{IC} (MPa) mean
1) Chen and Teng (2001)	0.0027	0.0053	427	854
2) Neubauer and Rostasy (2002)	0.0026			
3) Concrete Society (2000)	0.0060-0.0080		960-1280	
4) German Inst. of Construction (2001)	0.0065-0.0085		1040-1360	
5) Adelaide FRP beam tests (1999)	0.0046-0.0052		782-884	
6) Adelaide FRP beam tests (2002)	0.0025-0.0027		425-459	
7) Adelaide FRP beam tests (2002) (2.4 mm)	0.0015		255	

Table 2-3 Magnitudes of shear stresses in rectangular beam cross-sections for different values of (b/a) (Timoshenko and Goodier 1970).

$\frac{b}{a}$	$\frac{\tau_{xz}}{3P/2A}$	$\frac{\tau_{yz}}{3P/2A}$
0	1.000	0.000
2	1.390	0.310
4	1.988	0.968
6	2.582	1.695
8	3.176	2.452
10	3.770	3.226
15	5.255	5.202
20	6.740	7.209
25	8.225	9.233
50	15.650	19.466

Table 2-4 Range of parameters in the ACI 440 Bond Task Group Database (see Appendix A).

Parameter	Range
Beam height (h), in. (mm)	3.1 (78) – 32.5 (825)
Test span (L), ft. (m)	2.95 (0.9) – 29 (8.84)
Shear span / height ratio (a/h)	1.78 – 9.07
Concrete compressive strength (f_c'), psi (MPa)	3090 (21.3) – 11600 (80)
Tension steel reinforcing ratio (ρ_s)	0.0013 – 0.0262
Compression steel reinforcing ratio (ρ_s')	0.0013 – 0.0078
Shear steel reinforcing ratio (ρ_v)	0.0007 – 0.0079
FRP tensile modulus (E_f), ksi (MPa)	2970 (20500) – 39300 (271000)
FRP ply thickness (t_f), in. (mm)	0.004 (0.11) – 0.075 (1.9)
FRP width / concrete substrate width (b_f/b)	0.07 – 1.00
FRP strain at debonding (ε_{fub}), με	1622 - 16450

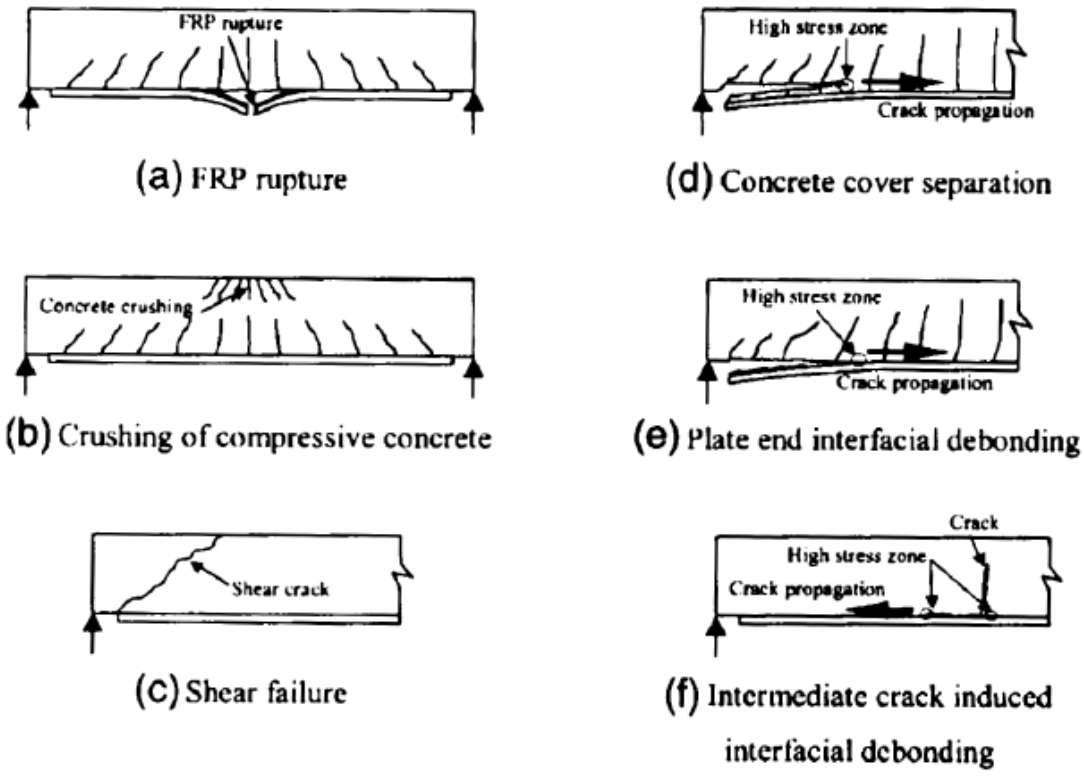

Figure 2-1: Failure modes of FRP plated RC flexural members
(J.G. Teng, J.F. Chen, S.T. Smith, L. Lam, 2002).

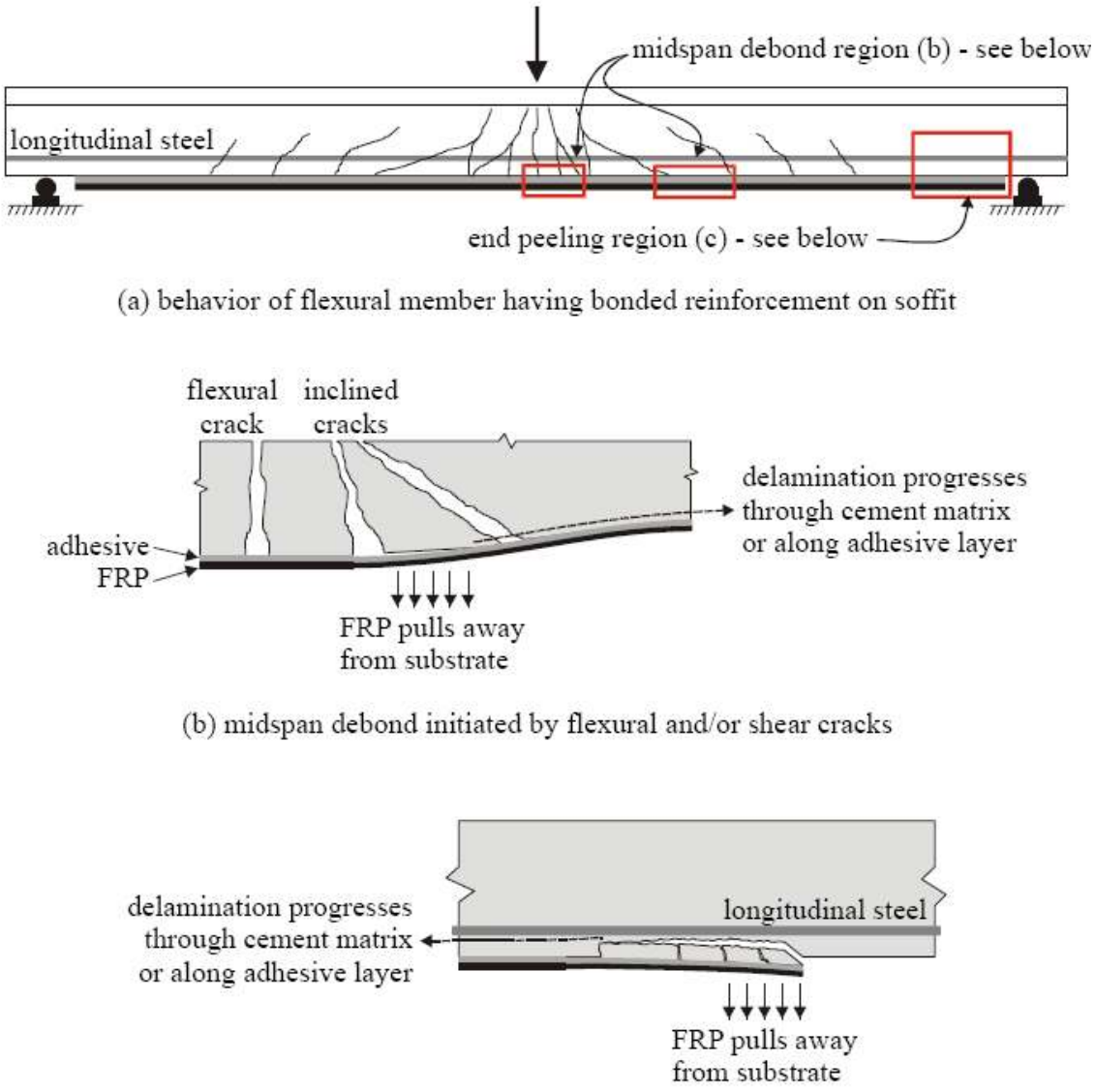

Figure 2-2 (b) IC and **(c)** PE modes of FRP delamination (Quattlebaum, 2003).

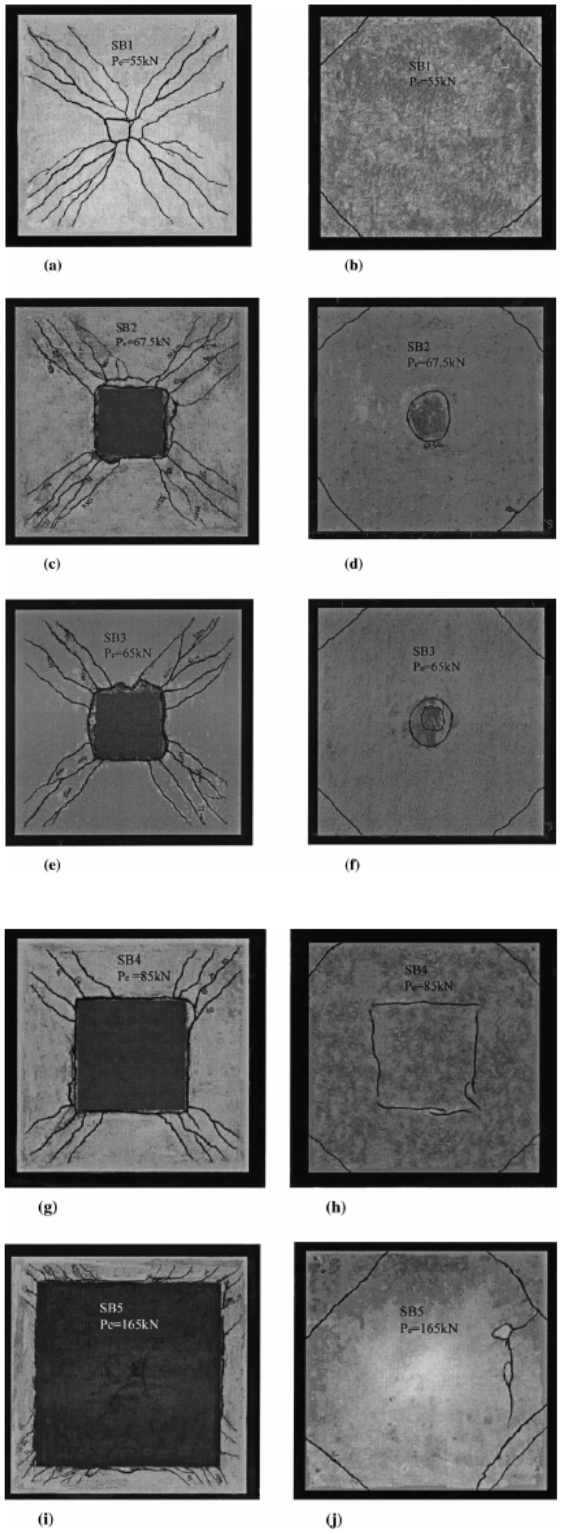

Figure 2-3 Final cracking patters of two-way RC slabs strengthened with steel plates (Zhang et al. 2001).

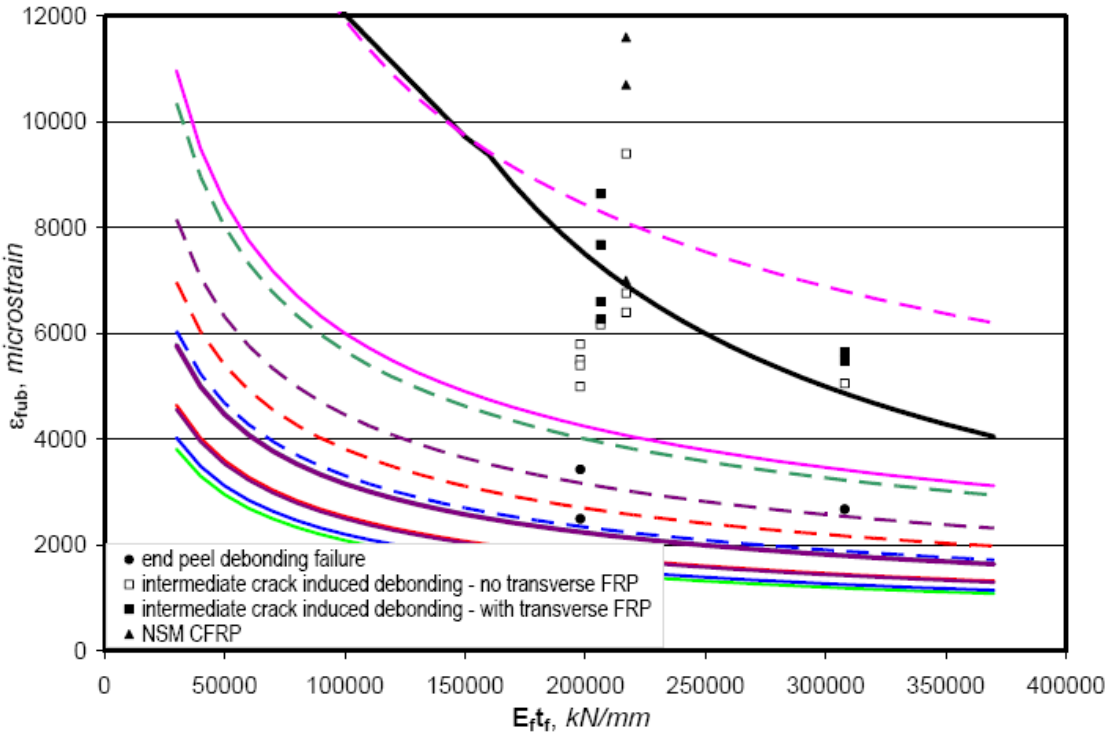

Figure 2-4 Various recommended limiting debonding strain relationships
Lines having the same color represent the same recommended relationships for the bounding cases of $b_f/b = 1$ (solid lines) and $b_f/b = 0$ (dashed lines). The ACI 440.2R-02 relationship is shown as the bold black curve. (Reeve 2005).

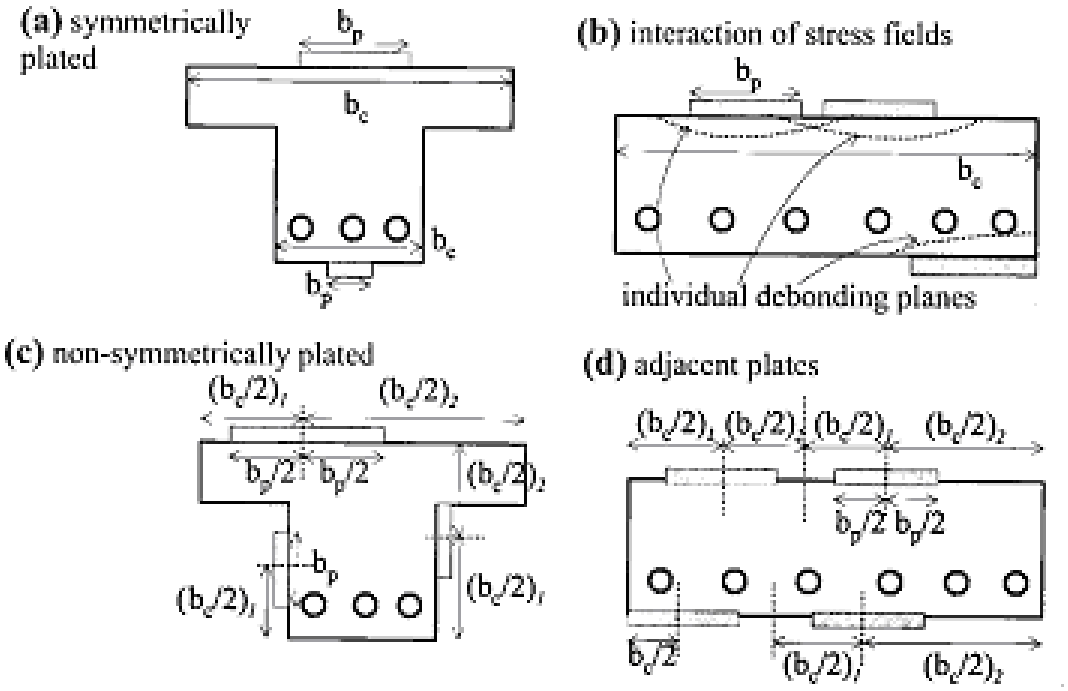

Figure 2-5 Effective widths of plates and interaction of stress fields (Oehlers and Seracino 2004).

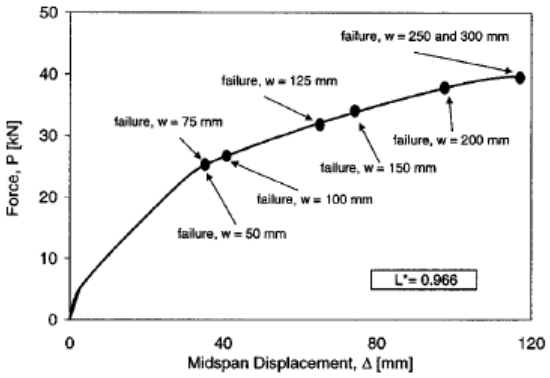

(a) Force-displacement response

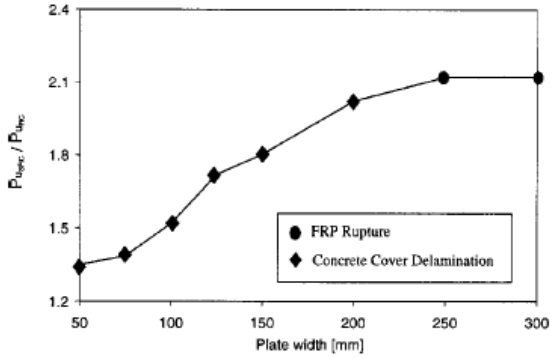

(b) Increase in ultimate load

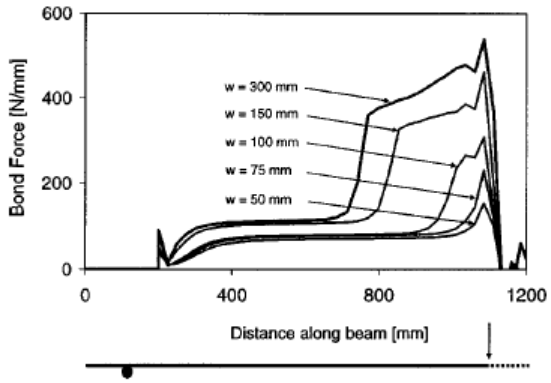

(c) Bond force distribution at failure

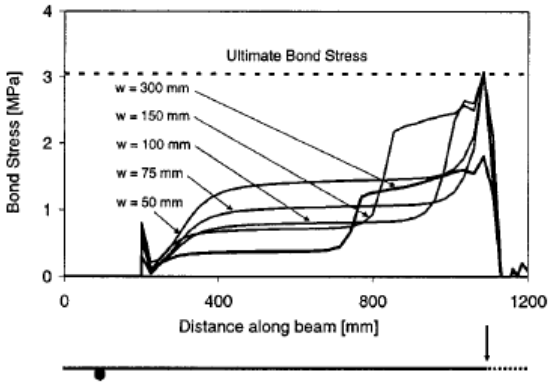

(d) Bond stress distribution at failure

Figure 2-6 Plots of various parameters for RC beams strengthened with CFRP plates of different widths (Thomsen et al. 2004).

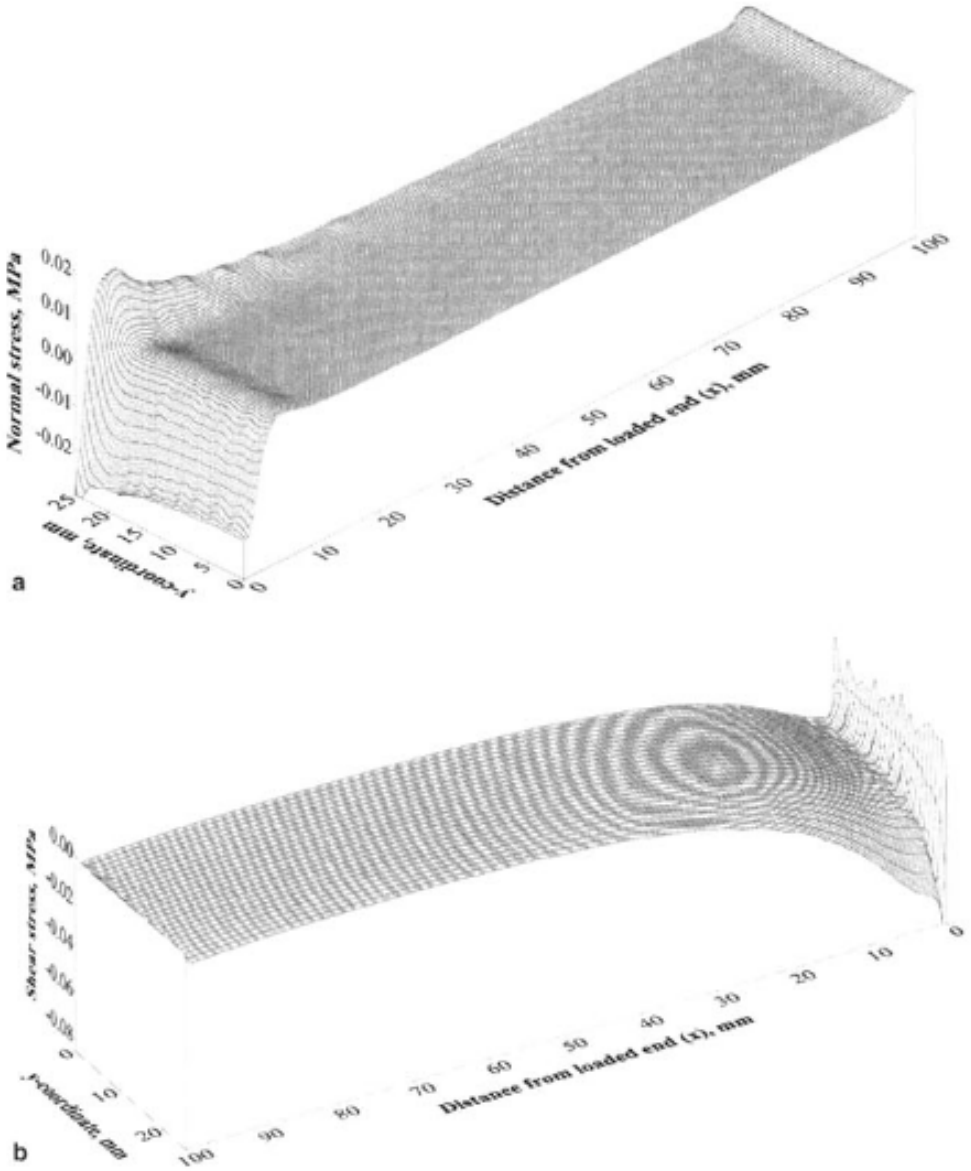

Figure 2-7 Stress distribution at the middle plane of the adhesive (a) normal (peeling) stress, (b) shear stress (Chen and Pan 2005).

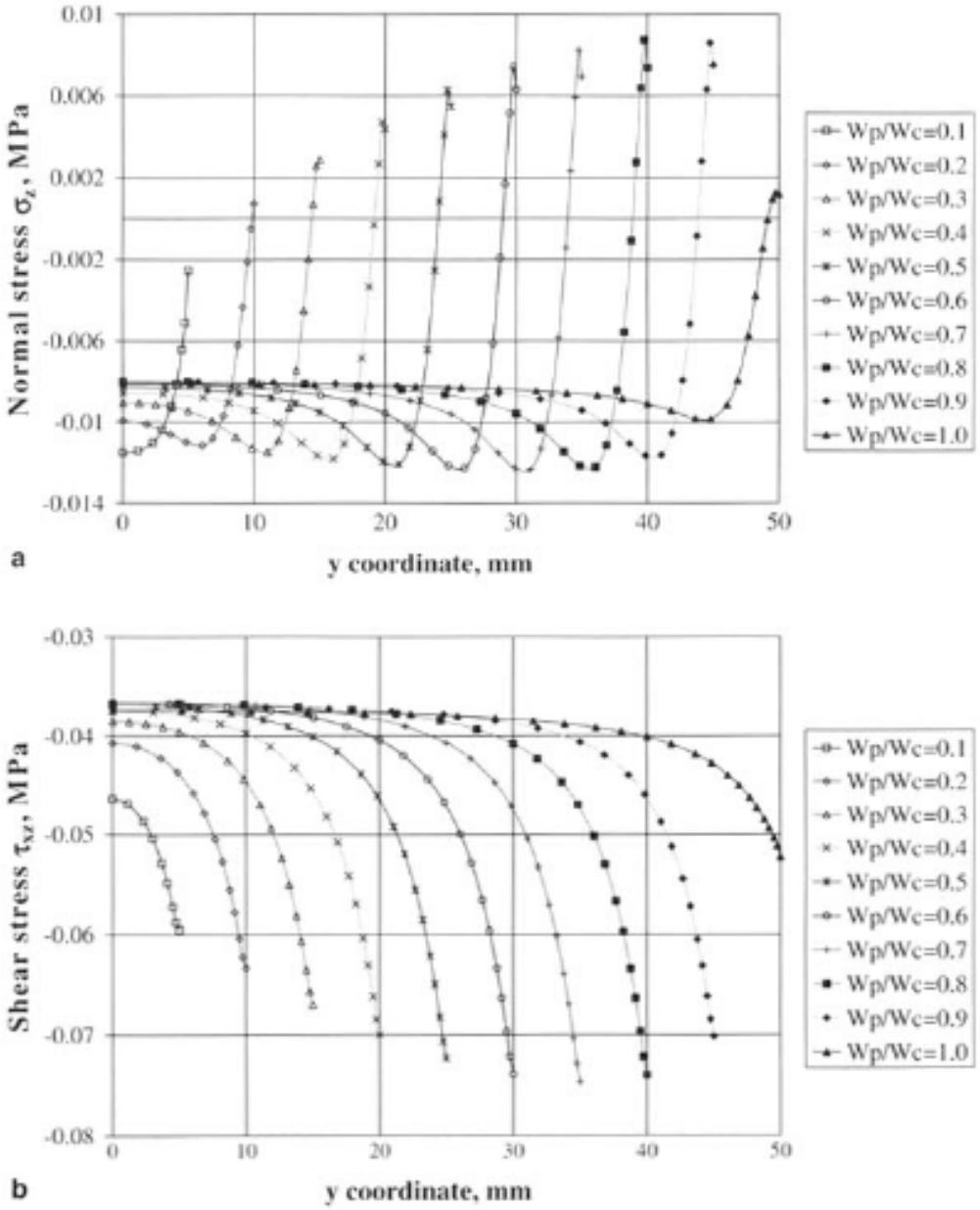

Figure 2-8 Stresses on the mid-section of adhesive for different plate width / substrate width ratio (a) normal (peeling) stress, (b) shear stress
(Chen and Pan 2005).

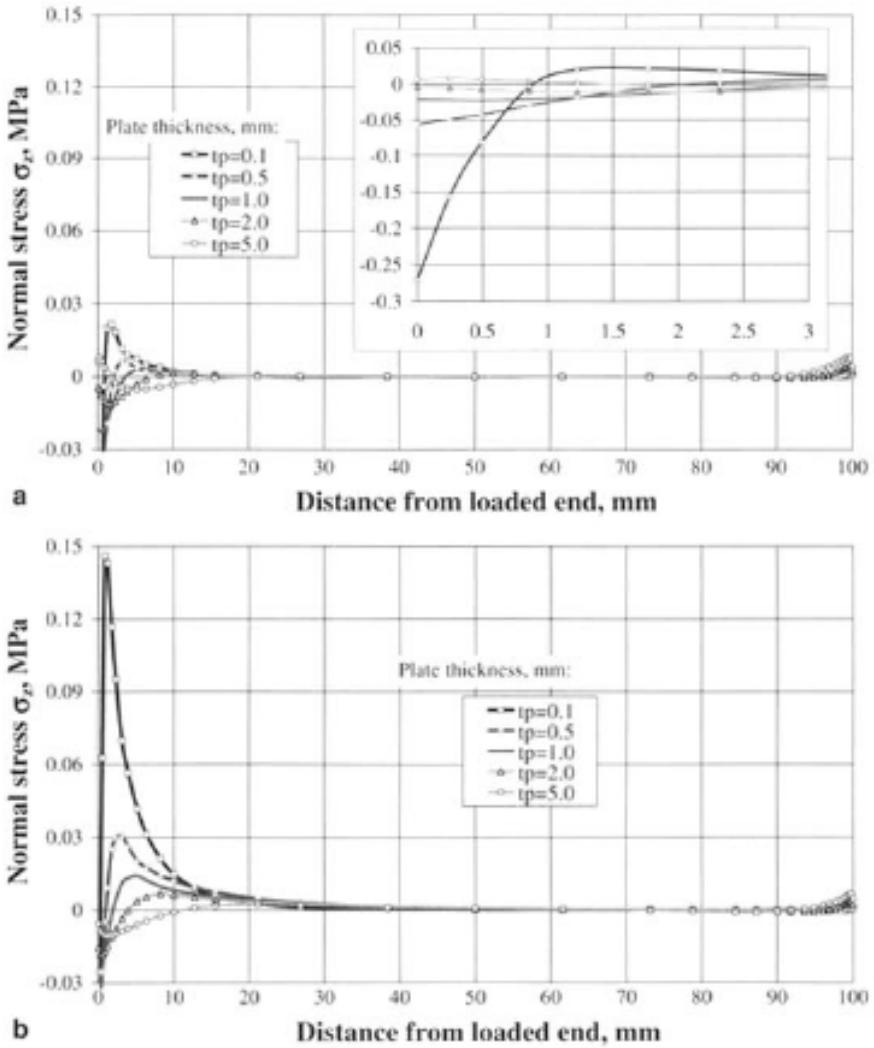

Figure 2-9 Effect of plate thickness on normal stress at mid-section of adhesive (a) middle of the plate, (b) edge of the plate
(Chen and Pan 2005).

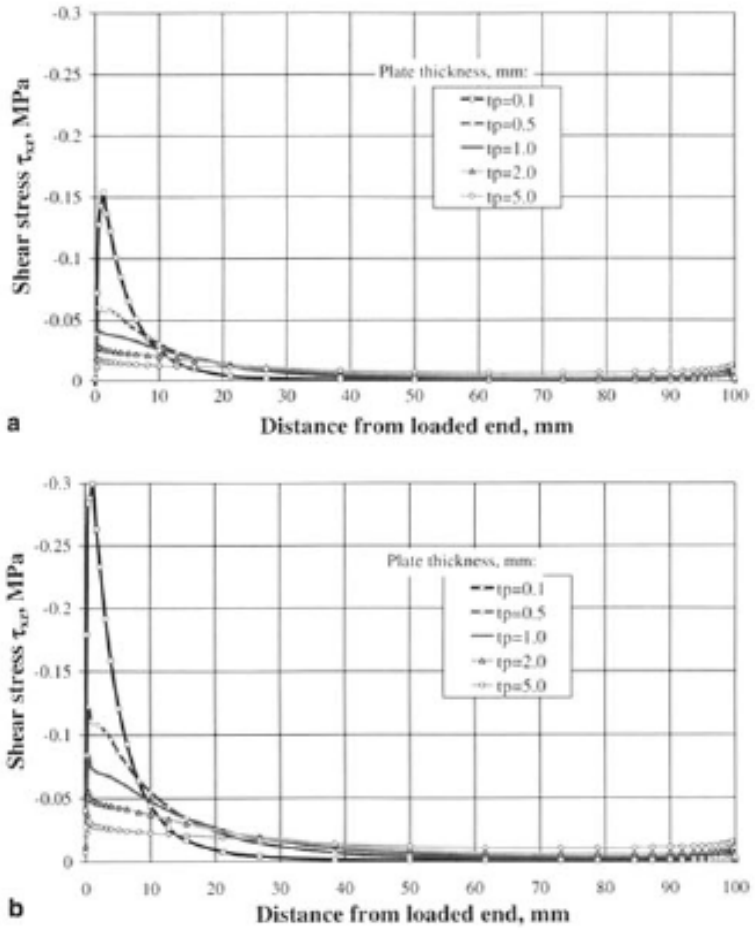

Figure 2-10 Effect of plate thickness on shear stress at mid-section of adhesive (a) middle of the plate, (b) edge of the plate
(Chen and Pan 2005).

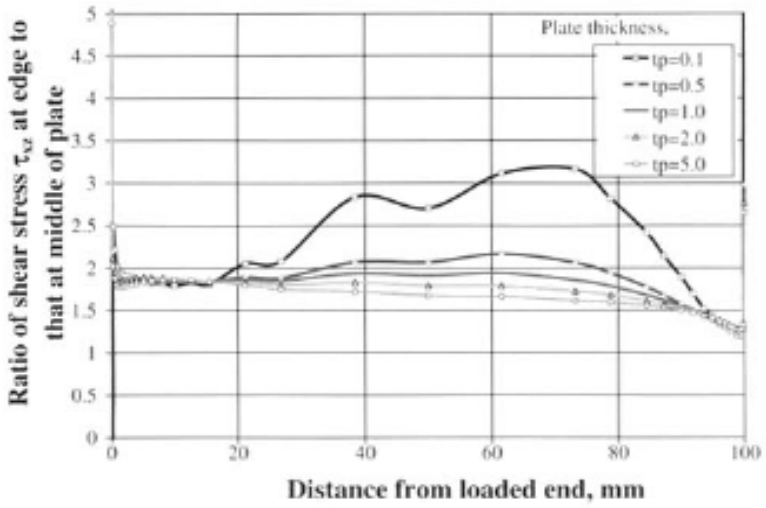

Figure 2-11 Effect of plate thickness on the ratio of shear stress at mid-section of adhesive at edge to that at the middle of the plate
(Chen and Pan 2005).

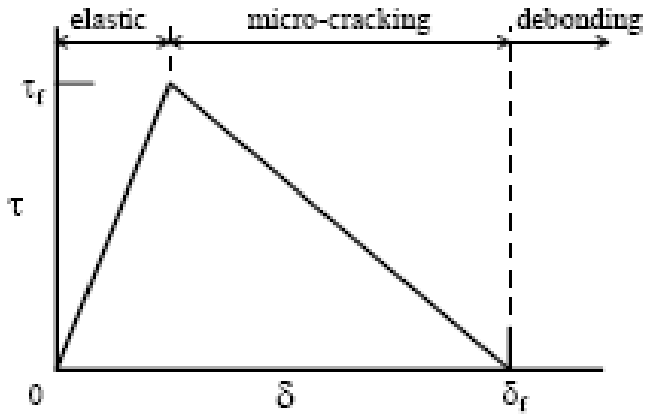

(a) Idealized τ/δ material characteristics

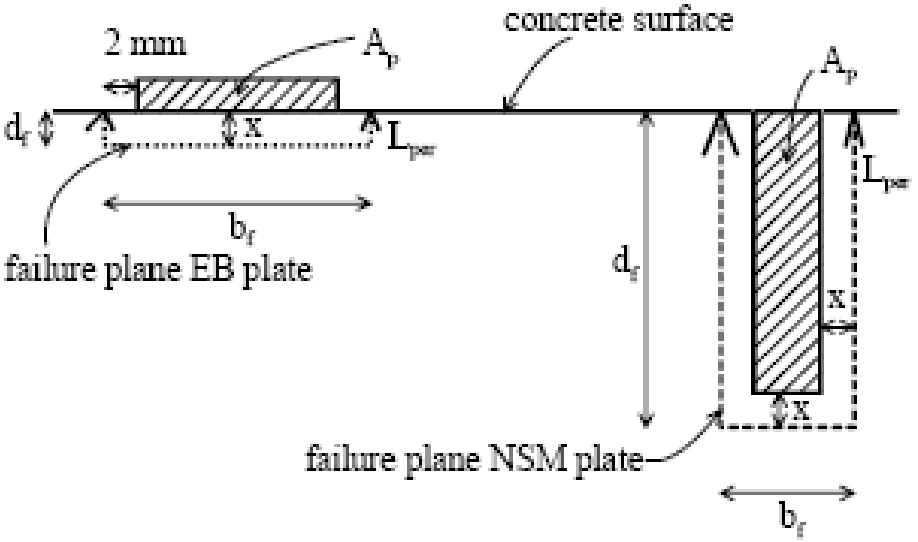

(b) Externally Bonded and Near Surface Mounted FRP plates

Figure 2-12 τ/δ material characteristics and FRP plate locations in FRP bonded RC members (Oehlers 2005).

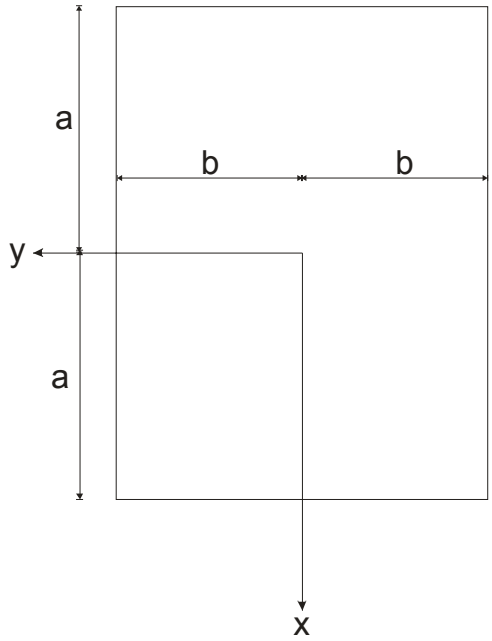

Figure 2-13 Diagram showing the beam cross-section and the coordinate system used (adapted from Timoshenko and Goodier 1970).

3.0 EXPERIMENTAL PROGRAM

This chapter reports details of the experimental program used in the study.

3.1 TEST SPECIMENS

Twelve identical reinforced concrete slabs were cast from a single batch of Portland Cement Concrete in the Watkins Haggart Structural Engineering laboratory at the University of Pittsburgh (Figure 3-2b). This work reports the testing of ten specimens inclusive of a Control Specimen. Two specimens were held in reserve and not used in this program.

The slabs were 50 in. (1270 mm) x 30 in. (762 mm) and 3 in. (76 mm) deep. Nine slabs were strengthened with various arrangements of carbon fiber reinforced polymer (CFRP) strips as described in the following paragraphs and one of them was left as an unretrofit control specimen (Control). The concrete had a measured 28 day compressive strength of 4860 psi (33.5 MPa). Details of the concrete mix as reported by the supplier are presented in Table 3-1.

Each slab contained seven numbers of #3 (9.5 mm diameter) longitudinal reinforcing steel bars at a spacing of 4 in. (100 mm) as primary flexural reinforcement. Additionally, four #3 bars transverse bars were provided to resist handling stresses due to inverting the slab for the application of CFRP. No additional shear reinforcement in the form of stirrups was provided.

Details of the slab reinforcement are shown in Figure 3-1a. Figure 3-2a and Figure 3-2b show the picture of the formwork prior to casting.

Commercially available 4 in. (102 mm) wide by 0.055 in. (1.4 mm) thick preformed unidirectional high strength carbon fiber reinforced polymer (CFRP) composite strips system were used in this study (Fyfe, 2005). The manufacturer reported material properties of the CFRP are presented in Table 3-2. The adhesive used to bond the FRP to the concrete substrate in the study was Fox Industries FX-776, a two-part ambient cure epoxy formulated for bonding to concrete and steel substrates. Manufacturer reported material properties of the adhesive are given in Table 3-3.

3.2 RETROFIT MEASURES

Nine retrofit measures were tested in this experimental research in order to investigate the effect of the CFRP width to spacing (b_f/s) ratio on the bond behavior. The CFRP strips were commercially available in widths of 4 in. (102 mm). These strips were then cut to widths of 2 in. (51 mm) and 1 in. (25 mm) as required.

Details of the nine specimens along with the number of CFRP strips and spacing for each specimen are given in Table 3-4. The first grouping of specimens had a slab with a single 4 in. CFRP strip bonded to its soffit, a slab with two 2 in. CFRP strips and a slab with four 1 in. CFRP strips. Thus, the area of CFRP applied to each slab was constant 0.22 in^2 (143 mm^2). The second grouping had a slab with two 4 in. strips, a slab with four 2 in. strips and a slab with eight 1 in. strips, resulting in an area of CFRP of 0.44 in^2 (286 mm^2). The third grouping had a slab with

three 4 in. strips, a slab with six 2 in. strips and a slab with twelve 1 in. strips bonded to its soffit, resulting in an area of CFRP of 0.66 in^2 (428 mm^2). CFRP details are shown in Figure 3-1b.

3.3 APPLICATION OF CFRP TO THE TEST SPECIMENS

This section outlines the procedure adopted for the application of CFRP to the slabs along with the surface preparation of slab and cutting of CFRP strips.

3.3.1 Concrete Surface Preparation

The concrete surface must be properly prepared to avoid failure at the adhesive-to-concrete interface. The surface must be clean, free of laitance and have minimal relief. It is generally accepted that a surface conforming to ICRI Surface Profile 4 or rougher is appropriate. The formed soffit of each test slab was prepared using an angle grinder with a wire wheel attachment to remove all laitance and dirt from the working surface of the concrete beam. Compressed air was then used to remove any concrete dust and dirt that settled on the slab. Once the surface was clean, the edge lines for strip alignment were marked.

3.3.2 Preparation of CFRP strips

The CFRP strips were provided in 4 in. (102 mm) widths and were cut to lengths of 46 in. (1168 mm) so that they did not extend to or beyond the end supports of the slab. The strips were then cut longitudinally to widths of 2 in. (51 mm) and 1 in. (25 mm) using a utility knife. Once

the CFRP was cut, it was cleaned and protected from dust, dirt, moisture and mechanical damage.

3.3.3 Application of CFRP

Once the CFRP was cut to width and length and the concrete surface prepared, the CFRP was ready for application. With the slabs inverted and having an unobstructed working surface on the (eventual) tension face of the beam, the retrofit process was begun. The adhesive was applied to the tension face of the slab using putty spatulas between the lines that were laid out for CFRP location. All possible care was taken to ensure that a uniform layer of adhesive was laid out. The adhesive was also applied in a similar fashion to one of the side of the CFRP strips. Each CFRP strip was then applied to the slab soffit. The strip was pushed firmly into the adhesive to remove any voids in the adhesive and assure a uniform application. Starting at the center of the strips and moving outward toward the supports locations, the strips were pressed onto the concrete with uniform pressure from fingertips. The exposed (unbonded) side of the CFRP strips was protected with masking tape in order to keep it clean of adhesive for eventual application of strain gages. The nine retrofitted one way slabs are shown in Figure 3-1b.

3.4 SPECIMEN DESIGNATION

The test specimens were designated as below

$$A \times B$$

where, A stands for the number of CFRP strips across the width of the slab; and

B stands for the width of the individual CFRP strips in inches.

The unretrofit control specimen was designated as Control and

1 x 4 is a slab with one 4 in. strip.

2 x 2 is a slab with two 2 in. strips.

4 x 1 is a slab with four 1 in. strips.

2 x 4 is a slab with two 4 in. strips.

4 x 2 is a slab with four 2 in. strips.

8 x 1 is a slab with eight 1 in. strips.

3 x 4 is a slab with three 4 in. strips.

6 x 2 is a slab with six 2 in. strips.

12 x 1 is a slab with twelve 1 in. strips.

3.5 TEST SETUP

All the ten specimens were tested to failure under a four point bending (flexural) load. The test frame, described below, was mounted in a universal testing machine with a capacity of 200,000 lbs (890 kN). Loading was applied at midspan using a system of two 1.5 in. (38 mm) diameter rollers spaced at 6 in. (152 mm) which loaded the slab uniformly across its entire width. The 30 in. (762 mm) wide by 50 in. (1270 mm) long one way slabs were simply supported over a clear span of 48 in. (1220 mm). Thus the shear span was 21 in. (533 mm) and the shear span-to-depth ratio was 7.

A steel reaction plate 51 in. (1296 mm) long, 31 in. (788 mm) wide and 3 in. (76 mm) thick was used to extend the lower platen of the test machine and permit relatively rigid support

over the 48 in. span. Two 9 x 9 x ¼ HSS (US designation) sections were welded to the base plate to support the slab with sufficient clearance that the soffit could be viewed during testing. Two 1.5 in. (38 mm) diameter rollers were used to support the slab across its entire width. At all four roller locations (midspan and supports), 0.25 in. (6.5 mm) thick steel shim plates were "capped" into place using high strength plaster (UltrCal 30) to ensure a uniform distribution of force into the slab and to mitigate local concrete crushing. A schematic representation and photographs of the test setup (and instrumentation) are shown in Figure 3-3 and Figure 3-4.

3.6 INSTRUMENTATION

As described earlier, ten instrumented slabs were tested. All the slabs were instrumented with four electrical resistance strain gages; two on each of the two #3 longitudinal reinforcing bars located on either side of the central bar (see Figure 3-1a). The two gages on each reinforcing bar were located 8 in. (203 mm) to either side of the centerline of the slab in all cases. These gages were designated S1, S2, S3 and S4 respectively (Figure 3-1a).

On each specimen, two CFRP strips were instrumented, each with four electrical resistance strain gages. The strips that were closest to the instrumented reinforcing bars were chosen and the strain gages were installed on them. The gages were located 8 in. (203 mm) and 12 in. (305 mm) to either side of the centerline of the slab in all cases. Specimen 1x4, having only a single strip, was only instrumented on this strip (4 gages). One objective of the testes was to investigate the transverse distribution across the CFRP strip and particularly, the presence of any shear lag effect. To do this, additional gages were located on Specimens 1x4, 2x2 and 4x1. Eight electrical resistance strain gages were installed for this purpose starting from one edge of

the CFRP strip at midspan and moving towards the center of the strip. The gages were positioned on alternating sides of the midspan to facilitate their close transverse spacing. Utmost care was taken to ensure that the adjacent gages were installed without a transverse gap in between them resulting in a transverse spacing between gages of 0.1 in. (2.54 mm) – the gage dimension. Owing to its thinner width, only six gages were installed on Specimen 4x1. Photographs of gage installations are shown in Figure 3-5.

Slab vertical displacement at midspan was monitored using two draw wire transducers (DWT) secured to the slab sides at mid-height. These DWTs also permitted monitoring of transverse "rocking" of the slab as the initial loads were applied and any torsional behavior (none was observed). The universal testing machine load cell, the two DWTs and all the strain gages were connected to a Vishay System 5100 Data Acquisition System.

3.7 TEST PROCEDURE

Ten reinforced one way slabs were tested under four point flexural loading to failure. The hydraulic universal testing machine was controlled manually in load control with load applied at rate of approximately 10 lbs per second. Each monotonic test was completed at failure of the specimen, defined by debonding of the CFRP strip or shear failure of the slab in the more heavily reinforced specimens. All data was recorded at a rate of 1 Hz, sufficient to capture all aspects of specimen behavior.

Table 3-1 Mix description and properties of concrete used.

Material	**Quantity** (per cubic yard)	**Type**	**Source**
Cement	675 lbs	1	Essroc Cement
Fine Aggregate	1122 lbs	Hi-Way	Tri-State River Pro.
Coarse Aggregate	1700 lbs	Shot	Tri-State River Pro.
Pozzolan	20% of cementitious	C-Ash	Essroc Cement
AE Agent	5 oz/cwt	VRC	Axim Concrete Tech.
WR Agent	4 oz/cwt	800N	Axim Concrete Tech.
HRWR	as required to pump	1000 SP-MN	Axim Concrete Tech.
water	265 lbs		
w/c ratio	0.39		
entrained air	6.8%		
Design Property	**Value**	**Notes**	
Strength	5000 psi	28 day cylinder strength = 4860 psi	
Unit Weight	139.3 pcf		
slump	5 in.	pumpable	
entrained air	4-5 to 7.5%		

Table 3-2 Manufacturer's reported properties of CFRP strips (Fyfe Tyfo UC).

Property	**ASTM Test Method**	**Fyfe Tyfo UC**
Material Type	NA	High Strength Carbon
Tensile Strength, *ksi (MPa)*	D3039	405 (2800)
Tensile Modulus, *ksi (GPa)*		22500 (155)
Elongation at rupture		0.018
Perpendicular Strength, *psi (Pa)*		negligible
Strip Thickness, *in (mm)*	NA	0.055 (1.4)
Widths used in testing, *in (mm)*	NA	4 (102); 2 (51); 1(25)

Table 3-3 Manufacturer's reported properties of adhesive system used (FX 776).

Property	**ASTM Test Method**	**FX 776**
Tensile Strength, *psi (MPa)*	D638	4500 (31)
Elongation at rupture		0.025
Tangent Modulus of elasticity, *ksi (GPa)*	D790	575 (3.9)
Thickness of application, in. (mm)	measured	approx. 0.1 (2.54)

Table 3-4 Details of the one way slab specimens.

Specimen	**Dimensions** ***in(mm)***	**Number of strips**	**Strip Width** ***in (mm)***	**Strip Spacing** ***in(mm)***
CONTROL	50 x 30 x 3 in. (1270 x 762 x 76 mm)	0	0 (0)	0 (0)
1x4		1	4 (102)	0 (0)
2x2		2	2 (51)	10 (254)
4x1		4	1 (25)	6 (152)
2x4		2	4 (102)	10 (254)
4x2		4	2 (51)	6 (152)
8X1		8	1 (25)	3.3 (84)
3X4		3	4 (102)	7.5 (191)
6X2		6	2 (51)	4.3 (109)
12X1		12	1 (25)	2.3 (58)

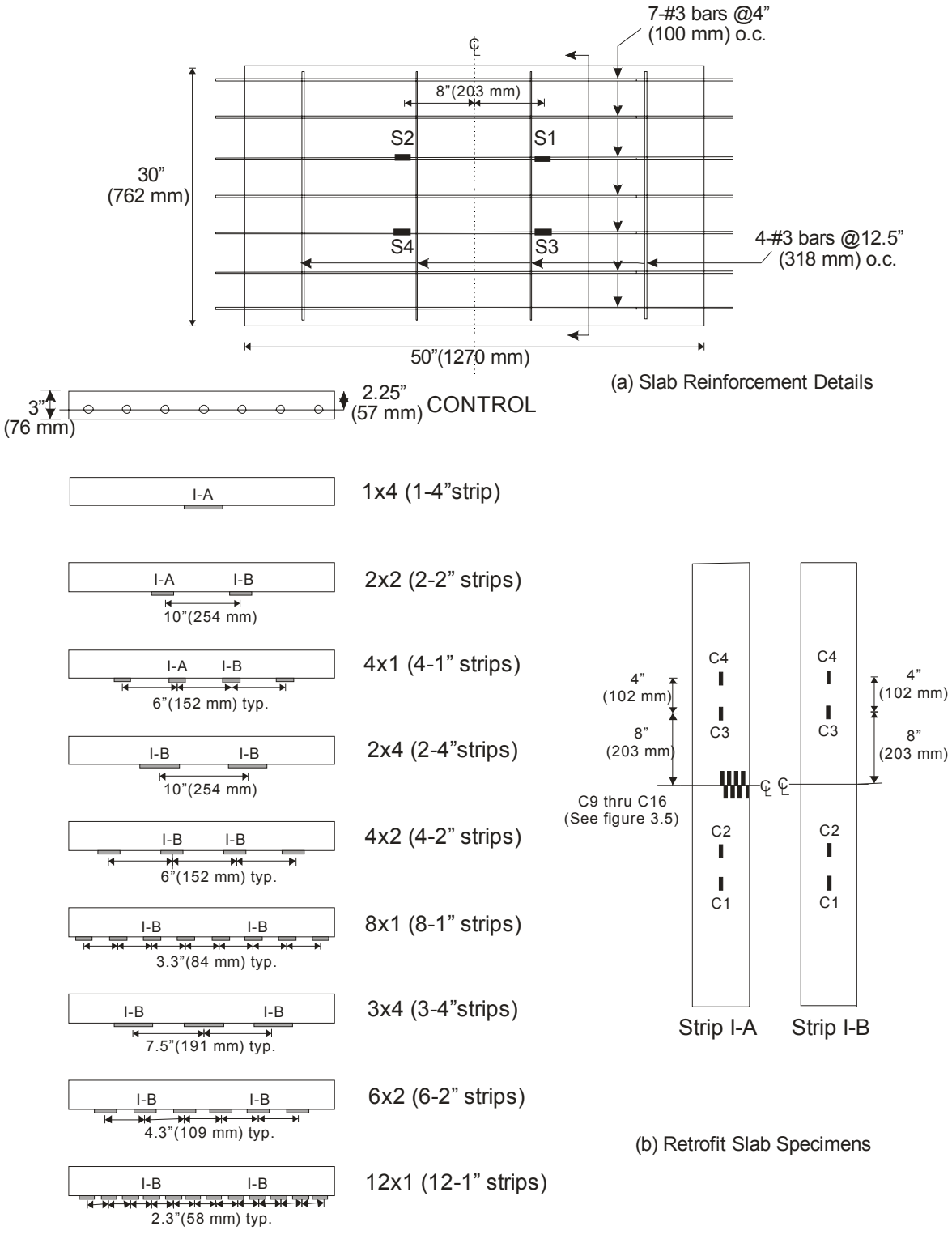

Figure 3-1 Details of slab reinforcement and retrofitted slab specimens.

(a) Typical Formwork

(b) Slab forms prior to casting

(c) Specimen 2x2

(d) Specimen 2x4

(e) Specimen 4x2

Figure 3-2 Typical retrofitted slab specimen and formwork.

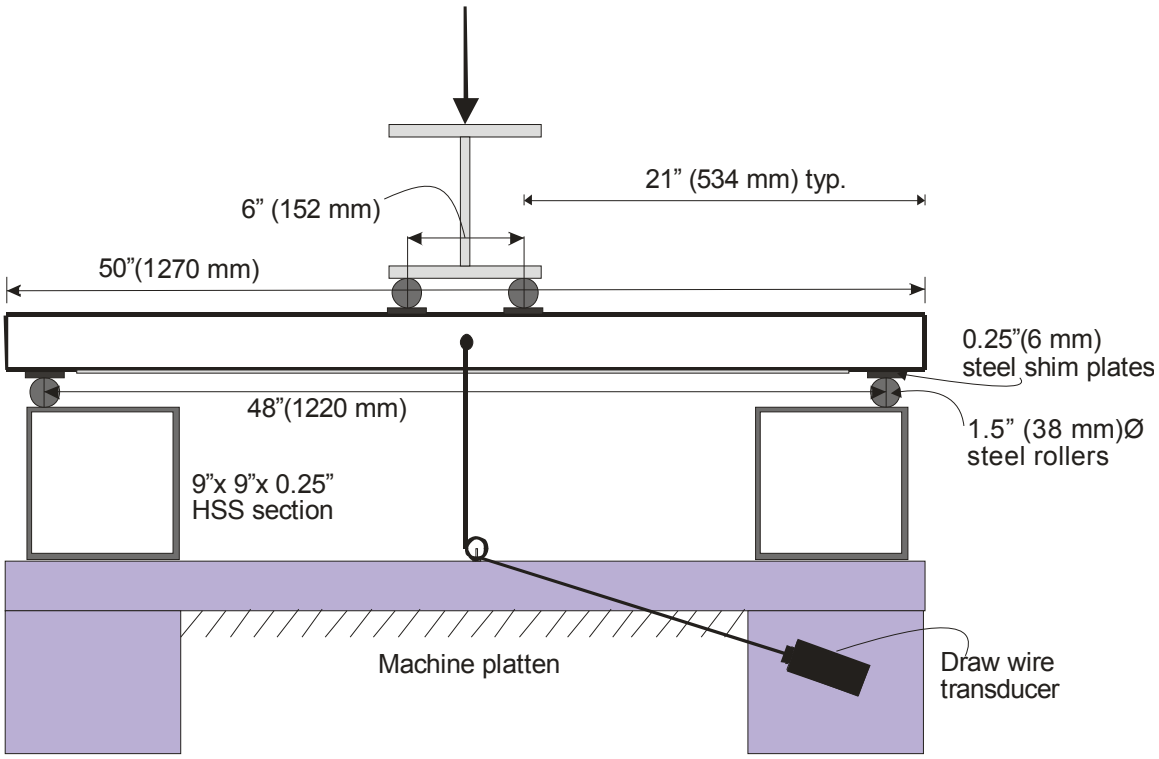

(a) Schematic of the test set up

(b) Photograph of the test set-up

Figure 3-3 Laboratory test set-up.

(a) Draw wire transducer details

(b) Details of the support

(c) Details of the loading arrangement

Figure 3-4 Details of the test set-up.

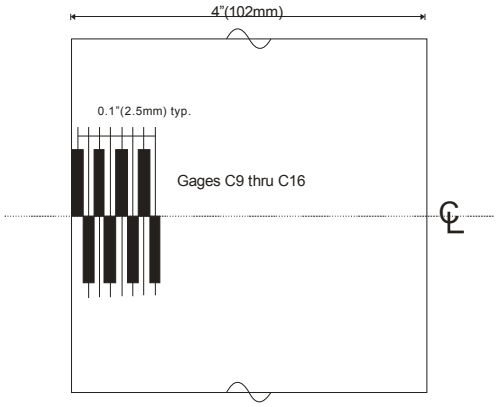

(a) Transverse Gage details on 4"(102mm) strip

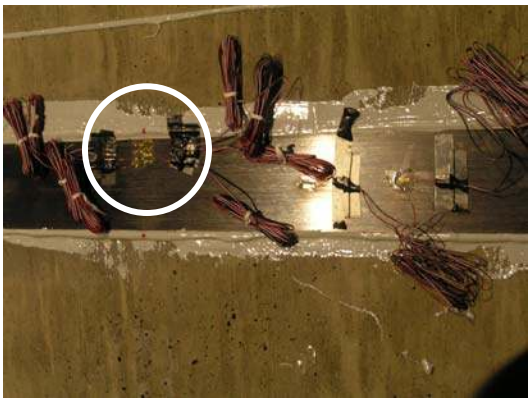

(b) Strain gages instrumented along the centerline of 4 in. (102 mm) wide CFRP strip of test specimen 2x2.

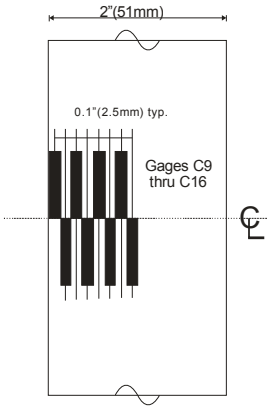

(c) Transverse Gage details on 2" (51 mm) strip

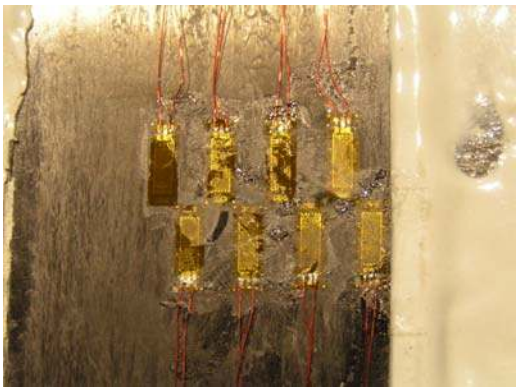

(d) Strain gages instrumented along the centerline of 2 in. (51 mm) wide CFRP strip of test specimen 2x2.

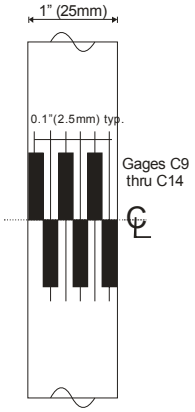

(e) Transverse Gage details on 1" (25 mm) strip

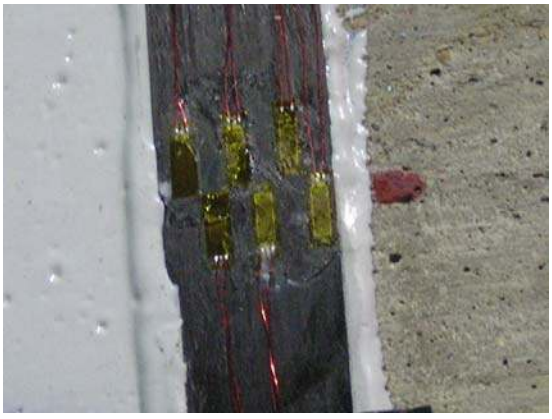

(f) Strain gages instrumented along the centerline of 1 in. (25 mm) wide CFRP strip of test specimen 2x2.

Figure 3-5 Transverse Gage details on CFRP strips.

4.0 TEST RESULTS AND TYPICAL SPECIMEN BEHAVIOR

This chapter presents the results of the experimental test program and a discussion of the behavior of each test specimen.

4.1 TEST RESULTS

Figure 4-1 thru Figure 4-10 show the applied load vs. mid span deflection curves for each of the test specimens that include nine retrofitted one way slab specimens and the control (unretrofit) specimen (Figure 4-1). The applied load vs. strain curves for all strain gages are shown in Figure 4-11 thru Figure 4-19. In all cases, the applied load is the total load applied to both load points, thus the shear in the slab (or support reaction) is one half this value. Strain curves are plotted for the coincidental reinforcing bar and CFRP gages at locations 8" (203 mm) from the midspan, the CFRP gages at all other locations i.e., at 12" (305 mm) from the midspan and the additional gages arranged transversely across the CFRP strip at the midspan. In these graphs, the strains are offset horizontally for clarity; the offset values are indicated in each case. Figure 4-20 thru Figure 4-22 show the strain vs. test time plots only for the coincidental rebar and CFRP gages; these curves help to identify debonding at the gage location where the test time is correlated with applied load. Figure 4-23 thru Figure 4-31 show the strain vs. test time plot for all the gages in all the retrofitted test specimens.

Figure 4-32 shows the transverse strain gradient in Specimens 1x4, 2x2 and 4x1. Figure 4-33 shows the longitudinal strain gradient in all retrofitted test specimens. Figure 4-34 thru Figure 4-37 are photographs obtained from the experiments. Results are discussed further in the following sections.

For all slabs, applied load is given in terms of the total load applied to the specimen over both load lines. Thus the maximum moment in the constant moment region due to the applied load, P, is:

$$M = (P/2)(21) \text{ (lb-in) or } M = (P/2)(0.533) \text{ (N-m)} \quad 4.1$$

The maximum shear (and support reaction) is:

$$V = P/2 \quad 4.2$$

The approximately 375 lb (1.67 kN) self weight of the slab is neglected in these calculations and all subsequent discussion.

A summary of the key results from each specimen are presented in Table 4-1 and Table 4-2. The details of individual specimen behavior are also presented in Table 4-3 thru Table 4-12. The following are the description for the data presented in each of these tables:

Σb_f/slab width: ratio of total width of CFRP used to slab width (30 in. (762 mm)).

b_f/s: ratio of individual CFRP strip width to spacing used on specimen.

Cracking load: applied load and corresponding midspan displacement at the first concrete crack. Cracking is determined by changes in stiffness in the load-displacement and load-reinforcing bar strain curves.

Maximum load: applied load and midspan displacement corresponding to the maximum applied load resisted by the specimen.

Ultimate load: applied load and midspan displacement corresponding to the eventual failure of the specimen. Ultimate load is defined as the greater of: the load corresponding to failure of the specimen, or the load at which the load carrying capacity falls below 80% of the maximum load obtained.

Maximum CFRP strain: CFRP and coincident reinforcing bar strain corresponding to the greatest observed CFRP strain for each specimen. This condition typically occurs following the maximum load being attained.

Initiation of debonding: CFRP and coincident reinforcing bar strain corresponding to CFRP debonding for each specimen. The CFRP strain at which debonding apparently initiates are determined by comparing strain time histories (see Figure 4-20, Figure 4-21 and Figure 4-22) of the CFRP strips and coincident reinforcing bars. Additional knowledge of the debonding mechanism is also assumed: Intermediate crack-induced debonding is hypothesized to initiate at a crack location having a large moment-to-shear ratio (but still in the shear span, nonetheless). Thus debonding will occur near a point of applied load but outside of the constant moment region. Debonding, once initiated, propagates in the direction of decreasing moment (toward the support). Thus, as the debonding propagates past the point of the outermost CFRP gages, C1, C4, C5 or C8, the strains in these gages should decrease relative to their corresponding reinforcing bar gages, S1, S2, S3 or S4. This decrease is due to the loss of shear transfer along the newly debonded CFRP-concrete interface as the incremental stress once transferred by bond is locally redistributed to the reinforcing steel. Observations of slab behavior and eventual complete debonding are used to verify the location of debonding identified by the strain data. For some specimens, videos were obtained illustrating the initiation and propagation of debonding as described above.

As an illustrative example, in Figure 4-20, showing specimen 1x4, CFRP strain gage C3 and its corresponding reinforcing bar strain gage S2 can be seen tracking each other through most of the test; both plots increase proportionally with increased loads/deflections (as represented by the test time). This behavior indicates that plane sections are remaining plane and thus bond is sound at this location; that is, there is no slip along the bond line. The behavior is also marked, as one would expect, by the CFRP strains being higher than those in the reinforcing steel which is much closer to the neutral axis of the section in this case. CFRP strain gage C3 and its corresponding reinforcing bar strain gage S4 can also be seen tracking each other until about 350 seconds when the two plots begin to diverge from each other. The rates of change of the strains in the reinforcing bar and CFRP are now independent of each other, indicating that plane sections are no longer plane and that the CFRP is likely slipping and/or debonding has initiated at a location away from this gage. In the latter case, the stress (and therefore strain) gradient in the CFRP will increase if the debonding is within a distance equal to the effective bond length (Teng et al 2003) of the debonding location – this is analogous to the development for reinforcing bars adjacent a crack. The CFRP strain value for the apparent initiation of debonding is reported as debonding passes CFRP strain gage C3 at about 800 seconds (when the CFRP strain drops markedly) and the two plots (of strain gages C3 and S2 and also C3 and S4) begin to cross over each other as the reinforcing steel attracts greater stress following debonding. From this stage onward, CFRP gauge C3 tracks with the adjacent CFRP gages C1, C2 and C4 (although these gages are not shown in this plot). This identical behavior of the gages can be clearly seen in Figure 4-23 wherein all the CFRP gages behave in a similar manner. Debonding has occurred at each location and thus the CFRP stress should be relatively uniform between these locations. It is noted that although debonding has occurred, some stress transfer may still

be affected through friction and aggregate interlock along the failure plane, explaining the minor differences between the adjacent debonded gages. This sequence of events is seen in each of Figure 4-23 thru Figure 4-31.

4.2 SPECIMEN BEHAVIOR

Initial cracking of the concrete was observed at an applied load ranging from 250 to 2460 pounds (1.11 to 10.94 kN) (Table 4-1). This variability is consistent with the high variability of concrete cracking behavior. The anticipated cracking moment for the slab specimens, based on modulus of rupture of $6\sqrt{f_c'}$ ($0.5\sqrt{f_c'}$ in SI units) is 18,800 lb-in (2124 N-m) corresponding to an applied load P = 1580 pounds (7.04 kN). All specimens behaved in an essentially linear manner having a flexural stiffness proportional to the amount of CFRP provided up to the initial yield of steel. As the specimens yielded, a softening of the flexural stiffness was observed. The post yield flexural stiffness of the system is proportional to the amount of CFRP provided. During the post yield response, the propagation of debonding was evident as "popping" noises and occasional "wisps of concrete dust" emanating from the CFRP/concrete interface region in case of the specimens 1x4, 2x2 and 4x1. The following sections summarize the typical behavior exhibited by different specimens during the testing program. Behavior was characterized as flexure-dominated or shear dominated depending on the equivalent flexural reinforcing ratio provided by the additional CFRP. The equivalent flexural reinforcement ratio is defined as follows:

$$\rho_{equivalent} = \frac{A_s}{bh} + \frac{A_f}{bh}\frac{E_f}{E_s} \qquad 4.3$$

where, bh = gross area of concrete section, equal to 90 in^2 (58,000 mm^2) in this study

A_f = cross sectional area of CFRP; $A_f = t_f b_f$ (Table 3-2)

A_s = cross sectional area of existing internal tension steel reinforcement, equal to 0.77 in^2 (500 mm^2) in this study.

E_f = modulus of CFRP, taken as 22500 ksi (155 GPa) (Table 3-2)

E_s = modulus of steel reinforcement, taken as 29000 ksi (200 GPa)

For all specimens in this study, the first term in Equation 4.3, (A_s/bh) is equal to 0.86%.

4.2.1 Control Specimen

The control specimen was dominated by flexural behavior in the constant moment region. The reinforcing steel is assumed to yield based on the near- and greater-than-yield values reported for gages S2 and S4 in the shear span. The specimen eventually failed having sustained a peak load of 9000 lb (40 kN) and a deflection of 0.58 in. (14.7 mm). Failure was characterized by compression failure of the concrete in the constant moment region which should be expected for a section having a short effective depth.

4.2.2 Test Specimens 1x4, 2x2 and 4x1

Specimens 1x4, 2x2 and 4x1 had the least increase in equivalent flexural reinforcement, 0.19%, resulting in an equivalent flexural reinforcement ratio, $\rho_{equivalent}$ = 1.05%. These specimens were dominated by flexural behavior as their ratio of shear capacity to retrofit flexural capacity remained below unity. Intermediate crack induced interfacial debonding failures characterized the behavior of test specimens 1x4, 2x2 and 4x1. In each of these retrofit slab

specimens; failure was relatively brittle and was characterized by a rapid complete CFRP debonding initiating beneath a point load and progressing toward one of the supports (Figure 4-35). A thin layer of concrete remained attached to the strips indicating that failure occurred in the concrete, adjacent to adhesive-to-concrete interface (Figure 4-36). The mechanism of this type of failure can be summarized as follows. When a flexure or flexure-shear crack is formed in the concrete, the tensile stresses released by the cracked concrete are transferred to the CFRP strips. As a result, high local interfacial Mode-II (shear) stresses between the CFRP strips and the concrete are induced adjacent to crack. At a flexure-shear crack in the shear span, additional Mode I (peeling) stresses are developed at the crack opening (tensile on the side of the crack having "lower moment" and compressive on the other side). As discussed in the literature review, the toughness of the Mode II-resisting behavior is significantly diminished in the presence of even a small amount of Mode I tension-directed stress. As the applied loading increases, the tensile stresses in the CFRP strip and the interfacial Mode-I and II stresses between the CFRP strip and the concrete near the crack also increase. When these stresses reach critical values, debonding initiates at the crack and propagates in the direction of decreasing moment gradient i.e.: towards the nearest support (Figure 4-35).

4.2.3 Test Specimens 2x4, 4x2, 8x1, 3x4, 6x2 and 12x1

Specimens 2x4, 4x2 and 8x1 had equivalent flexural reinforcement ratios, $\rho_{equivalent}$ = 1.24% while specimens 3x4, 6x2 and 12x1 had $\rho_{equivalent}$ = 1.43%. These ratios represent 44% and 66% increases in equivalent flexural reinforcing, respectively. The increased flexural reinforcement increased the flexural capacity of the slabs without affecting the shear capacity. In these cases, the shear capacity provided was insufficient to develop the full flexural capacity of

the retrofitted slabs. The nominal capacity of the slabs based on the ACI 318 (2005) prescribed concrete shear strength of $2\sqrt{f_c'}$ ($0.17\sqrt{f_c'}$ in SI units) is 17,233 lbs (76.6 kN). Based on observed behavior (Table 4-1), it would appear that the average shear capacity of the slabs in this study was approximately 21,900 lbs (97.4 kN), corresponding to a shear stress of $2.5\sqrt{f_c'}$ ($0.21\sqrt{f_c'}$). This latter value falls between the conventionally accepted (ACI 318 2005 and ACI 445 1999) lower and upper bounds for nominal shear capacity of a member having no shear reinforcement: $2\sqrt{f_c'}$ and $3.5\sqrt{f_c'}$ respectively.

As a result of the increased flexural capacity, shear failure characterized the ultimate behavior of these specimens. The failure was extremely brittle and occurred at the slab ends emanating from the supports (Figure 4-37). This behavior highlights the need to consider all limit states in a strengthening project rather than simply the limit states for which the strengthening is intended.

While it was understood that shear failures were likely, the ultimate behavior of the slabs is not at issue in the present study. Rather the effect of the b_f/s ratio on bond performance is the focus of the work. As indicated by the data presented in this chapter and the discussions in the subsequent chapter, assessment of bond performance is easily made and compared for load levels up to that which shear became dominant. It should be noted that increasing the shear capacity of a slab, rather than a beam, is difficult in practice. Thus existing shear capacity places a *de facto* limit on flexural strengthening of slab elements.

4.3 TRANSVERSE STRAIN GRADIENT

Figure 4-32 shows the transverse strain data obtained laterally across the CFRP strips for the test specimens 1x4, 2x2 and 4x1. The strain gage arrangement in the lateral (transverse) direction for each of these test specimens is shown in Figure 3-1 and Figure 3-5. Figure 4-32 shows that the strain distribution is essentially uniform across the width of the strips, although a small increase is evident near the edges (gage 1, in each case). An increase near the edges is expected due to shear lag effects (Section 2.6.1), however the extent of the observed increase is modest and less than may be expected. It is supposed that the first gage was not located close enough to the edge of the CFRP strip to capture this effect clearly. As seen in Figure 3-5, gage 1 was centered slightly more than 0.1 in. (2.5 mm) from the edge. Additionally, the gages used have a gage width of 0.062 in. (1.6 mm); thus strains are effectively averaged over this dimension. It is believed that the resulting gage setup geometry is unable to capture the highly localized shear lag effect.

Table 4-1 Summary of key results.

Specimen			Control	1x4	2x2	4x1	2x4	4x2	8x1	3x4	6x2	12x1
Concrete age at testing[1]		days	73	75	89	90	80	82	83	87	86	88
□b_f/slab width				0.13	0.13	0.13	0.27	0.27	0.27	0.40	0.40	0.40
b_f/s			--	0.13	0.20	0.17	0.40	0.33	0.30	0.53	0.46	0.44
First Cracking	Load	kip	0.25	0.35	2.46	0.52	0.47	1.92	1.45	0.89	1.18	1.50
	Deflection	in	0.001	0.01	0.026	0.001	0.001	0.01	0.001	0.001	0.006	0.036
Maximum Load	Load	kip	9.00	13.6	14.9	16.8	17.65	23.1	22.2	20.6	22.2	21.4
	Deflection	in	0.67	0.45	0.55	0.68	0.48	0.55	0.55	0.45	0.39	0.48
	Strain in CFRP	με	n.a.	3046	3944	4242	2899	4331	3624	2571	2649	2774
	Rebar strain	με	2178	1572	1905	2035	1374	1996	1995	1293	1265	1269
Ultimate Load	Load	kip	7.91	9.48	11.98	13.59	14.12	18.46	17.74	16.51	17.78	17.10
	Deflection	in	0.97	0.63	0.64	0.71	0.78	0.58	0.73	0.65	0.79	0.54
at Maximum CFRP Strain	Strain in CFRP	με	n.a.	3523	4366	4635	2899	4331	3624	2571	2649	2774
	Corresponding Rebar strain	με	n.a.	13568	5169	2676	1438	1996	1995	1296	1265	1269
at Initiation of Debonding[3]	Strain in CFRP	με	n.a.	2057	3331	4629	≥ 2899	≥ 4331	≥ 3624	≥ 2571	≥ 2649	≥ 2774
	Corresponding Rebar strain	με	n.a.	1445	2043	1846	≥ 1438	≥ 1996	≥ 1995	≥ 1296	≥ 1265	≥ 1269

[1] FRP was applied to specimens at a concrete age of 55 days.
[2] The reinforcing bars in the specimen have not yielded.
[3] Specimens not exhibiting debonding are reported as having debonding strains greater than the maximum observed

Table 4-2 Strains recorded in each gage corresponding to the maximum load in each specimen.

Specimen	Maximum Load (lbs)	S1	S2	S3	S4	C1	C2	C3	C4	C5	C6	C7	C8
Control	9023	2092	2154	1862	2603	n.a.	n.a.	n.a.	n.a.	n.a.	n.a.	n.a.	n.a.
1x4	13569	n.a.	1665	n.a.	1478	2850	2885	3046	2157	3523	3429	3428	3439
2x2	14900	1397	326	1622	1905	2648	3336	3589	2760	2819	3538	3944	3177
4x1	16788	1950	2035	2103	--	3781	4227	4242	2866	3097	4513	4001	3009
2x4	17654	n.a.	1438	1247	1374	1912	2659	2538	2086	2155	2731	2899	2221
4x2	23080	n.a.	1996	1729	1697	2709	4331	3393	2556	3021	3576	3471	2964
8x1	22171	1995	1518	1985	1705	2508	3482	3251	2327	2405	3624	3382	2603
3x4	20634	1293	1151	1296	1126	2130	2571	n.a.	1825	n.a.	n.a.	n.a.	1911
6x2	22230	1166	1051	1265	1219	2168	2560	2375	1738	1915	2548	2649	1802
12x1	21242	1269	1094	1223	n.a.	1651	2211	2774	2237	1684	2514	2462	2025

n.a.: gage not present in the specimen
--: gage failed to provide reliable data

Table 4-3 Strains in reinforcing bar gages in Control specimen.

Load (lbs)	S1	S2	S3	S4	Comments on failure
2000	459	621	606	702	The failure was a compression failure of concrete in the constant moment region.
4000	849	1032	962	1160	
6000	1221	1393	1330	1639	
8000	1684	1838	1634	2281	

Table 4-4 Strains in coincidental gages on the rebar and CFRP strips in test specimen 1x4.

Load (lbs)	C2	S2	C3	S4	Comments on failure
2000	226	129	311	143	Intermediate crack induced debonding was observed initiating at a point of applied load. Some evidence of end peel was also observed.
4000	685	419	807	398	
6000	1174	537	1281	603	
8000	1633	732	1748	789	
10000	2082	1002	2126	931	
12000	2562	1364	2591	1161	

Table 4-5 Strains in coincidental gages on the rebar and CFRP strips in test specimen 2x2.

Load (lbs)	S1	C2	S2	C3	S3	C6	S4	C7	Comments on failure
2000	44	147	72	204	39	128	74	221	Intermediate crack induced debonding was observed initiating at a point of applied load. Some evidence of end peel was also observed. The strip on the south western side debonded first followed by the other strip.
4000	279	729	368	902	342	727	408	941	
6000	496	1233	562	1448	586	1236	665	1528	
8000	737	1729	851	1948	833	1750	962	2087	
10000	953	2186	1058	2357	1035	2255	1210	2580	
12000	1159	2625	1149	2783	1240	2757	1437	3085	
14000	1336	3081	947	3298	1484	3307	1654	3633	

Table 4-6 Strains in coincidental gages on the rebar and CFRP strips in test specimen 4x1.

Load (lbs)	S1	C2	S2	C3	S3	C6	S4	C7	Comments on failure
2000	50	208	55	162	73	266	16	153	Intermediate crack induced debonding was observed initiating at a point of applied load. Some evidence of end peel was also observed. The third strip from the eastern end debonded first flowed by the second, first and fourth strips respectively.
4000	289	851	280	798	328	860	317	702	
6000	506	1361	561	1355	543	1332	557	1206	
8000	701	1835	816	1851	760	1814	778	1682	
10000	924	2335	1088	2289	999	2294	974	2196	
12000	1116	2731	1364	2721	1204	2765	1180	2648	
14000	1325	3259	1640	3304	1426	3151	1394	3128	
16000	1624	4215	1912	3970	1704	3752	1733	3686	

Table 4-7 Strains in coincidental gages on the rebar and CFRP strips in test specimen 2x4.

Load (lbs)	S2	C3	S3	C6	S4	C7	Comments on failure
2000	44	118	33	123	48	138	The specimen failed in shear. A shear cracked developed on the southern side of the slab.
4000	286	464	137	414	223	468	
6000	479	804	294	747	418	840	
8000	650	1112	436	1061	589	1216	
10000	822	1425	580	1380	749	1574	
12000	984	1728	717	1695	904	1917	
14000	1147	2035	878	2066	1067	2265	
16000	1306	2315	1069	2429	1241	2611	

Table 4-8 Strains in coincidental gages on the rebar and CFRP strips in test specimen 4x2.

Load (lbs)	S2	C3	S3	C6	S4	C7	Comments on failure
2000	32	103	40	101	32	119	The specimen failed in shear. A shear cracked developed on the southern side of the slab. Concrete was completely lost at this end both at the top and bottom and reinforcement could be clearly seen.
4000	141	311	181	305	127	352	
6000	345	628	407	656	290	695	
8000	998	547	967	590	1076	468	
10000	726	1380	736	1291	651	1474	
12000	899	1753	879	1624	813	1831	
14000	1074	2083	1024	1965	968	2163	
16000	1252	2288	1158	2319	1119	2496	
18000	1473	2551	1286	2699	1270	2820	
20000	1701	2822	1421	3051	1426	3067	
22000	1892	3159	1604	3402	1600	3241	

Table 4-9 Strains in coincidental gages on the rebar and CFRP strips in test specimen 8x1.

Load (lbs)	S1	C2	S2	C3	S3	C6	S4	C7	Comments on failure
2000	44	86	41	131	39	101	60	143	The specimen failed in shear. A shear cracked developed on the northern side the slab. The crack was first seen on the western face and it then began to propagate towards the eastern face.
4000	282	490	170	448	194	321	256	499	
6000	441	699	329	744	420	581	384	739	
8000	630	971	1148	1055	662	887	533	1032	
10000	815	1254	608	1352	893	1213	686	1320	
12000	976	1543	769	1665	1067	1452	834	1594	
14000	1151	1835	915	1959	1238	1699	990	1879	
16000	1336	2139	1058	2257	1440	2113	1149	2230	
18000	1536	2476	1205	2566	1650	2605	1311	2571	
20000	1747	2928	1346	2874	1824	3159	1478	2921	
22000	1969	3431	1502	3222	1973	3584	1684	3346	

Table 4-10 Strains in coincidental gages on the rebar and CFRP strips in test specimen 3x4.

Load (lbs)	S1	C2	Comments on failure
2000	34	118	The specimen failed in shear. A shear cracked developed on the southern side of the slab. Cracks were visible at the rebar locations on the southern face of the slab. Popping sounds were heard at loads close to 7500 lbs; no indication of their cause was established.
4000	123	337	
6000	285	619	
8000	408	871	
10000	540	1130	
12000	667	1380	
14000	796	1633	
16000	930	1879	
18000	1065	2131	
20000	1216	2423	

Table 4-11 Strains in coincidental gages on the rebar and CFRP strips in test specimen 6x2.

Load (lbs)	S1	C2	S2	C3	S3	C6	S4	C7	Comments on failure
2000	29	102	21	87	33	100	31	100	The specimen failed in shear. A shear cracked developed on the northern side of the slab. Failure was very sudden.
4000	95	274	60	223	105	258	84	244	
6000	185	542	178	445	248	506	205	496	
8000	293	839	298	689	383	770	329	777	
10000	410	1115	404	937	506	1030	458	1035	
12000	537	1393	509	1201	626	1289	581	1267	
14000	654	1646	607	1458	744	1544	705	1499	
16000	768	1881	705	1706	869	1795	831	1741	
18000	888	2088	814	1956	993	2048	956	1997	
20000	1015	2308	923	2203	1117	2295	1073	2291	
22000	1144	2518	1035	2362	1251	2537	1203	2607	

Table 4-12 Strains in coincidental gages on the rebar and CFRP strips in test specimen 12x1.

Load (lbs)	S1	C2	S2	C3	S3	C6	Comments on failure
2000	34	99	36	142	34	101	The specimen failed in shear. A shear cracked developed on the southern side of the slab. Cracks were observed on the north eastern face beginning to propagate at loads close to 5500 lbs. A crack was seen at the central reinforcing bar location on the northern face at loads close to 10,000 lbs.
4000	145	307	224	500	169	372	
6000	309	528	322	738	278	597	
8000	457	764	392	995	400	826	
10000	570	998	485	1247	521	1052	
12000	677	1231	590	1497	648	1302	
14000	773	1456	697	1744	771	1552	
16000	867	1678	806	2028	891	1819	
18000	992	1877	914	2303	1015	2084	
20000	1158	2082	1017	2580	1139	2354	

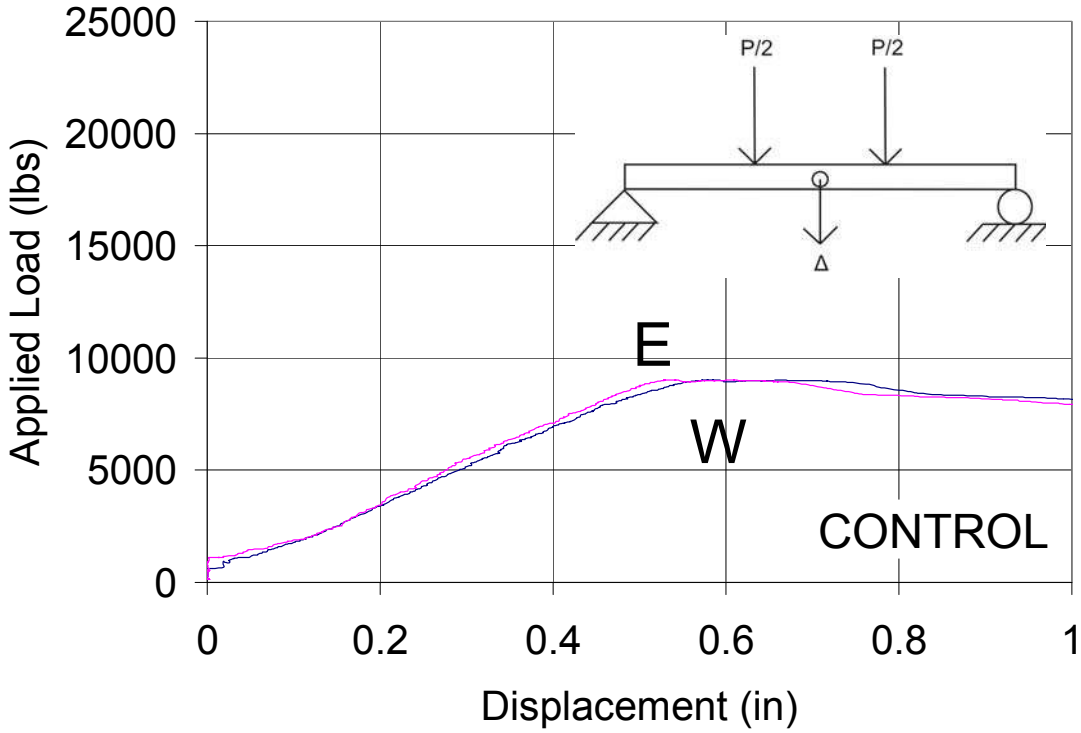

Figure 4-1 Plot of Load vs. Displacement for Control.

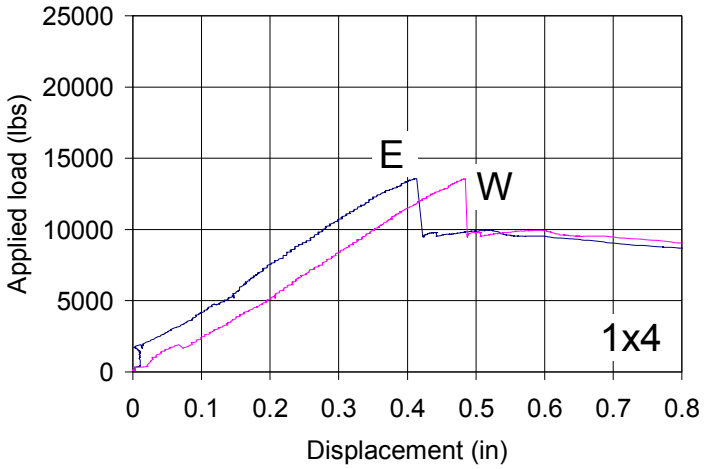

Figure 4-2 Plot of load vs. displacement for specimen 1x4.

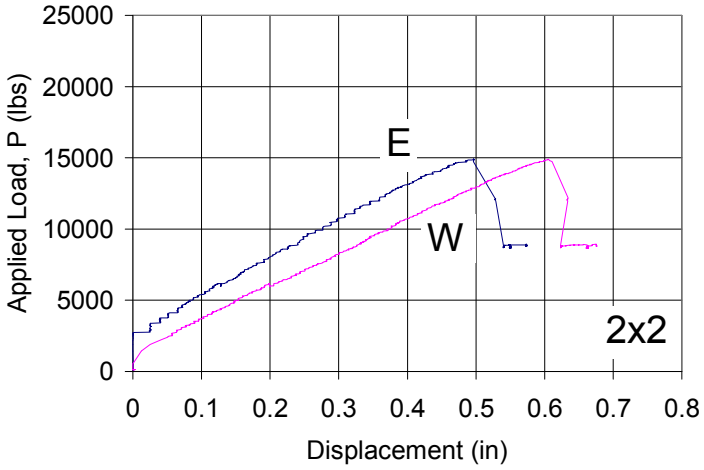

Figure 4-3 Plot of load vs. displacement for specimen 2x2.

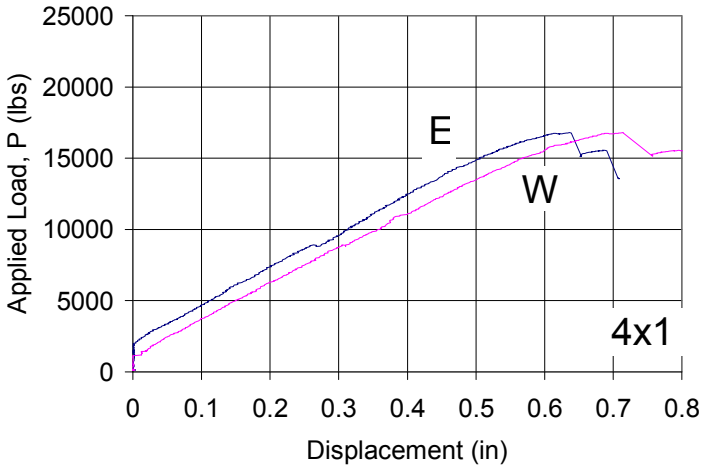

Figure 4-4 Plot of load vs. displacement for specimen 4x1.

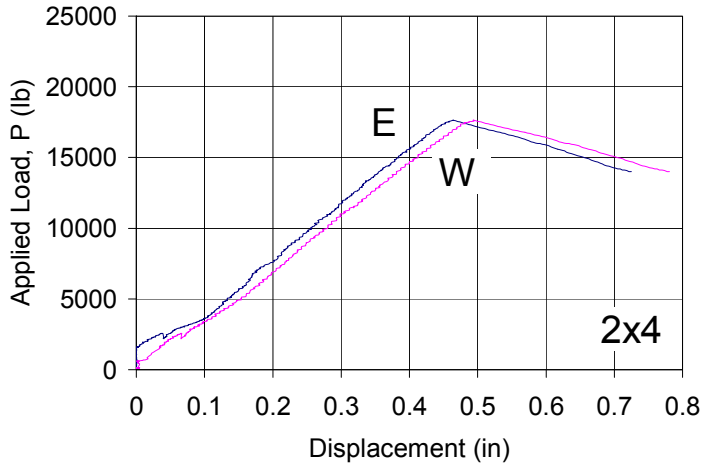

Figure 4-5 Plot of load vs. displacement for specimen 2x4.

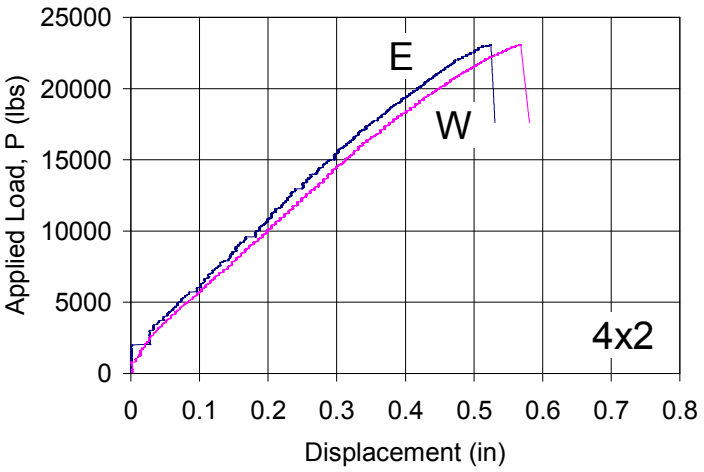

Figure 4-6 Plot of load vs. displacement for specimen 4x2.

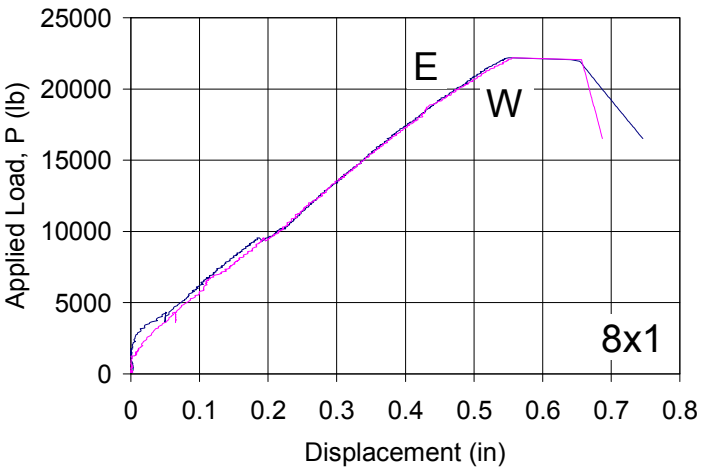

Figure 4-7 Plot of load vs. displacement for specimen 8x1.

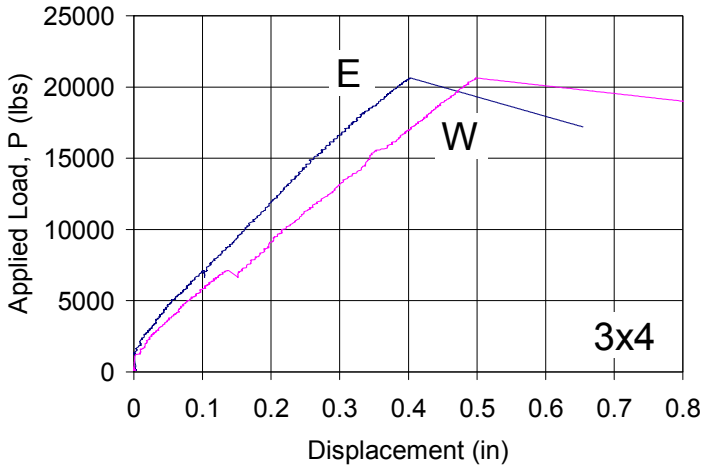

Figure 4-8 Plot of load vs. displacement for specimen 3x4.

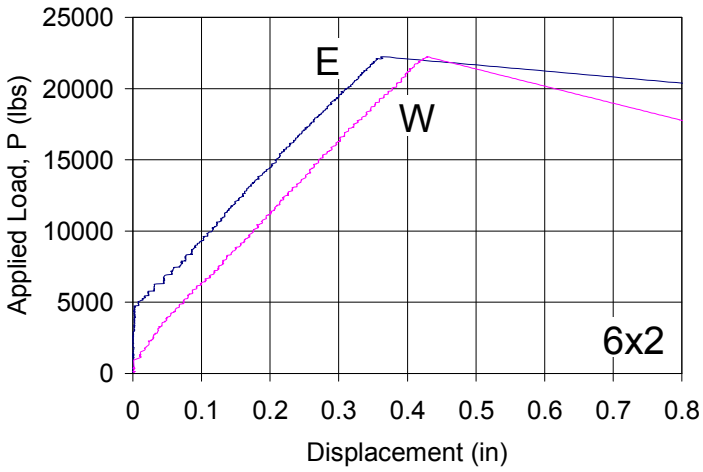

Figure 4-9 Plot of load vs. displacement for specimen 6x2.

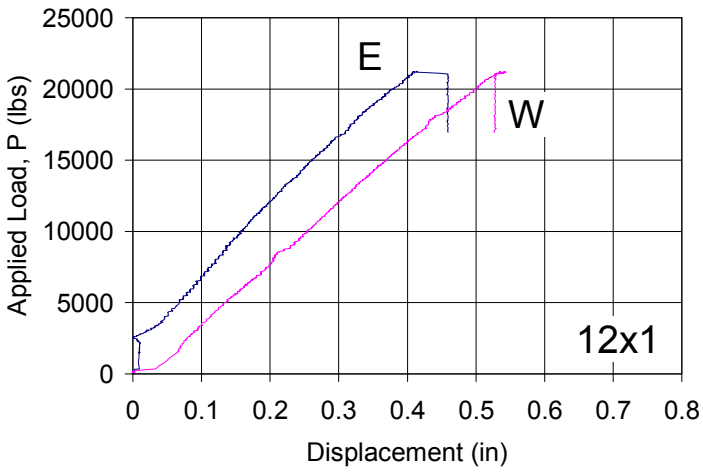

Figure 4-10 Plot of load vs. displacement for specimen 12x1.

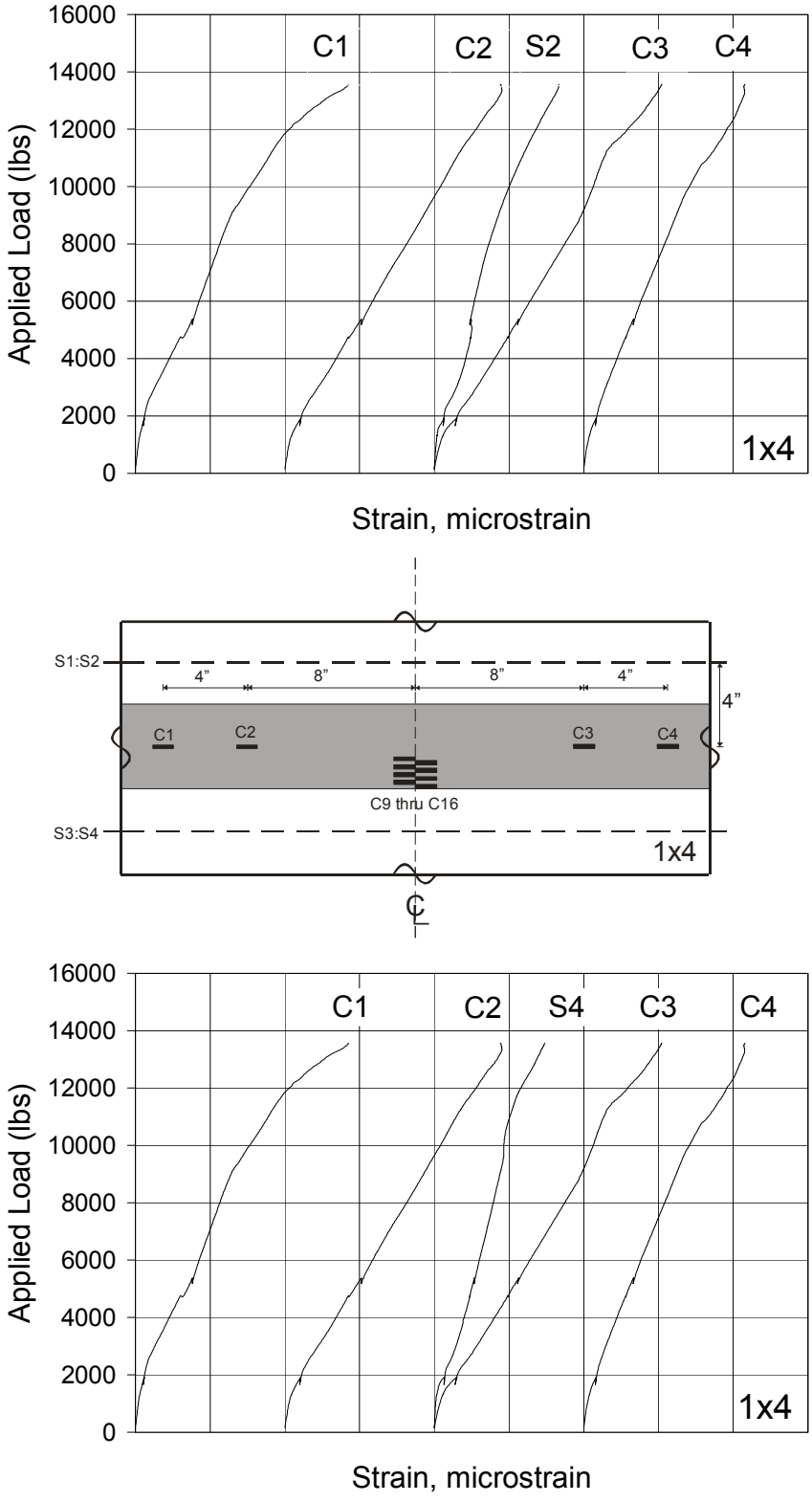

Figure 4-11 Plot of load vs. strain for the specimen 1x4.
Vertical gridlines spaced at 1000 microstrain.
Curves are horizontally offset 2000 microstrain for clarity.

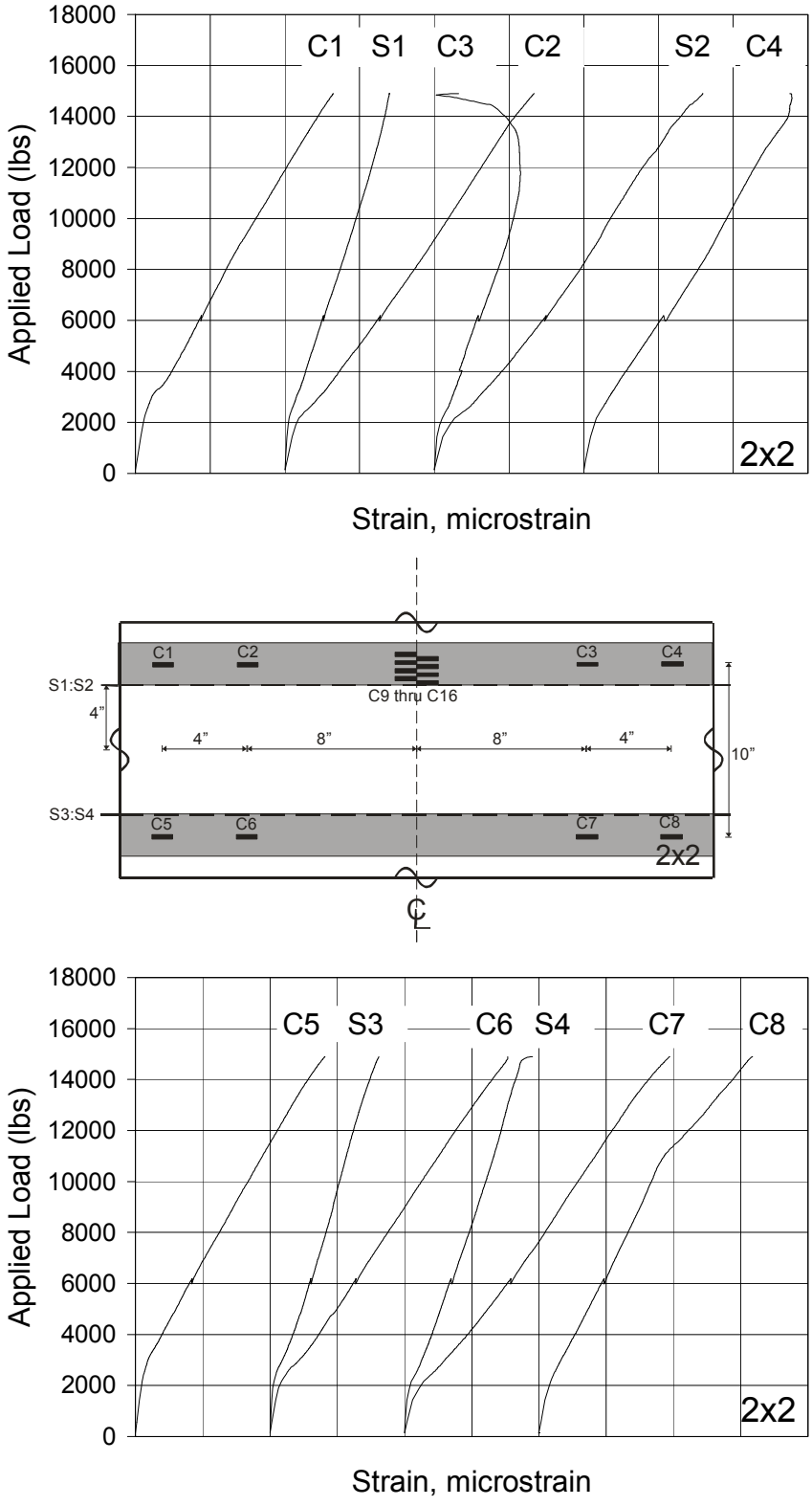

Figure 4-12 Plot of load vs. strain for the specimen 2x2.
Vertical gridlines spaced at 1000 microstrain.
Curves are horizontally offset 2000 microstrain for clarity.

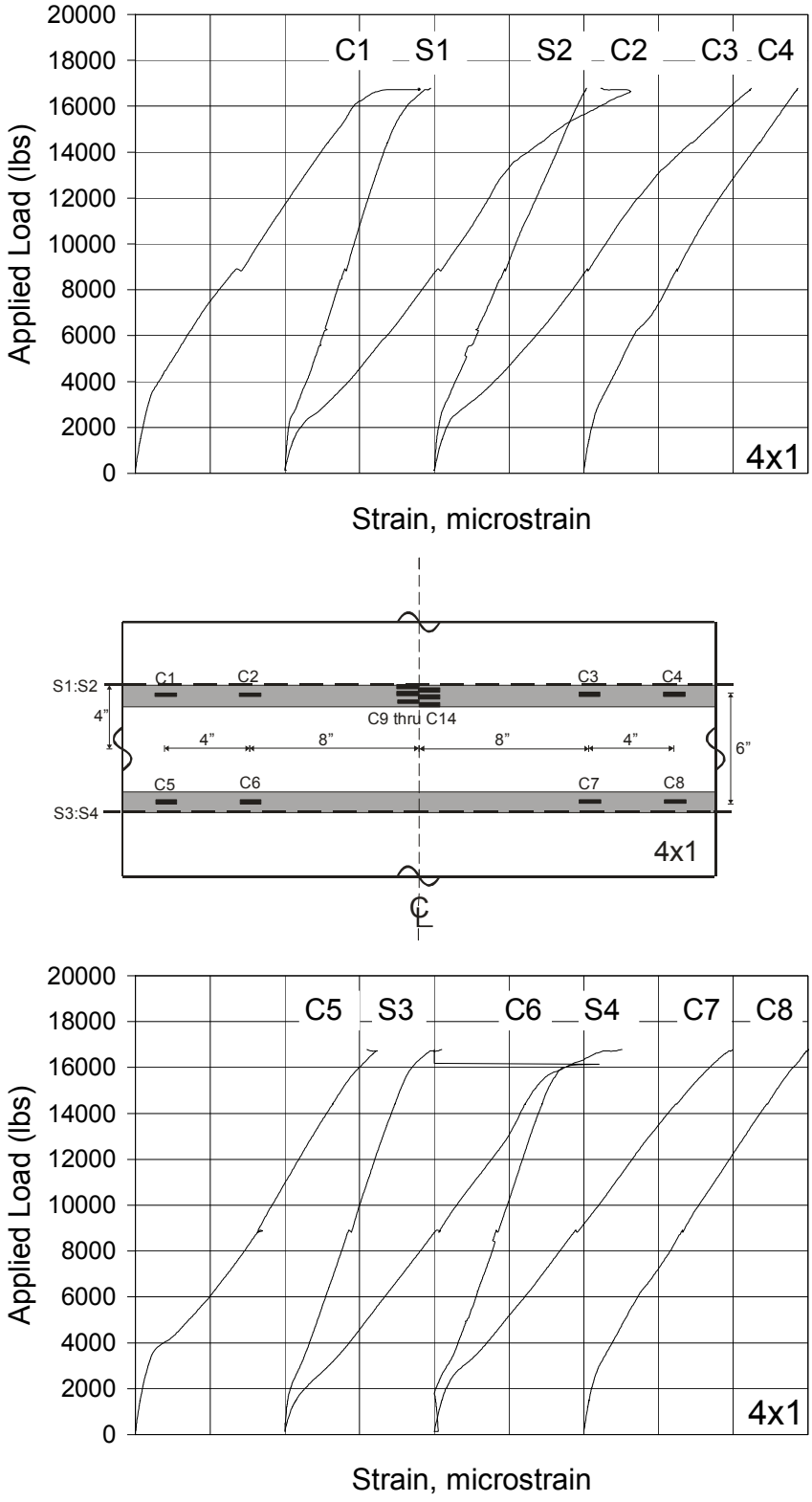

Figure 4-13 Plot of load vs. strain for the specimen 4x1.
Vertical gridlines spaced at 1000 microstrain.
Curves are horizontally offset 2000 microstrain for clarity.

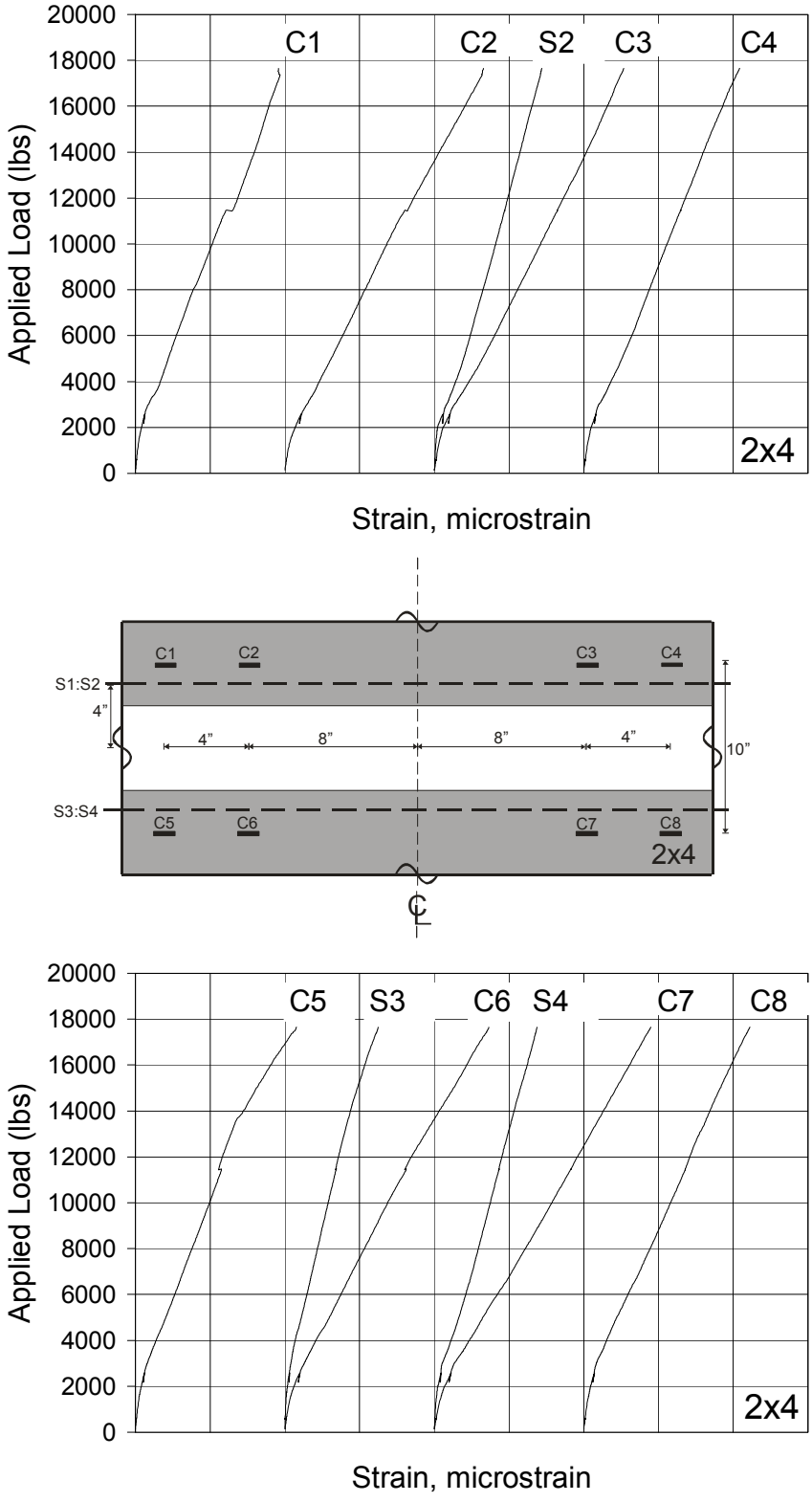

Figure 4-14 Plot of load vs. strain for the specimen 2x4.
Vertical gridlines spaced at 1000 microstrain.
Curves are horizontally offset 2000 microstrain for clarity.

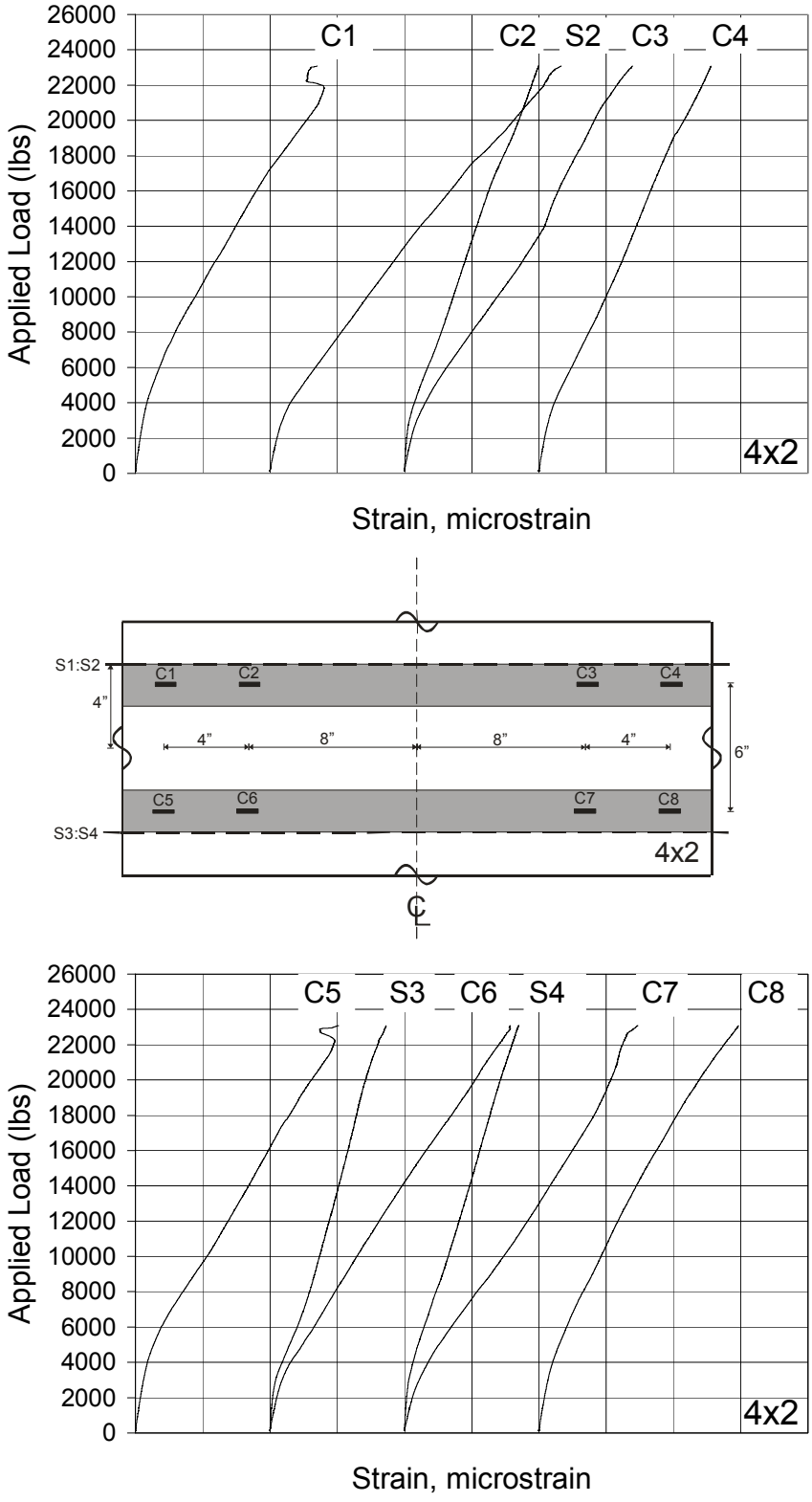

Figure 4-15 Plot of load vs. strain for the specimen 4x2.
Vertical gridlines spaced at 1000 microstrain.
Curves are horizontally offset 2000 microstrain for clarity.

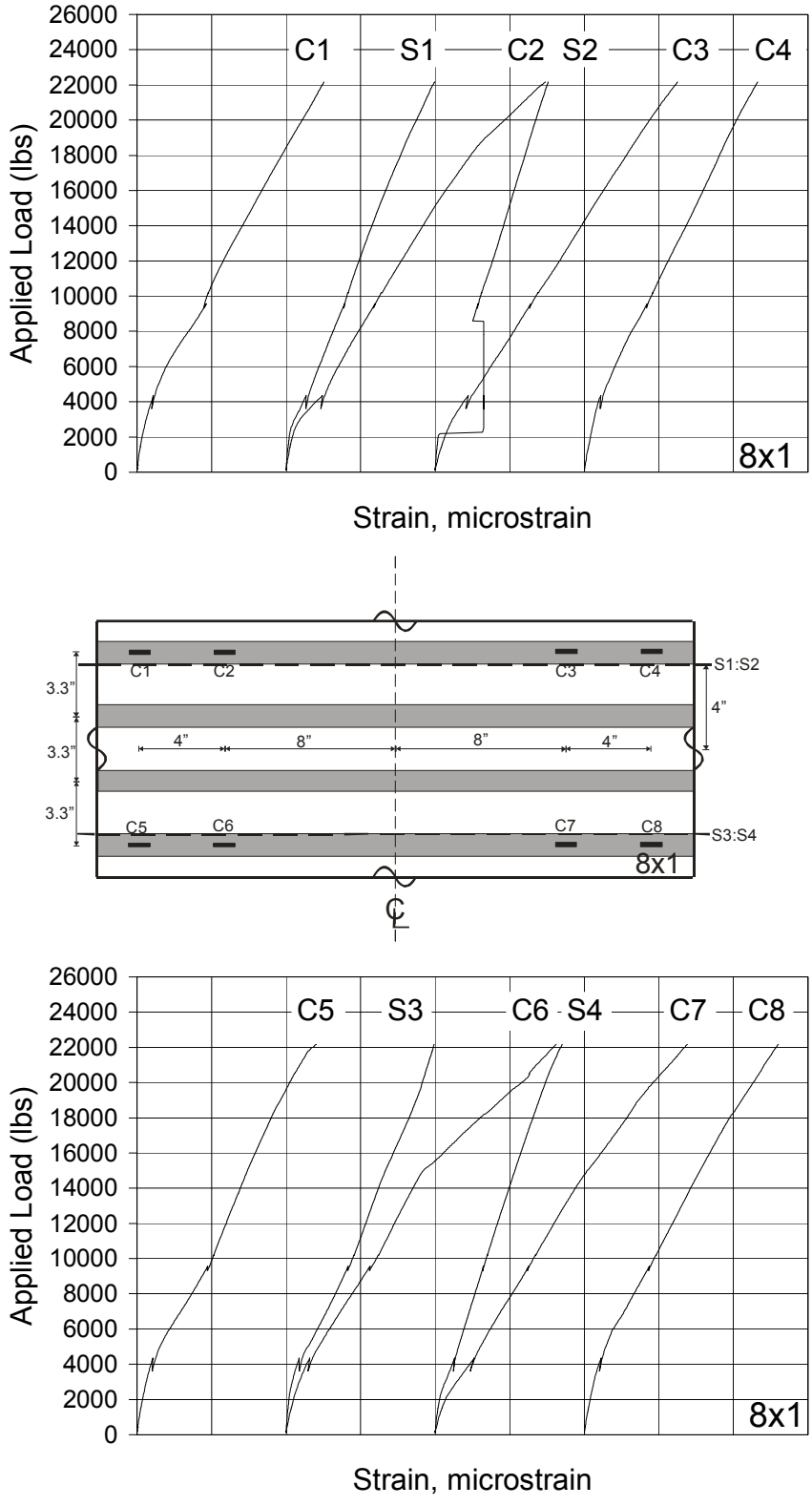

Figure 4-16 Plot of load vs. strain for the specimen 8x1.
Vertical gridlines spaced at 1000 microstrain.
Curves are horizontally offset 2000 microstrain for clarity.

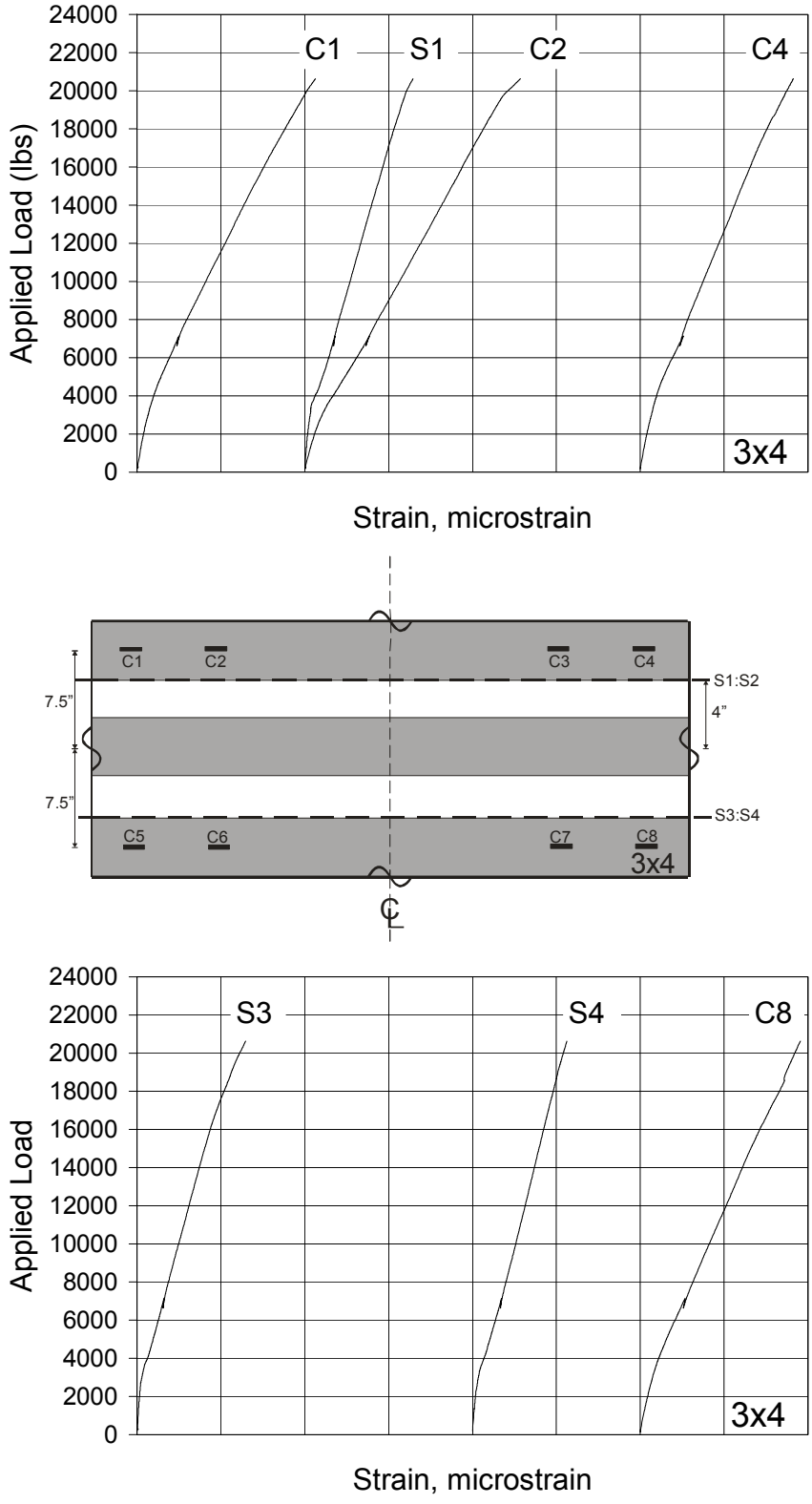

Figure 4-17 Plot of load vs. strain for the specimen 3x4.
Vertical gridlines spaced at 1000 microstrain.
Curves are horizontally offset 2000 microstrain for clarity.

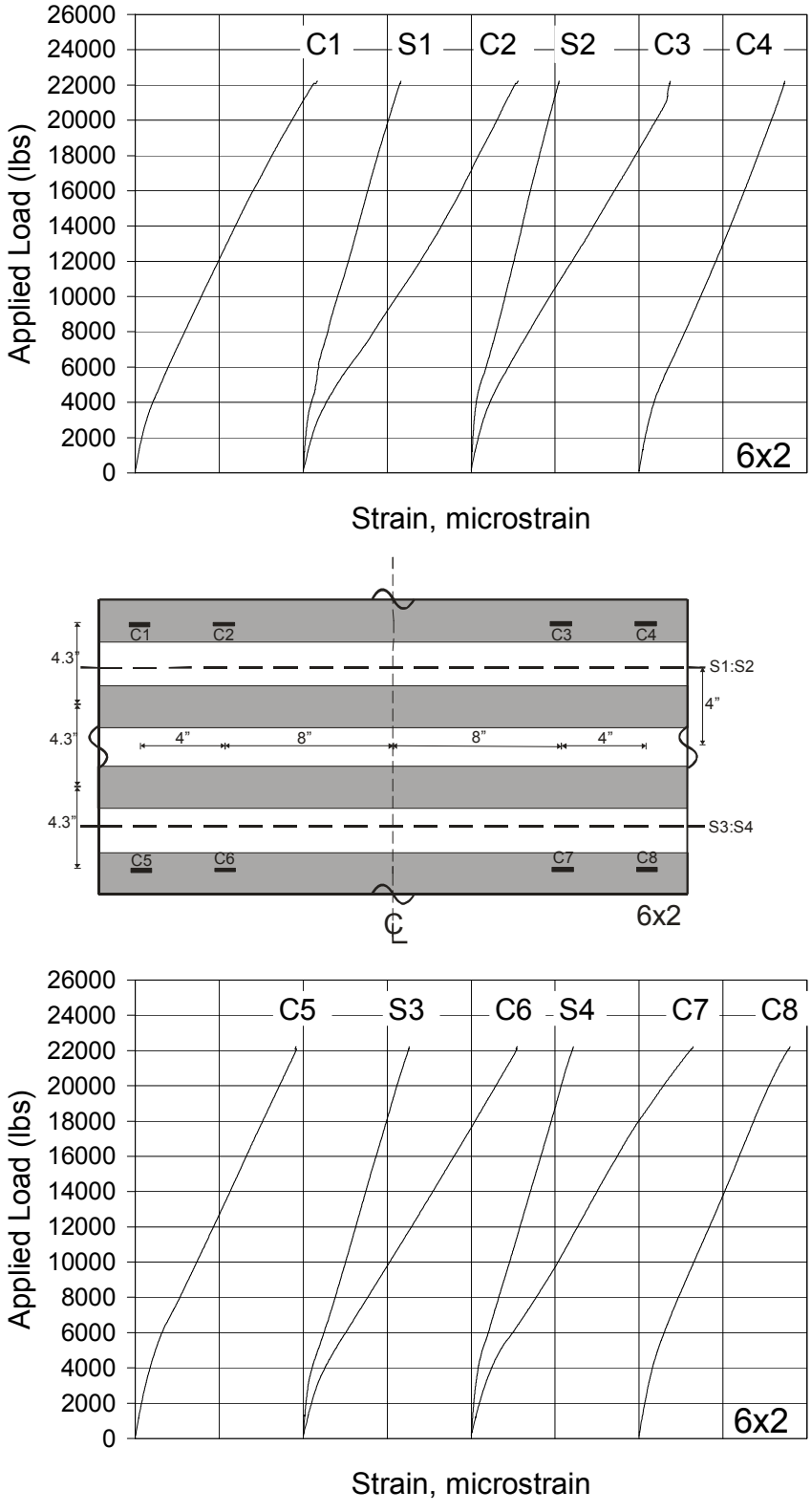

Figure 4-18 Plot of load vs. strain for the specimen 6x2.
Vertical gridlines spaced at 1000 microstrain.
Curves are horizontally offset 2000 microstrain for clarity.

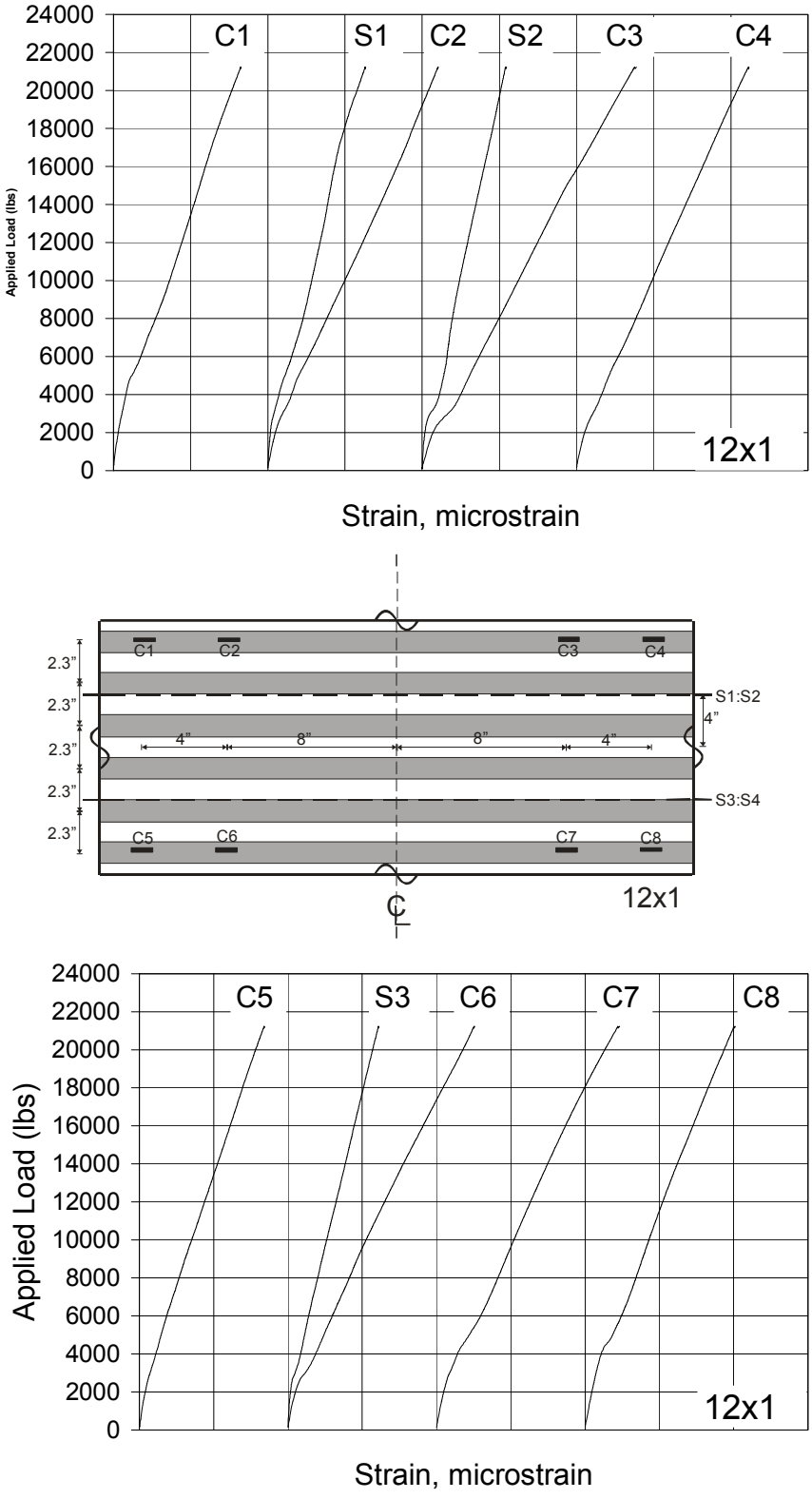

Figure 4-19 Plot of load vs. strain for the specimen 12x1.
Vertical gridlines spaced at 1000 microstrain.
Curves are horizontally offset 2000 microstrain for clarity.

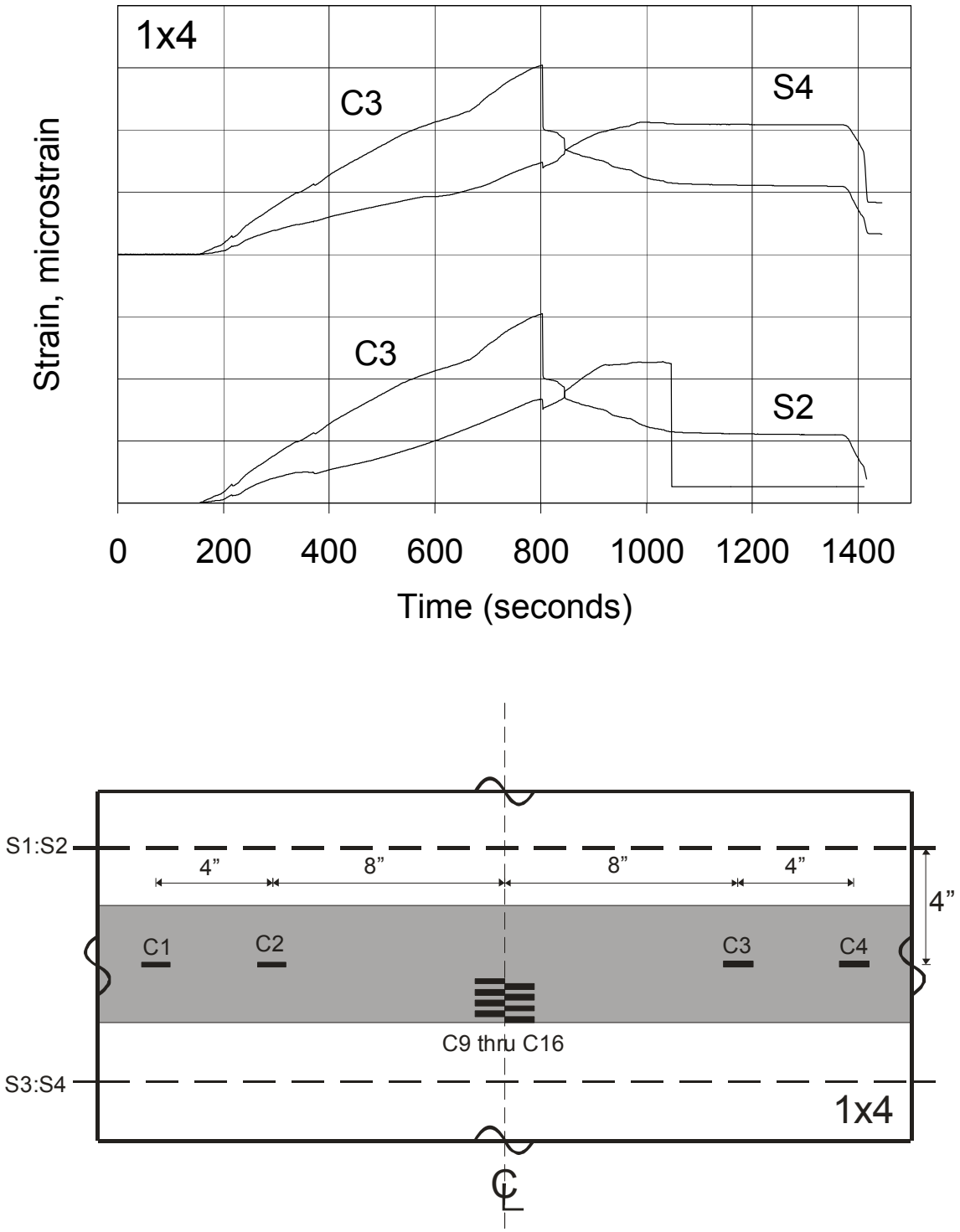

Figure 4-20 Plot of strain vs. time for the specimen 1x4.
Horizontal gridlines spaced at 1000 microstrain.
Curves are vertically offset 4000 microstrain for clarity.

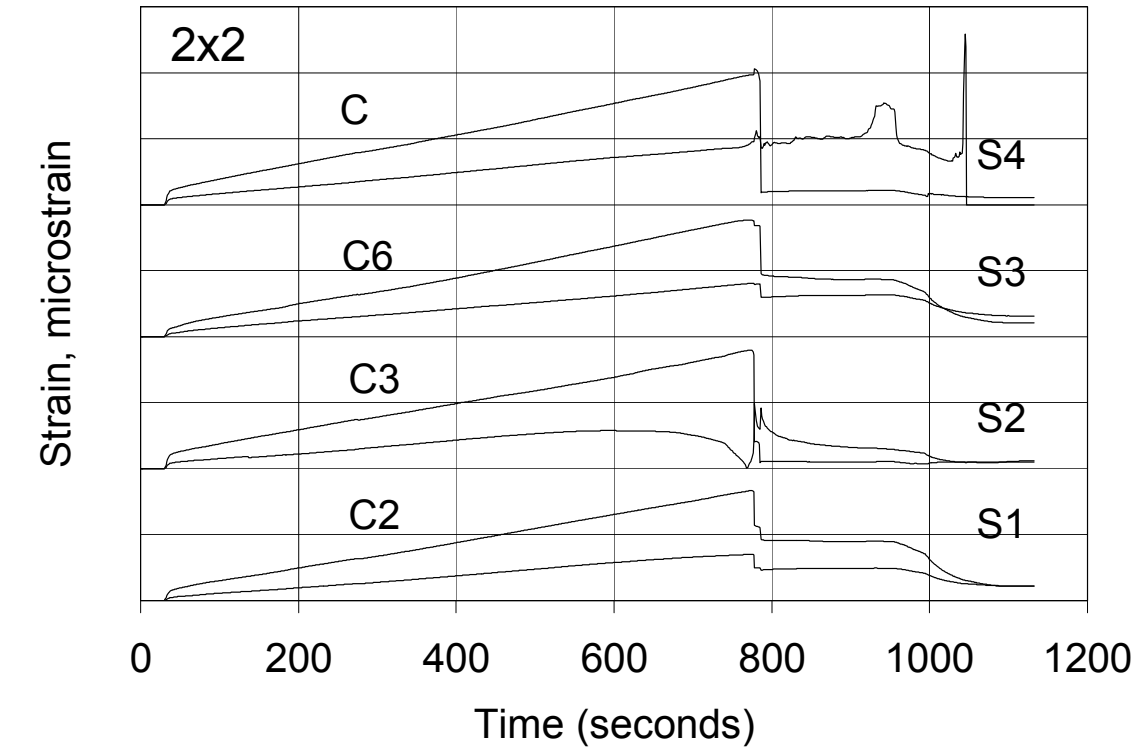

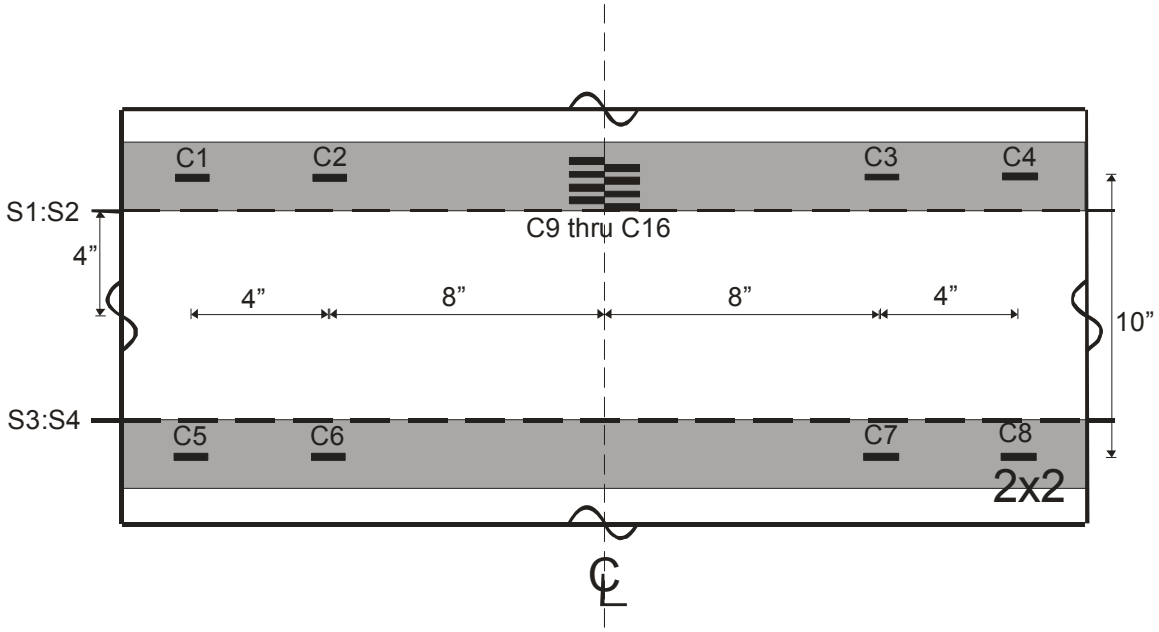

Figure 4-21 Plot of strain vs. time for the specimen 2x2.
Horizontal gridlines spaced at 2000 microstrain.
Curves are vertically offset 4000 microstrain for clarity.

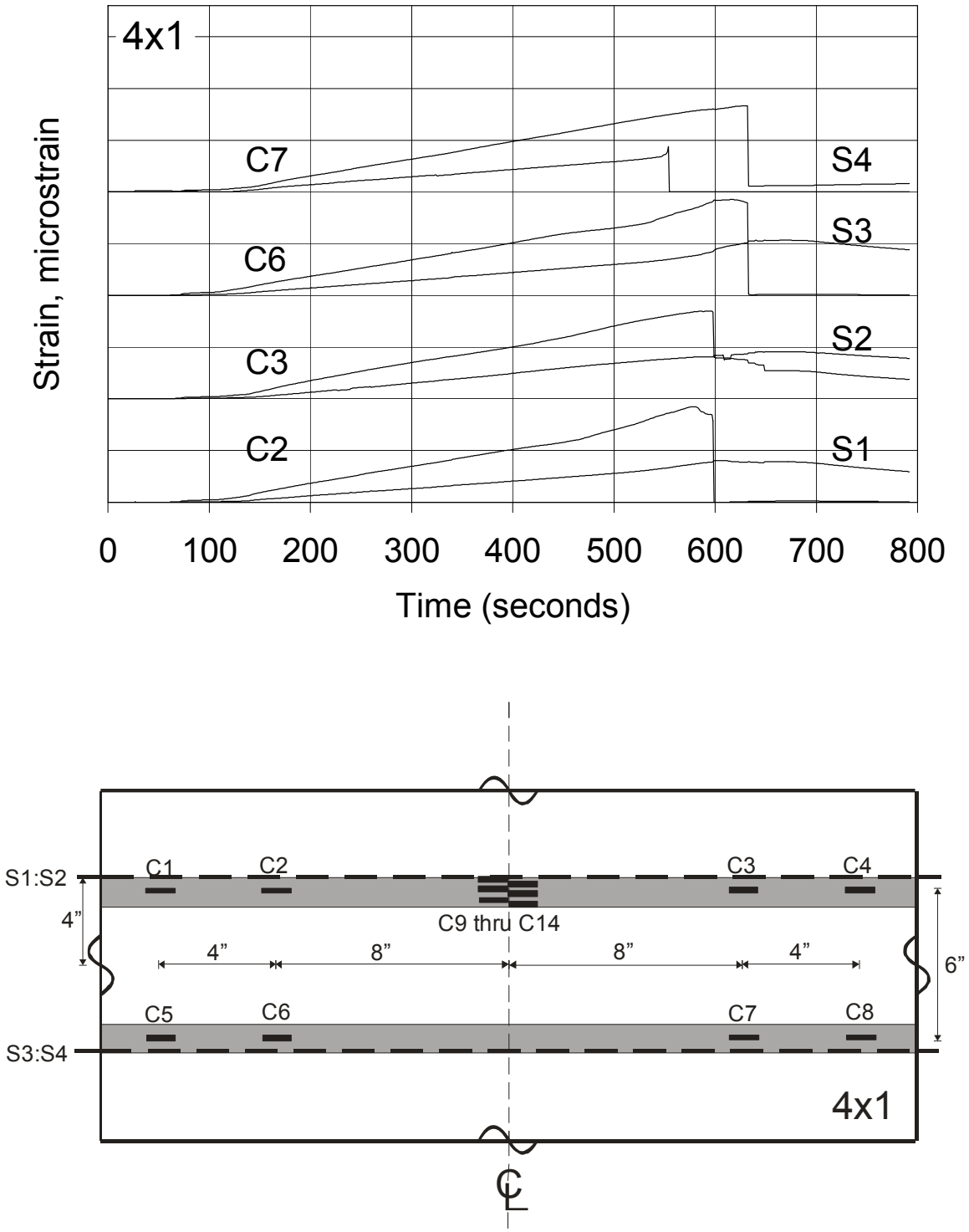

Figure 4-22 Plot of strain vs. time for the specimen 4x1.
Horizontal gridlines spaced at 2500 microstrain.
Curves are vertically offset 5000 microstrain for clarity.

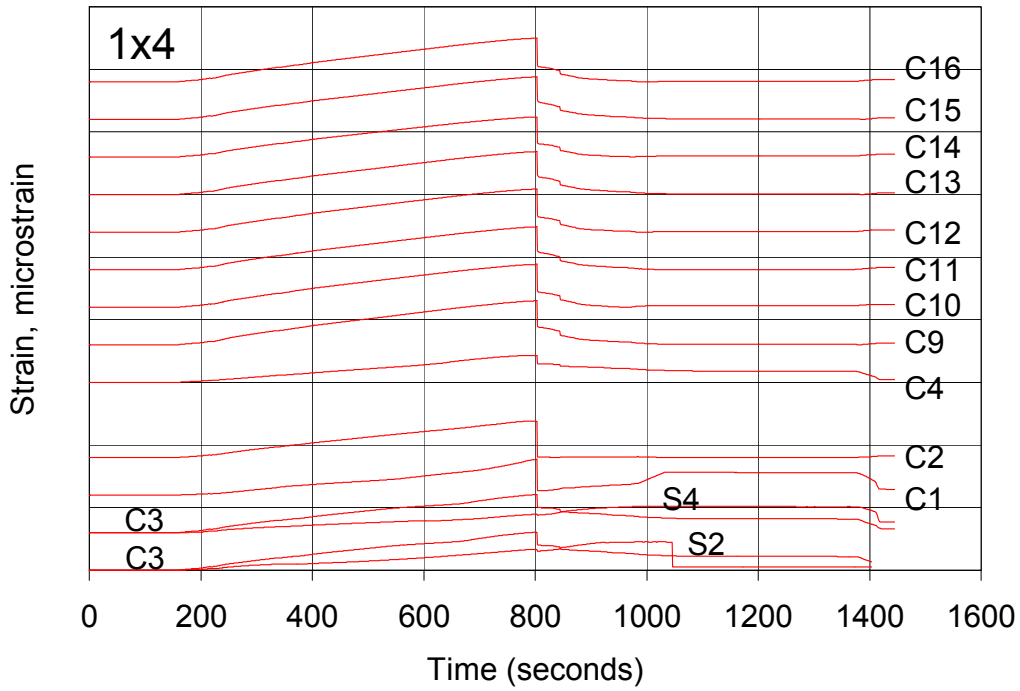

Figure 4-23 Strain time plot for all CFRP and rebar gages in specimen 1x4.
Horizontal gridlines spaced at 5000 microstrain.
Curves are vertically offset 3000 microstrain for clarity.

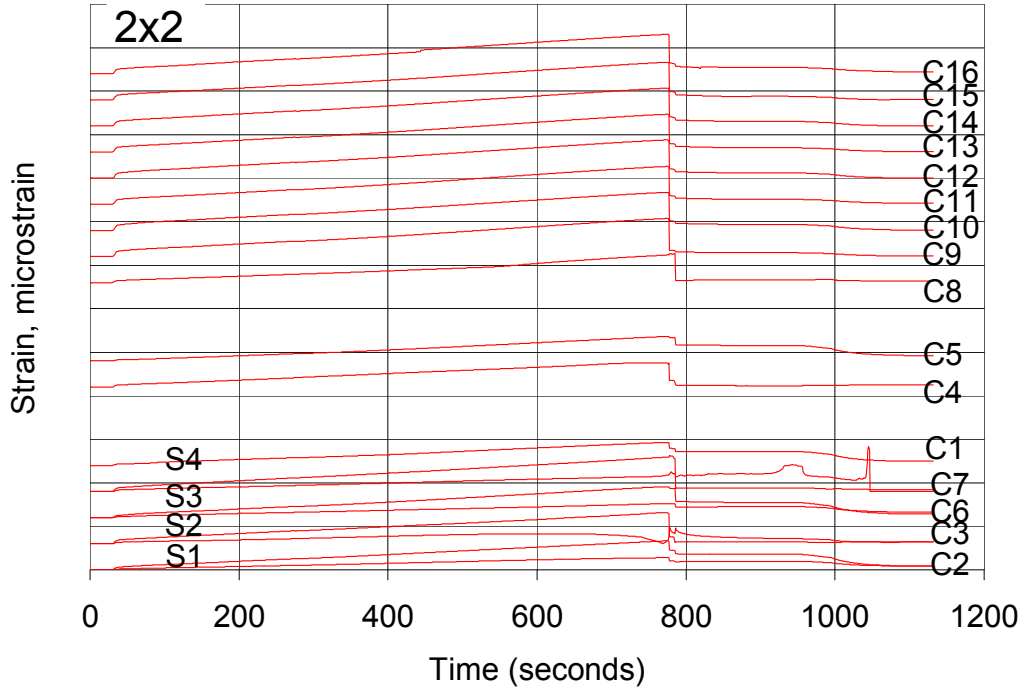

Figure 4-24 Strain time plot for all CFRP and rebar gages in specimen 2x2.
Horizontal gridlines spaced at 5000 microstrain.
Curves are vertically offset 3000 microstrain for clarity.

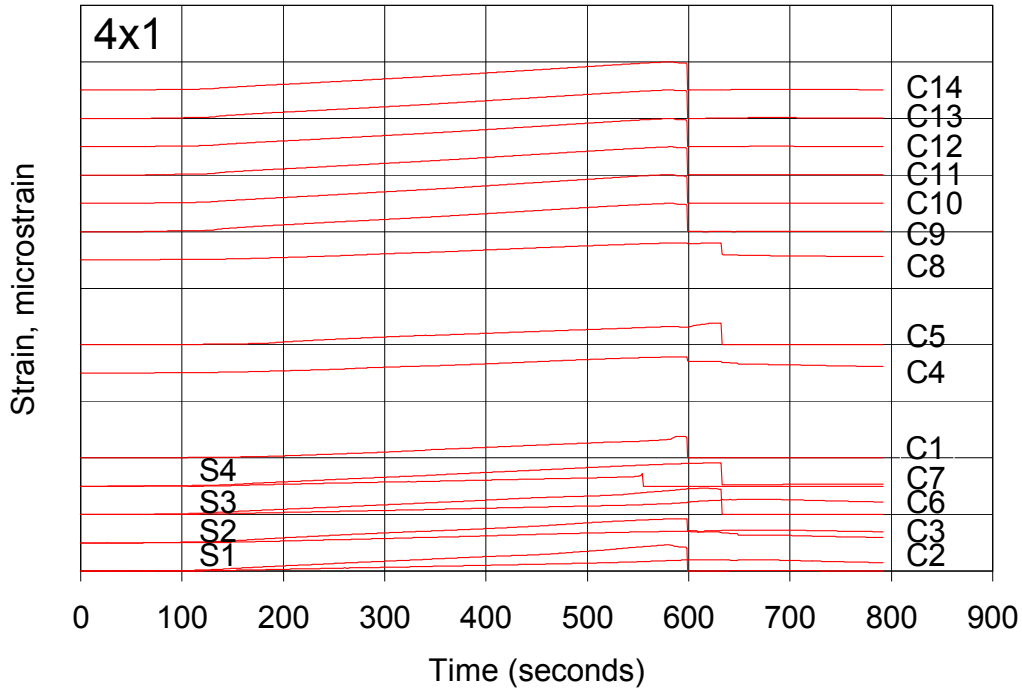

Figure 4-25 Strain time plot for all CFRP and rebar gages in specimen 4x1.
Horizontal gridlines spaced at 1000 microstrain.
Curves are vertically offset 5000 microstrain for clarity.

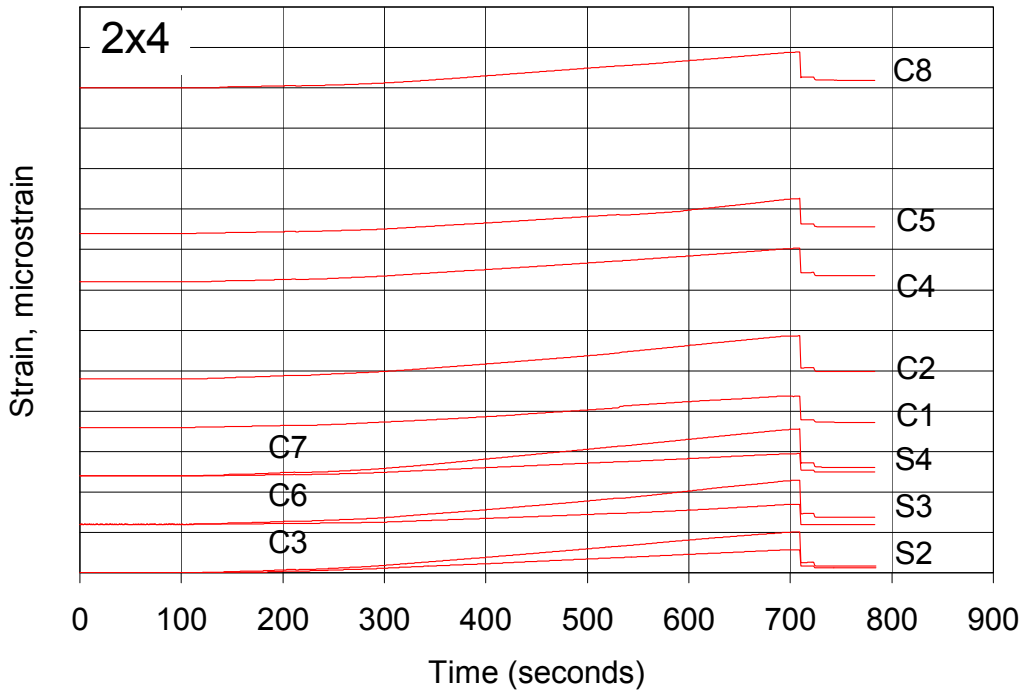

Figure 4-26 Strain time plot for all CFRP and rebar gages in specimen 2x4.
Horizontal gridlines spaced at 2500 microstrain.
Curves are vertically offset 3000 microstrain for clarity.

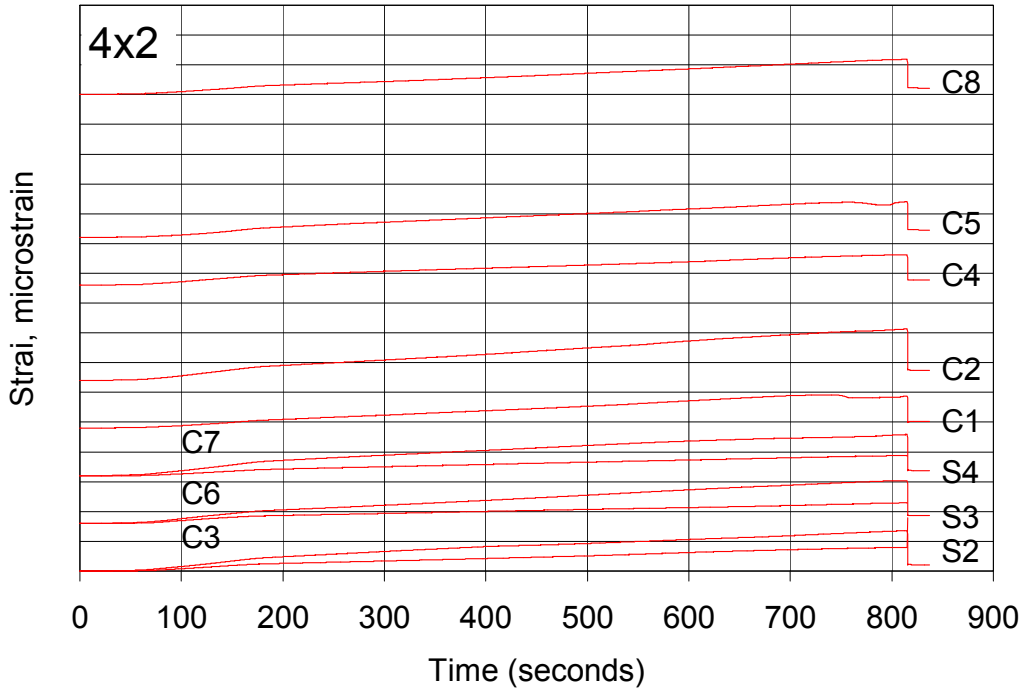

Figure 4-27 Strain time plot for all CFRP and rebar gages in specimen 4x2.
Horizontal gridlines spaced at 2500 microstrain.
Curves are vertically offset 4000 microstrain for clarity.

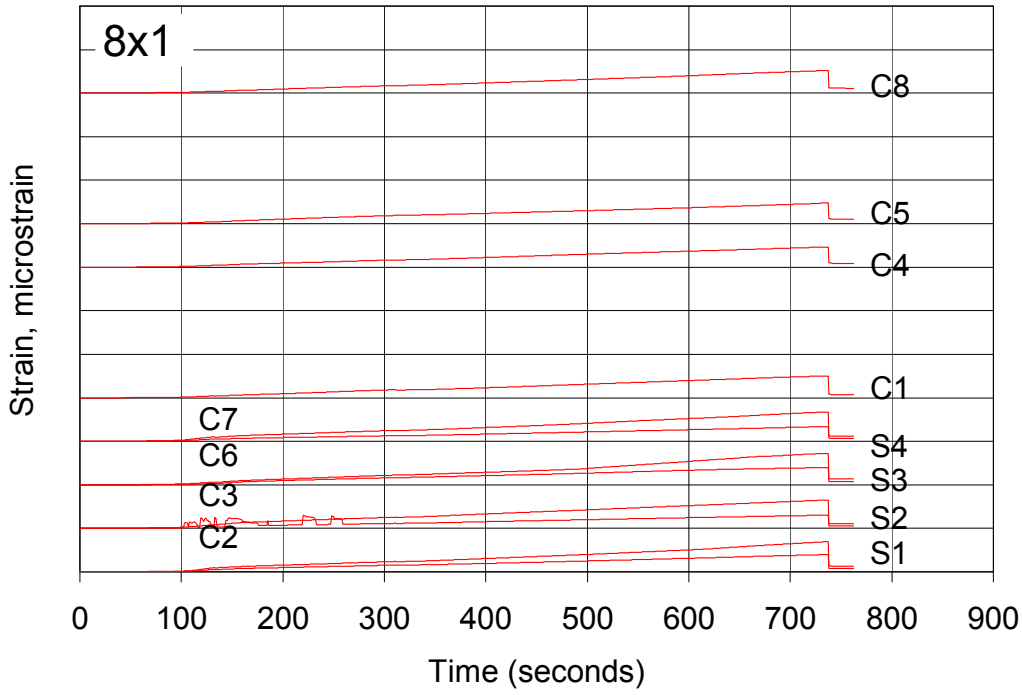

Figure 4-28 Strain time plot for all CFRP and rebar gages in specimen 8x1.
Horizontal gridlines spaced at 5000 microstrain.
Curves are vertically offset 5000 microstrain for clarity.

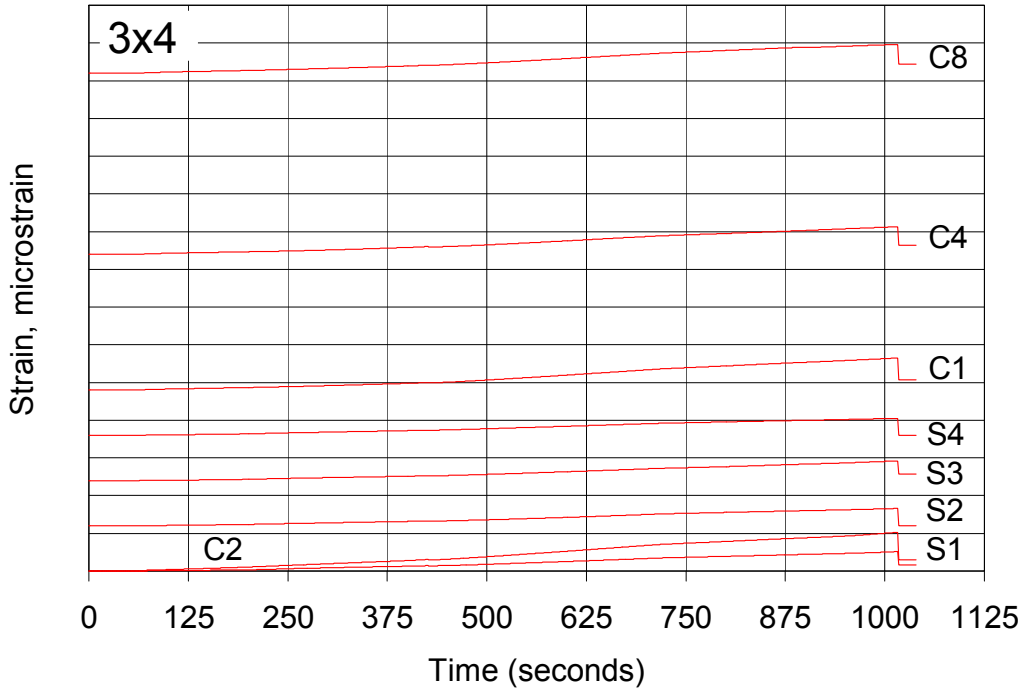

Figure 4-29 Strain time plot for all CFRP and rebar gages in specimen 3x4.
Horizontal gridlines spaced at 2500 microstrain.
Curves are vertically offset 3000 microstrain for clarity.

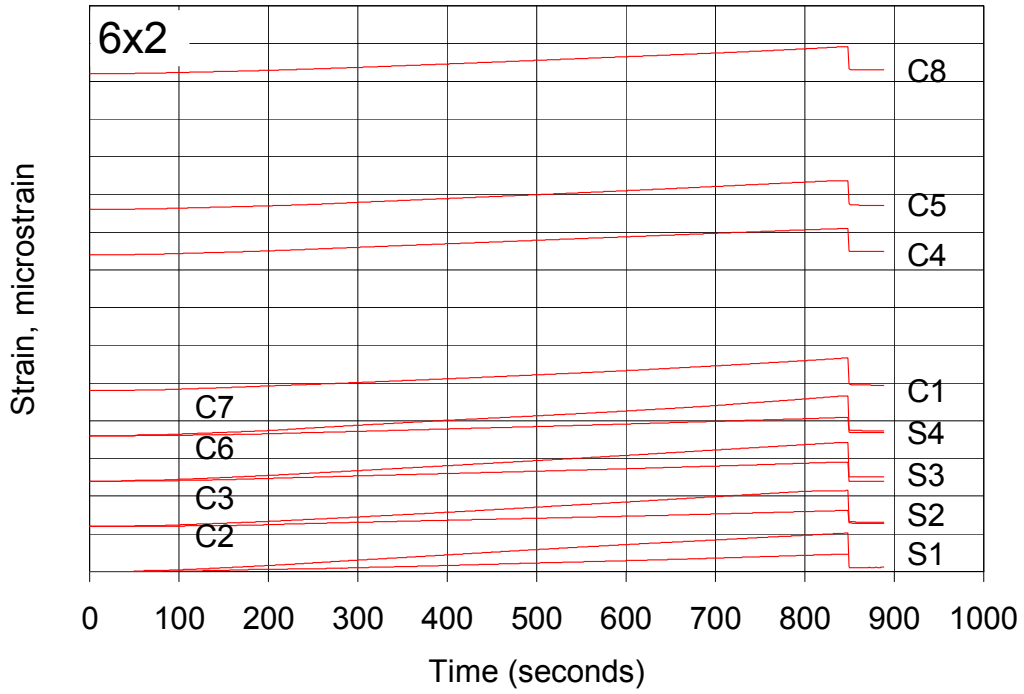

Figure 4-30 Strain time plot for all CFRP and rebar gages in specimen 6x2.
Horizontal gridlines spaced at 2500 microstrain.
Curves are vertically offset 3000 microstrain for clarity.

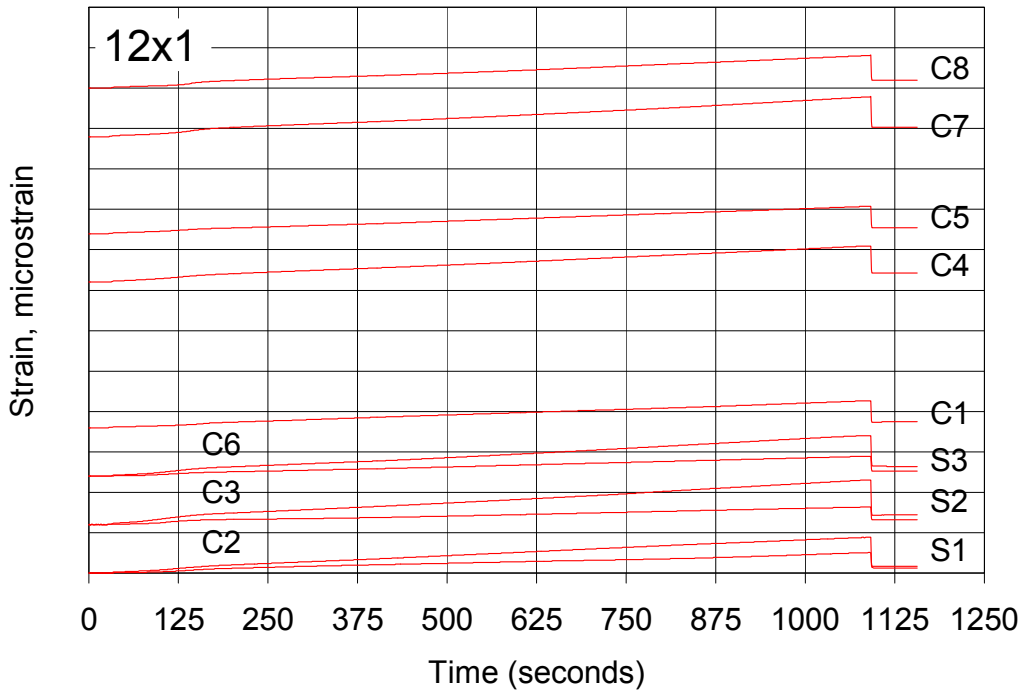

Figure 4-31 Strain time plot for all CFRP and rebar gages in specimen 12x1.
Horizontal gridlines spaced at 2500 microstrain.
Curves are vertically offset 3000 microstrain for clarity.

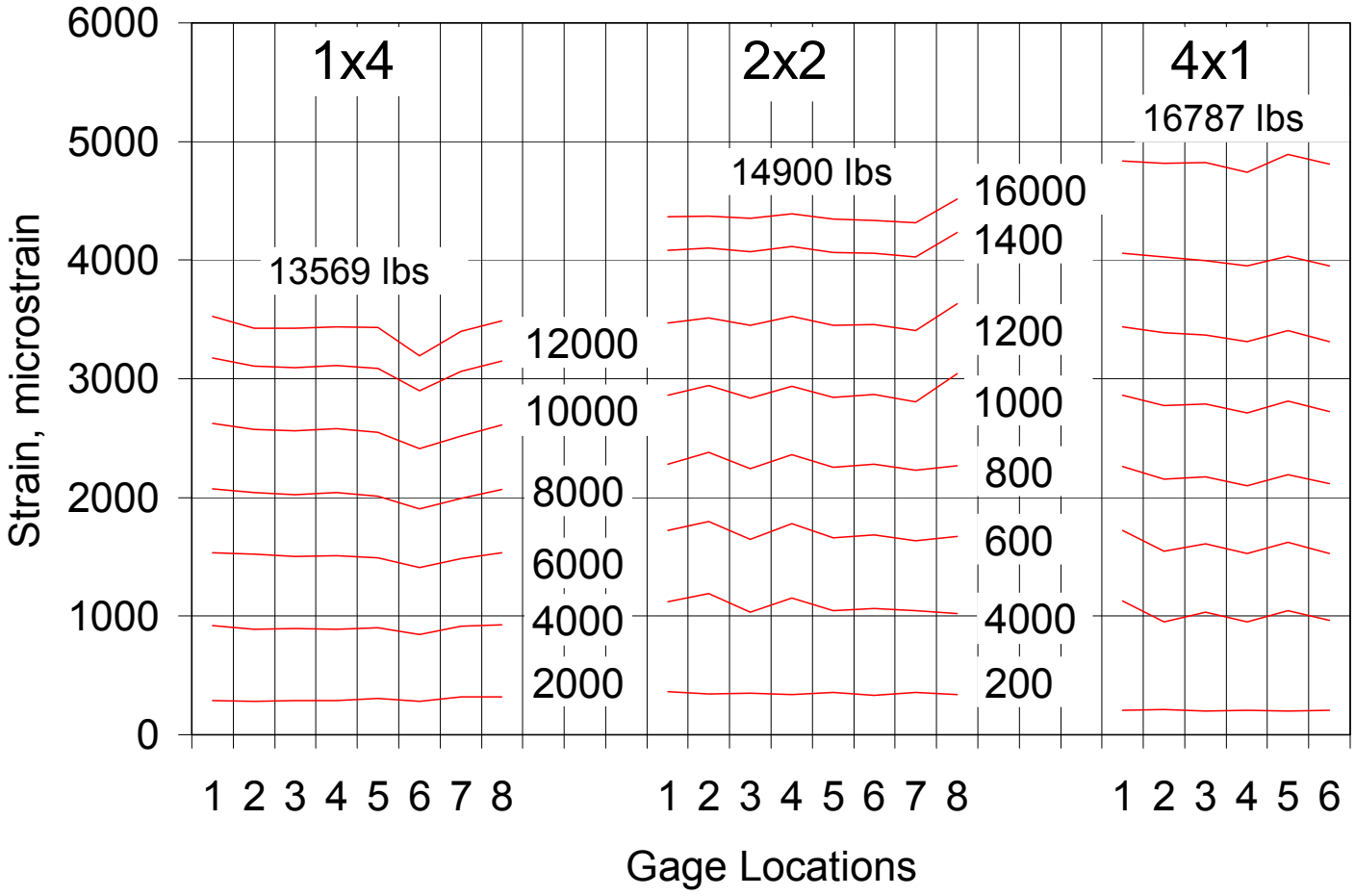

Figure 4-32 Strain distribution in transverse direction (across) of CFRP strips.
Gage1 located at the outside edge of the CFRP strip and the gages are spaced horizontally at 0.1in. (2.54 mm).
(No vertical offsets in this Figure)

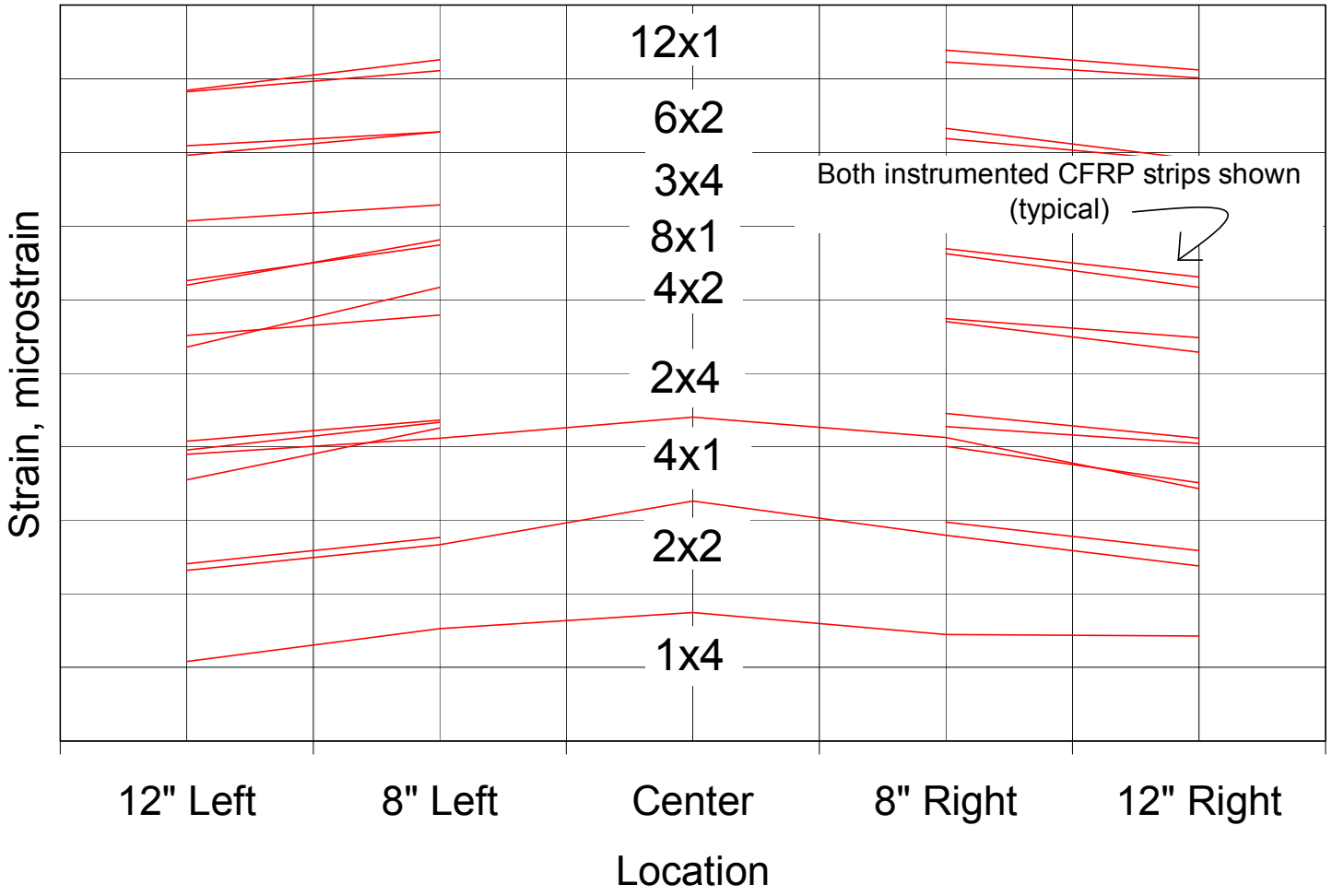

Figure 4-33 Longitudinal strain distributions in the test specimens.
Vertical gridlines spaced at 2000 microstrain.
Curves are vertically offset 2000 microstrain for clarity.

(a) overall view of failure (b) close-up of constant moment region

Figure 4-34 Failure of Control specimen.

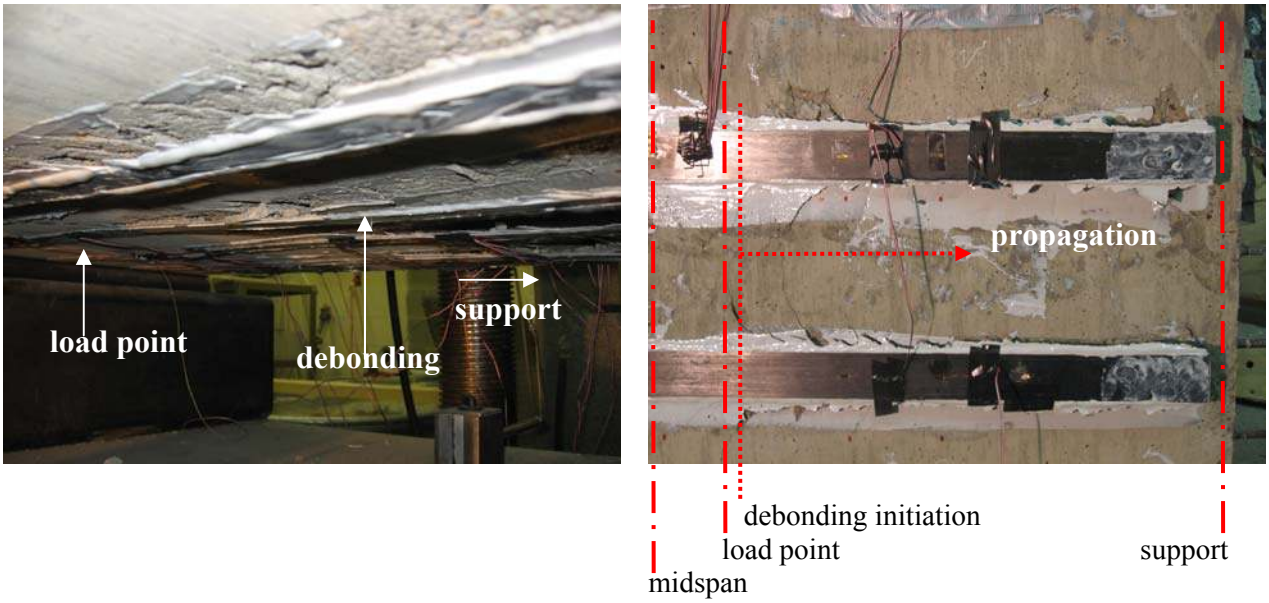

(a) debonding of Specimen 4x1 during testing (b) Specimen 2x2 after testing

Figure 4-35 Debonding failures.

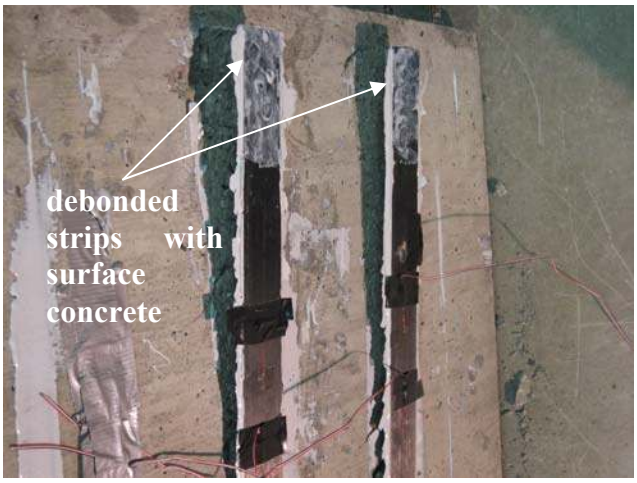

(a) debonded strip from Specimen 2x2

(b) Specimen 1x4 after testing

Figure 4-36 Debonded strips with cover concrete.

(a) failure of Specimen 2x4

(b) diagonal shear crack on the northwestern face of Specimen 4x2

(c) Specimen 6x2 after testing

(d) crack at the level of reinforcing bars on the southern face of Specimen 12x1

Figure 4-37 Shear failures.

5.0 DISCUSSION OF EXPERIMENTAL RESULTS

This chapter reports interpretations of and results derived from the experimental data reported in Chapter 5. Basis for these interpretations is also reported.

5.1 COMPARISON OF TEST SPECIMENS

Test specimen nomenclature is outlined in Section 3.4. Figure 4-1 thru Figure 4-10 show the observed load deflection behaviors for the control specimen and all nine retrofit test specimens. A summary of the key results of this test program is given in Table 4-1 and definitions for all parameters reported are given in Section 4.1. For direct comparison, the plots of all nine retrofitted specimens and the control specimen are shown in Figure 5-1 on a single graph.

It can be clearly seen from Figure 5-1 that the behavior changes from being ductile in case of the control specimen, to brittle in case of the heavily retrofitted specimens. As expected, the load carrying capacity increases with the application of the CFRP. The response seen in Figure 5-1 is indicative of the change in behavior from a flexural-dominated behavior for the control specimen to a behavior clearly limited by shear capacity of the slab as the amount of reinforcement is increased.

Initial cracking of the loaded slabs occurred over a wide range of loading for all test specimens, varying over a range of about 2000 lbs. (9350 N). The lowest observed applied load to cause cracking was 250 lbs (1110 N) in case of the control specimen and the greatest was 2460 lbs (10.95 kN) for Specimen 2x2. Such variation should be expected and reflects the expected variability in the modulus of rupture of the concrete (usually expressed as $7.5\sqrt{f_c'}$ (ACI 318 2005)). The apparent modulus of rupture corresponding to the 250 lb cracking load of the control specimen is $1.6\sqrt{f_c'}$ while that for Specimen 2x2 is $9.8\sqrt{f_c'}$ (both include effects of self weight and loading apparatus dead load). The low value for the control specimen may reflect a flaw in the specimen or damage while handling nut is nonetheless within the range of typically observed values. The higher cracking loads of the retrofit specimens reflect the marginal improvement in cracking performance affected by externally bonded CFRP. Such an effect is observed in most studies of external FRP retrofit of initially uncracked specimens. It should be noted that in most practical applications, the structure will be cracked prior to application of the CFRP retrofit.

From Table 4-1 it can be seen that with an increase in the amount of CFRP, the maximum loads carried by the specimen increases. Also from Table 4-1 it can be seen that for the same amount of CFRP, the slabs retrofitted with a multiple thinner strips have greater load carrying capacities when compared to slabs retrofitted with fewer wider strips. However it can be seen that there is an apparent upper limit to the load carrying capacity of the slabs tested. Specimens 4x2 and 8x1 have higher maximum loads when compared to 3x4, 6x2 or even 12x1, although the variability between these is nominal. This observed behavior reflects the shear dominated behavior in case of the second and third series specimens. In these cases, the CFRP, while increasing the flexural capacity, has no effect on the shear capacity of the slabs, thus the behavior

evolves from being flexure-critical to being shear-critical with the application of additional CFRP. This behavior underlines the interaction of moment and shear that must be considered in design. For slab structures, while flexural retrofit is relatively simple, increasing the existing shear capacity is difficult (unlike for beams where the vertical sides are accessible for external retrofit). Thus there is an important limit to the flexural strengthening that may be applied to slabs. As described in Section 4.2.3, the ultimate behavior of the slabs is not critical in the present study.

Specimen 4x2 has the highest load carrying capacity of 23.1 kips. This corresponds to a support (maximum) shear of 11.55 kips. For the slab of cross section having width, b = 30 in., an effective depth, d = 2.06 in. and compressive strength of concrete, $f_c^{'}$ = 4860 psi, this corresponds to concrete shear strength of $2.7\sqrt{f_c^{'}}bd$ which is in the expected range defined by ACI 318 (2005) as discussed in Section 4.2.3.

Further it was observed that the maximum strains obtained in the CFRP strips increases with larger number of smaller strips when compared to a smaller number of wider strips. This is most clearly seen in the flexure-critical specimens where the total width of CFRP reinforcement provided is 4 in. (102 mm). In this family of specimens, 1x4, 2x2 and 4x1, it can be seen that debonding initiates at a higher strain in case of specimen 4x1 when compared to specimen 1x4. Thus it is quite evident that it is more effective to use multiple thinner strips of CFRP.

A summary of the key results, with all data normalized to the control specimen values is given in Table 5-1. A graphical representation of the normalized result analysis is given in Figure 5-2. These graphs plot the ratio of the test specimen parameter to the control specimen parameter versus the equivalent reinforcement ratio ($\rho_{equivalent}$) of the test specimen, already defined in Equation 4.3 (Section 4.2) as:

$$\rho_{equivalent} = \frac{A_s}{bh} + \frac{A_f}{bh}\frac{E_f}{E_s}$$

where, bh = gross area of concrete section, equal to 90 in^2 (58,000 mm^2) in this study

A_f = cross sectional area of CFRP; $A_f = t_f b_f$ (Table 3-2)

A_s = cross sectional area of existing internal tension steel reinforcement, equal to 0.77 in^2 (500 mm^2) in this study.

E_f = modulus of CFRP, taken as 22500 ksi (155 GPa) (Table 3-2)

E_s = modulus of steel reinforcement, taken as 29000 ksi (200 GPa)

For all specimens in this study, the first term in the above equation, (A_s/bh) is equal to 0.86%.

In Figure 5-2 and all subsequent figures in this chapter, the first series of specimens (1x4, 2x2 and 4x1) are denoted by squares, the second series (2x4, 4x2 and 8x1) are denoted by diamonds and the third series (3x4, 6x2 and 12x1) are denoted by triangles. In each series, the 4 in. strips are denoted by solid black shapes, the 2 in. strips by gray, and the 1 in. strips with open shapes. In each case it can be seen that the slabs with a greater number of thinner strips performed better than slabs with fewer wider strips. This is clearly evident in cases of the first cracking load (Figure 5-2(a)) and the maximum load (Figure 5-2(b)). Thus it is established that the retrofit geometry has some influence on the overall retrofit performance and that multiple thinner strips are preferable to fewer wider strips in terms of performance. This observation supports the premise that the strips engage a region of concrete wider than their own width; i.e. there is a degree of stress transfer spreading into the concrete layer. Since debonding is typically observed to occur a small distance into the concrete substrate, this observation is further supported. In Figure 5-2(b), it is seen that in case of the second and third series of slab specimens, the maximum loads are similar owing to the behavior being dominated by shear capacity of the slab. This again emphasizes the interaction of flexure and shear and illustrates

increases in retrofit reinforcement do not result proportionate increases in the load carrying capacity.

Table 5-1 Analysis of Key Results Summary (see Figure 5-2).

Specimen	1x4	2x2	4x1	2x4	4x2	8x1	3x4	6x2	12x1
$\sum b_f$/slab width	0.13	0.13	0.13	0.27	0.27	0.27	0.40	0.40	0.40
b_f/s	0.13	0.20	0.17	0.40	0.33	0.30	0.53	0.46	0.44
$\rho_{equivalent}$	1.05	1.05	1.05	1.24	1.24	1.24	1.43	1.43	1.43
Ratio of first cracking load to that of control specimen	1.4	9.84	2.08	1.88	7.68	5.8	3.56	4.72	6.00
Ratio of maximum load to that of control specimen	1.51	1.66	1.87	1.96	2.57	2.47	2.29	2.47	2.38
Ratio of deflection at maximum load to that of control specimen	0.67	0.82	1.01	0.72	0.82	0.82	0.67	0.58	0.72

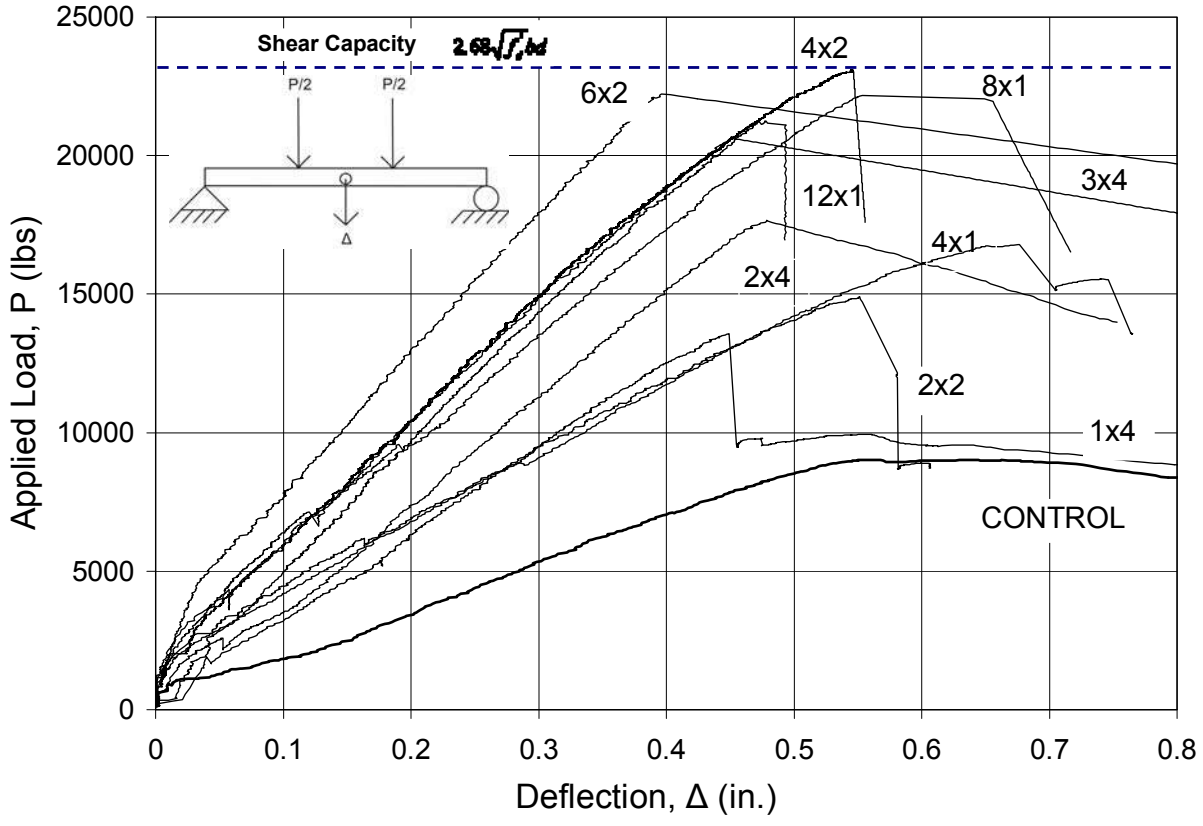

Figure 5-1 Load vs. Deflection curves for all test specimens.

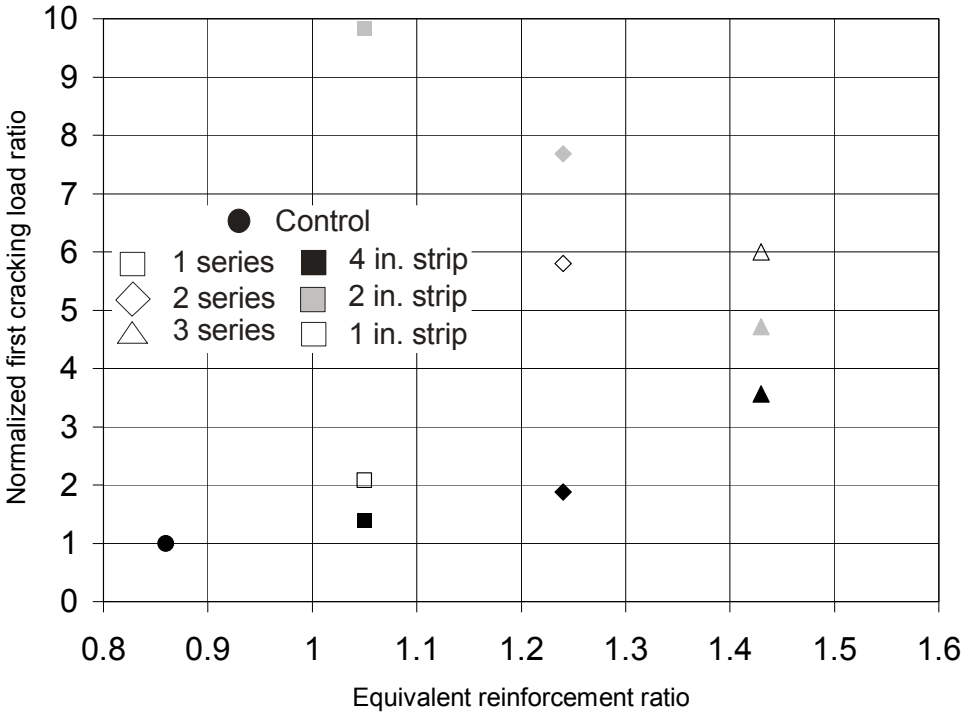

(a) Normalized first cracking load vs. Equivalent reinforcement ratio ($\rho_{equivalent}$)

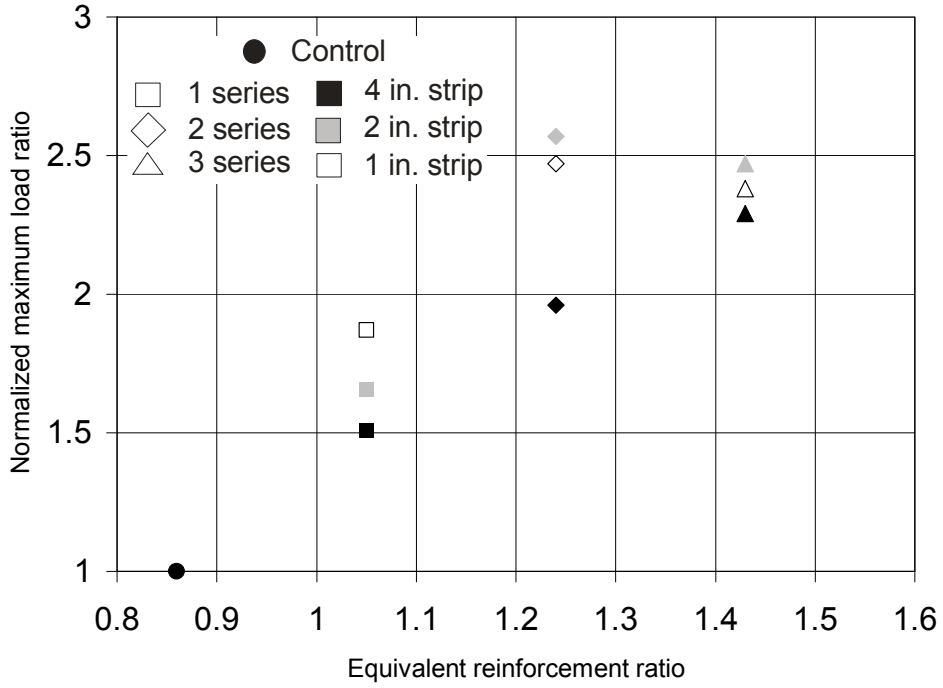

(b) Normalized maximum load vs. Equivalent reinforcement ratio ($\rho_{equivalent}$)

Figure 5.2 Analysis of key results: ratio of retrofit test specimens to control specimen.

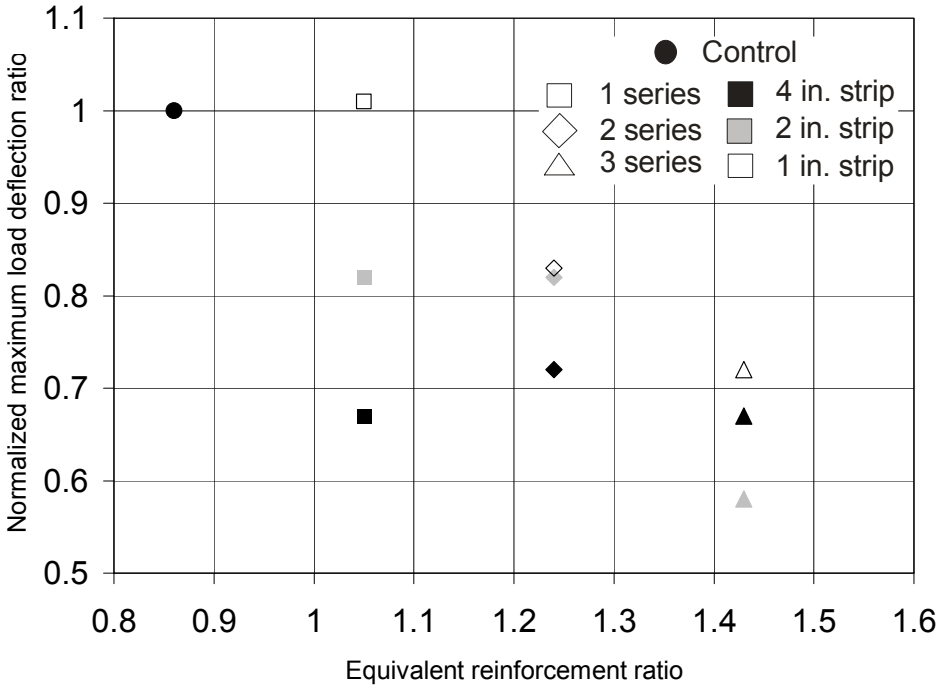

(c) Normalized deflection at maximum load vs. Equivalent reinforcement ratio ($\rho_{equivalent}$)

Figure 5-2 Analysis of key results: ratio of retrofit test specimens to control specimen.

6.0 DEBONDING BEHAVIOR

This chapter reports a discussion of observed debonding behavior and places this in the context of debonding criteria proposed in various national standards and by other researchers. In this chapter, only intermediate crack induced debonding, where it is a controlling limit state is considered. Therefore the experimental results from the first series of slabs (1x4, 2x2 and 4x1) are of primary interest.

6.1 DEBONDING BEHAVIOR

As discussed in Section 2.5, values of the critical strain above which debonding is likely, ε_{fub} are recommended in a number of standards and proposed by number of researchers. Many of these are discussed in this chapter.

In all cases discussed, it is assumed that the CFRP strips are sufficiently long to be fully "developed"; for example: in the case of recommendations of Teng et al. (2001) the factor accounting for bond length, k_L, is taken as 1 for all test specimens since $L_b >> L_{bmax}$. Additionally, it is assumed that cover delamination (end peel debonding) has been effectively mitigated by extending the CFRP close to the support along the relatively long shear span.

As recommended by the Task Group on Bond (2005) the value $\alpha = 0.9$ will be used in applying the equations recommended by Teng et al. (2001) and Teng et al. (2004) as this value has been

shown to result in better fit over a broad range of available data. (Teng et al. determined a value of $\alpha = 1.1$ using a more limited database of test results.)

The 28-day compressive strength of 4860 psi (33.5 MPa), given in Table 3-1 is used in all the calculations. The tensile strength of concrete is taken as $6\sqrt{f_c'}$ ($0.5\sqrt{f_c'}$ in MPa) in all cases corresponding to f_{ct} = 420 psi (2.9 MPa).

Figure 6-1 shows plots of the design equations for maximum allowable strain, ε_{fub} given by the following:

- ACI 440.2R-07;
- ACI 440.2R-02;
- Teng et al. (2004);
- Teng et al. (2001);
- fib Bulletin 14 (2001);
- JSCE Recommendations (2001);
- Concrete Society TR55 (2000);
- Italian CRN DT 200 (2004);
- Chinese CECS-146 (reference 2006); and
- the draft Australian guideline (2006).

Where appropriate (see Table 2-1) the recommended equations are plotted using values of b_f/s equal to those used for the first series of tests in this study: 0.13, 0.20 and 0.17. It can be seen in Figure 6-1 that varying the value of b_f/s within this small range has little effect on the predicted debonding strains.

The observed values of the strain in the CFRP at the initiation of debonding for specimens 1x4, 2x2 and 4x1 are also shown in Figure 6-1. The second and third series of slab specimens are

not represented in these plots since they did not exhibit intermediate crack-induced debonding limit states.

For clarity, a subset of Figure 6-1 showing only the relationships recommended by ACI 440.2R-07 and those recommended by Teng et al. (2004) is plotted in Figure 6-2. Again the three values of b_f/s used in this study: 0.13, 0.20 and 0.17 are applied to Teng et al. equation.

For the values of strain at initiation of debonding (obtained in this study and shown in Figure 6-1 and Figure 6-2) the following observations are made:

1. The present ACI 440.2R-07 equation is non conservative, overestimating the strain at which debonding occurs. However, this equation is an improvement over ACI 440.2R-02 which is highly non conservative. This observation is not as critical as it may seem in as far as the ACI 440.2R-07 equation represents a median response rather than a lower bound behavior. The ACI 440.2R-07 recommendation is based on the format of Teng et al. recommendations without considering the effect of b_f/s ratio; that is: k_b is taken as unity.
2. Both Teng et al. (2001 and 2004) recommendations and Chinese CECS-146 recommendation (also written by Teng) are also non conservative. Again, these recommendations must be understood to represent empirically derived median, rather than lower bound behavior.

The equations given by JSCE Recommendations, the Australian guideline, Concrete Society TR-55, fib Bulletin 14 and Italian CNR DT 200 provide conservative estimates of debonding strains. These recommendations, on the other hand, are understood to represent expected lower bound debonding behavior; thus this observation should be expected.

6.2 RETROFIT GEOMETRY PARAMETER

The k_b factor discussed in Section 2.6 is given by several researchers as a function of the ratio of FRP width to substrate width or FRP spacing, in the case of slabs: b_f/b or b_f/s, respectively.

Figure 6-3 shows plots of the maximum calculated debonding strains obtained using each of the equations discussed previously versus the experimentally observed debonding strains for Specimens 1x4, 2x2 and 4x1. The "predicted" axis represents the calculated debonding strains while the "observed" axis represents the experimentally observed strains at which debonding initiated.

Similar results were found for the recommendations made by ACI 440.2R-07, ACI 440.2R-02, Teng et al. (2007), Teng et al. (2002) and Chinese CECS-146. In all these cases, the prescribed equations provided conservative values of the maximum allowable strain, ε_{fub}. ACI 440.2R-02, Teng et al. (2002) and Chinese CECS-146, in particular, overestimate the debonding strain.

The Concrete Society TR-55, Italian CNR DT 200, fib Bulletin 14 and Australian guidelines resulted in non conservative estimates of the maximum allowable strain, ε_{fub}. These equations under estimate the strain at which debonding initiates.

The same predictions of debonding strain although neglecting the b_f/s term; that is, setting $k_b = 1$ in all cases where this term is used, are also shown in Figure 6-3. Due to the lower values of b_f/s for the first series (1x4, 2x2 and 4x1), setting k_b to unity results in reduced predicted values of debonding strain and, therefore, an improvement in the predictions resulting from the recommended equations.

The observations reported in Sections 6.1 and 6.2 are generally consistent with the nature of the recommendations (median or lower bound empirical equation) discussed although they suggest that the behavior of FRP-retrofit slabs may differ from that of beams. All recommendations reported are empirical in nature and are based on databases populated exclusively by beam tests. Only Teng et al. (2001) recognizes the effect of structure geometry in recommending different values of the modification factor, α, for simple and cantilever structures (α = 1.1 and 0.72, respectively).

6.3 DISCUSSIONS OF THE ACI 440 BOND TASK GROUP DATABASE

As discussed in Chapter 2, the ACI Committee 440 Task Group on Bond was charged with assessing the existing 440.2R-02 bond equations and determining an appropriate relationship to capture the limits associated with debonding behavior to be incorporated into 440.2R-07[4]. The task group has an extensive database of experimental tests of flexural members having FRP retrofits. The database includes 282 tests from 42 citable sources of which 102 have sufficient information to assess the FRP debonding strains and behavior. Of these 102 tests, 72 tests reported FRP delamination (FIC/SIC) failures; only these, and the three first series tests reported here, have been considered in the subsequent discussions. The range of parameters encompassed in these 72 tests is given in Table 2-4; the database of the 72 test results is given in Appendix.

[4] As of this writing (January 2008), the revisions to ACI 440.2R-02 reported in this thesis as ACI 440.2R-07 have been approved by Committee 440 and ACI TAC. Publication of ACI 440.2R-08 is expected in the spring of 2008.

As stated in Chapter 2, the ACI 440.2R-02 provisions were found to be generally non conservative. Figure 6-4 shows debonding strain values calculated using ACI 440.2R-02 and ACI 440.2R-07 guidelines: results from the task group data base and the experimentally observed results from this study are also shown. In this figure, the ACI 440.2R-07 equation is plotted for two concrete compressive strengths values: 4000 psi (25.6 MPa) and 7500 psi (51.7 MPa). These values represent the range of compressive strength values of the 72 tests in the database as shown in Table 2-4. It can be seen that the ACI 440.2R-02 is indeed generally non conservative and that the proposed ACI 440.2R-07 equation is a better representation of the median (or "best fit") of the available debonding strain data. It is noted that most of the data where the experimentally obtained debonding strain is observed to exceed the ACI 440.2R-02 recommendations, and all of the highest such observed values, originated from the same laboratory (Juvandes 1999 and Dias 2001) and may indicate a different definition of debonding strain being used (the database is self-reported and verified only through available citations).

Figure 6-5, repeats the form of Figure 6-3 but with all results from the database (circular shapes) and the present test results (square shapes). In each case, calculations have been made considering values of k_b based on b_f/b or b_f/s (solid shapes) parameters and those calculated setting k_b equal to unity (open shapes). In some cases, the figures have just open shapes because these respective provisions do not include a k_b factor.

6.3.1 Correlation of Experimentally Observed and Equation-Prescribed Data

Table 6-1 reports correlation coefficients between the experimentally-observed debonding strains and the equation-prescribed strains for each of the specifications considered.

The correlation coefficient $\rho_{X,Y}$ between two random variables X and Y with expected values μ_X and μ_Y and standard deviations σ_X and σ_Y is defined as:

$$\rho_{X,Y} = \frac{\operatorname{cov}(X,Y)}{\sigma_X \sigma_Y} = \frac{E((X-\mu_X)(Y-\mu_Y))}{\sigma_X \sigma_Y} \qquad (6.1)$$

Where E is the expected value operator and cov means covariance. Since, $\mu_X = E(X)$ and $\sigma_X{}^2 = E(X^2) - E^2(X)$ and likewise for Y, the correlation coefficient may also be written as:

$$\rho_{X,Y} = \frac{E(XY) - E(X)E(Y)}{\sqrt{E(X^2) - E^2(X)}\sqrt{E(Y^2) - E^2(Y)}} \qquad (6.2)$$

The correlation is 1 in the case of an increasing linear relationship, −1 in the case of a decreasing linear relationship, and some value in between -1 and 1 in all other cases, indicating the degree of linear dependence between the variables. The closer the coefficient is to either −1 or 1, the stronger the correlation between the variables.

From Table 6-1 it can be clearly seen that improved correlation is obtained when the retrofit geometry parameter, k_b is considered rather than neglected (k_b = 1). This is illustrated in the case of Teng et al. (2004) recommendations where the correlation coefficient is 0.65 considering the k_b value and only 0.53 when k_b = 1 is used. It is noted that in setting k_b = 1, the fit coefficient used in the equation (0.54 in the case of Teng et al. 2004) may change, however this will have no impact on the correlation coefficient. Table 6-1 additionally illustrates that the Teng et al. (2004) recommendations have the best correlation with experimental data. For cases where k_b = 1, the ACI 440.2R-07, fib Bulletin 14 and Teng et al. (2004) recommendations result in similar correlation coefficients.

Table 6-2 gives the correlation coefficients for the experimentally-observed strains and equation-prescribed strains using the ACI 440.2R-07 recommendations modified by the k_b

factors prescribed by Teng et al. (2001 and 2004). The correlation is calculated for the entire useful database of 72 tests and a subset of this database defined by specimens having an overall depth greater than or equal to 10 inches (250 mm). The 10 in. depth was selected arbitrarily as a dividing point between small- and moderate-scale specimens in addition to maintaining a reasonable dataset size (43 test results). The correlation coefficients, $\rho_{X,Y}$, were obtained for the ACI 440.2R-07 equation (effectively $k_b = 1$) and for the same equation modified by k_b as specified by Teng et al. (2001) and Teng et al. (2004). Table 6-2 indicates a better correlation obtained using the k_b factor recommended by Teng et al. (2001).

6.3.2 Fit Coefficients

Having established that the inclusion of the k_b factor improves correlation of observed and predicted results, it is necessary to establish the correct fit coefficient, α (see Equation 6.3). In the following exercise, a number of assumptions are made:

1. The general format of the debonding strain equation will take that recommended by Teng et al. (2004) and adopted by ACI 440.2R-07. This is given as:

$$\varepsilon_{fub} = \alpha \sqrt{\frac{f_c^{'}}{nE_f t_f}} \qquad (6.3)$$

2. Based on the test results shown in Table 6.2, the k_b factor recommended by Teng et al. (2001) will be adopted, as indicated in Equation 6.4:

$$\varepsilon_{fub} = \alpha k_b \sqrt{\frac{f_c^{'}}{nE_f t_f}} = \alpha \sqrt{\frac{2 - b_f / b}{1 + b_f / b}} \sqrt{\frac{f_c^{'}}{nE_f t_f}} \qquad (6.4)$$

Based on these assumptions, values of α are determined resulting in the average ratio of experimentally-observed strains to the strains calculated from Equations 6.3 and 6.4 being equal to unity.

As indicated in Table 6-3, when k_b is neglected as in the present ACI 440.2R-07 recommendations, α = 0.41 yields the best fit to the mean data. When k_b is considered, this value is decreased marginally to 0.39 to fit the mean data. As indicated in Table 6-2, the correlation is improved in the latter case as represented by a reduction in the standard deviation of the ratio of observed to predicted results (Table 6-3).

It is therefore recommended that Equation 6.4, with a value of α = 0.39 be adopted. It is further noted that reducing the precision by setting α = 0.4 would not affect predicted results in any meaningful manner and better reflects the expected precision of such calculations.

Figure 6-6 shows the resulting plots of the resulting design equations for maximum allowable strain, ε_{fub} versus the FRP stiffness. The curves are plotted for a concrete compressive strength of 5000 psi (34.5 MPa) representing the average compressive strength of the tests listed in the database. Equation 6.4 is plotted for the upper and lower limiting values of k_b: $\sqrt{2}$ and $1/\sqrt{2}$, obtained when $b_f = 0$ and $b_f = 1$ respectively.

6.3.3 Effects of Specimen Size

Although not a focus of the present work, the effect of calibrating empirical design equations using an existing database is shown to be effected by the size of the specimens included in the database. In Table 6-2 and Table 6-3 reduced correlation coefficients and increased fit coefficients result from excluding small-scale (h < 10 in. (250 mm)) test results from the dataset

used to calculate the coefficients. This observation indicates the presence of a size effect. The following conclusions are drawn in this regard:

1. Reduced correlation at larger scales is a typically observed size effect as control of specimen parameters is better with smaller specimens.
2. The present guidance: using $\alpha = 0.41$ and/or $\alpha = 0.39$ is conservative when applied to larger specimens having realistic dimensions.

Nonetheless, caution should be practiced when using small-scale tests to calibrate such predictive equations.

Table 6-1 Correlation coefficients for different (calculated using Eq. 6.2).

Specification	Correlation Coefficient	
	Calculated k_b value	**$k_b = 1$**
ACI 440.2R-07	n.a.	0.52
ACI 440.2R-02	n.a.	0.37
fib Bulletin 14 (2001)	n.a.	0.54
JSCE Recommendations (2001)	n.a.	0.44
Concrete Society TR-55 (2000)	0.61	0.49
Italian INR DT-200 (2004)	0.57	0.51
Chinese CECS-146 (reference 2006)	0.53	0.39
The draft Australian Guideline (2006)	0.62	0.49
Teng et al. (2004)	0.65	0.53
Teng et al. (2001)	0.62	0.49

Table 6-2 Correlation coefficients for proposed ACI 440.2R-07 equation with and without kb factors specified by Teng et al. (2001) and Teng et al. (2004).

Debonding Strain $\varepsilon_{fub} = \alpha k_b \sqrt{\frac{f_c'}{nE_f t_f}}$	**Correlation Coefficient,** $\rho_{X,Y}$	
	Complete database (85 tests)	**Reduced database,** $h \geq 10$ *in.* **(43 tests)**
$\varepsilon_{fub} = 0.41(1.0)\sqrt{\frac{f_c'}{nE_f t_f}}$ (ACI 440.2R-07)	0.52	0.34
$\varepsilon_{fub} = 0.41\sqrt{\frac{2-b_f/b}{1+b_f/b}}\sqrt{\frac{f_c'}{nE_f t_f}}$ (Teng et al. 2001)	0.66	0.46
$\varepsilon_{fub} = 0.41\sqrt{\frac{2.25-b_f/b}{1.25+b_f/b}}\sqrt{\frac{f_c'}{nE_f t_f}}$ (Teng et al. 2004)	0.65	0.45

Table 6-3 α factors for the proposed ACI 440.2R-07 equation with and without kb factor specified by Teng et al. (2001).

Debonding Strain	**Complete database (85 tests)**			**Reduced database,** $h \geq 10$ *in.* **(43 tests)**		
	α	$\varepsilon_{observed} / \varepsilon_{calculated}$		α	$\varepsilon_{observed} / \varepsilon_{calculated}$	
		avg.	std. dev.		avg.	std. dev.
$\varepsilon_{fub} = \alpha\sqrt{\frac{f_c'}{nE_f t_f}}$	0.41	1.0047	0.38	0.44	1.014	0.35
$\varepsilon_{fub} = \alpha\sqrt{\frac{2-b_f/b}{1+b_f/b}}\sqrt{\frac{f_c'}{nE_f t_f}}$	0.39	1.0173	0.33	0.43	1.008	0.33

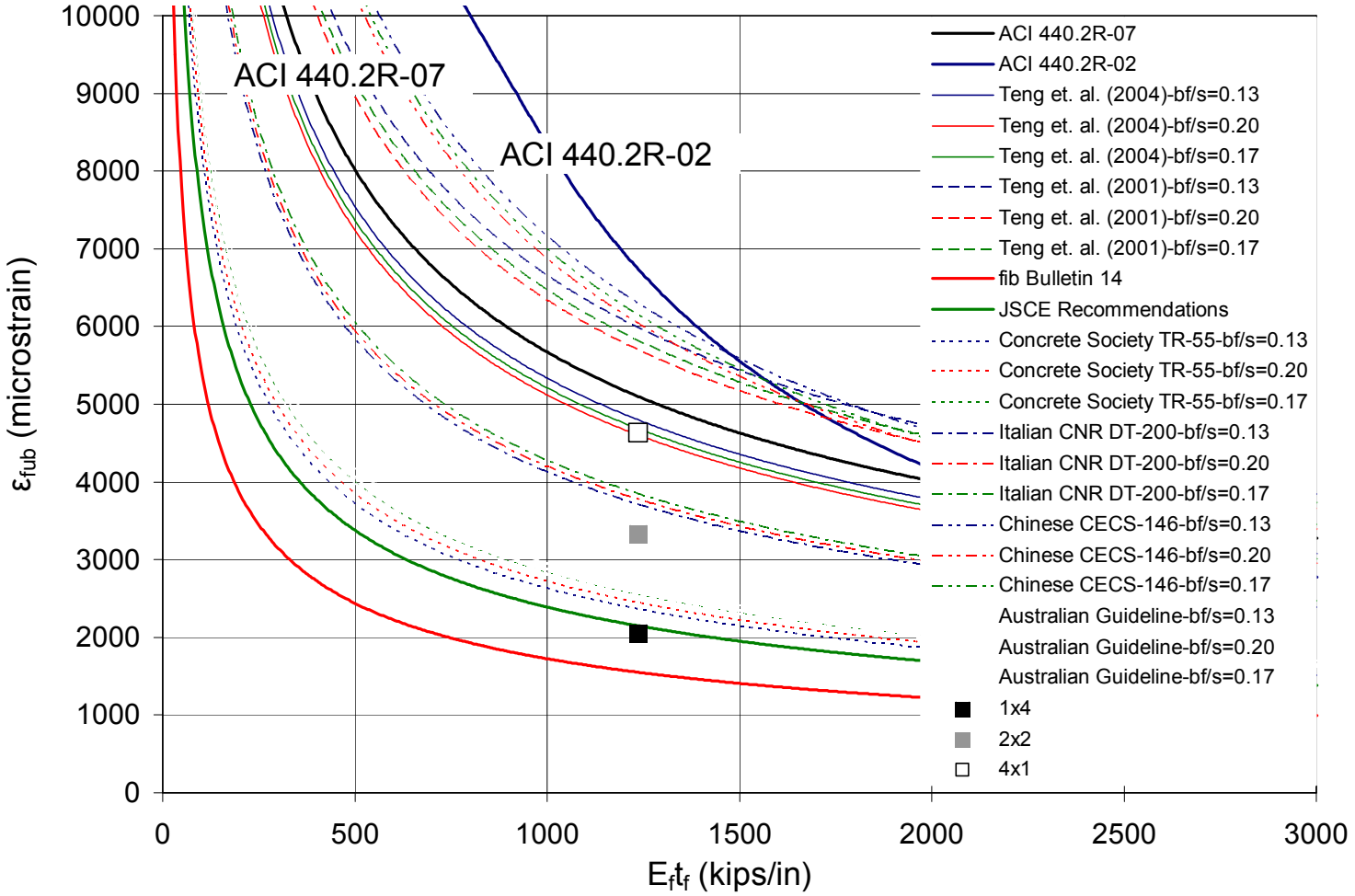

Figure 6-1 Experimentally observed strains vs. CFRP stiffness, compared with available strain equations proposed by various specifications and researchers.

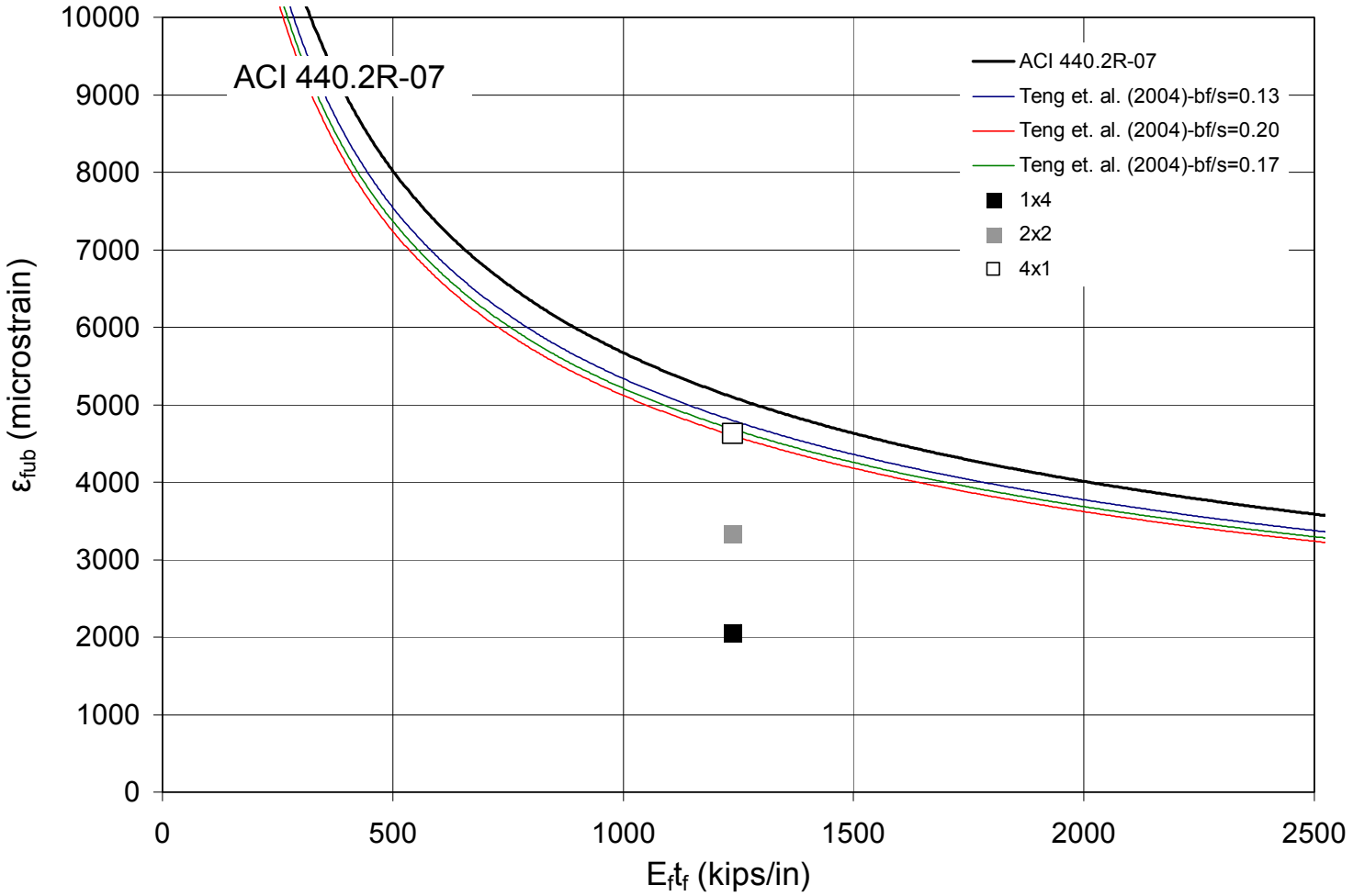

Figure 6-2 Experimentally observed strains vs. CFRP stiffness, compared with ACI 440.2R-07 and Teng et al. (2004) recommendations.

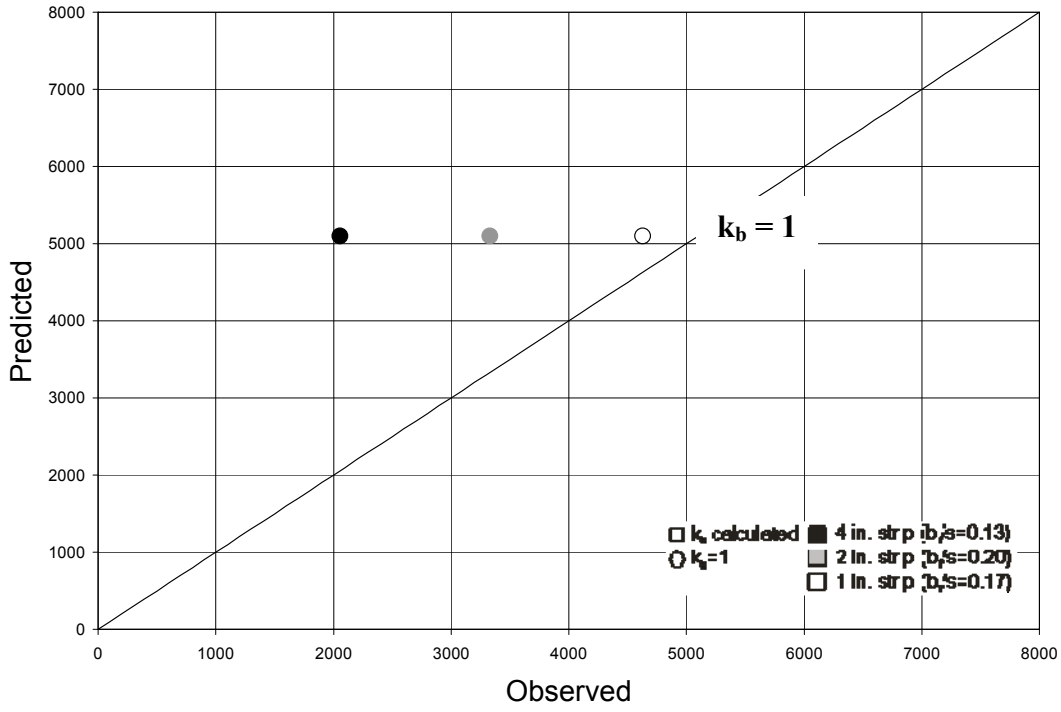

(a) Predicted vs. Observed strains based on ACI 440.2R-07

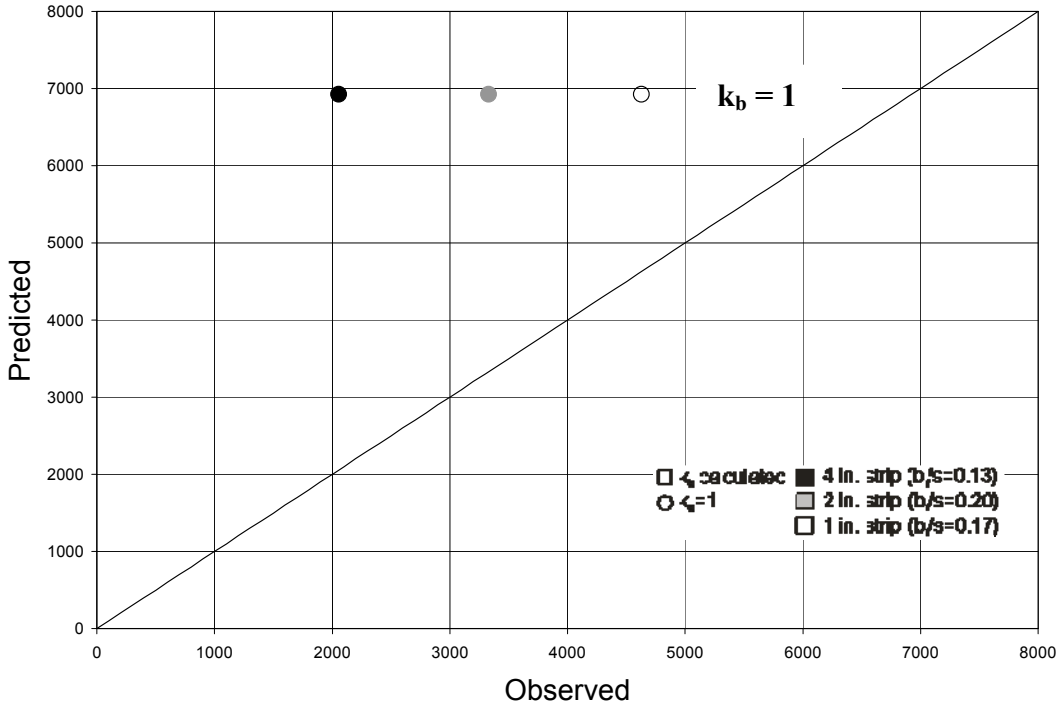

(b) Predicted vs. Observed strains based on ACI 440.2R-02

Figure 6.3 Predicted vs. Observed strains based on various specifications.

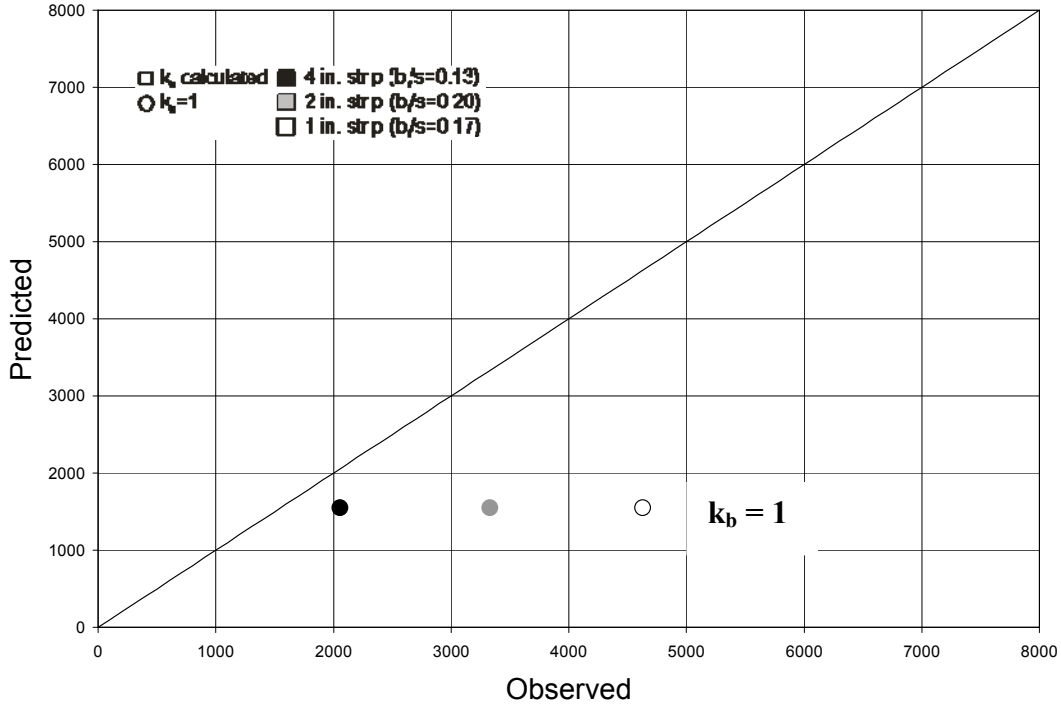

(c) Predicted vs. Observed strains based on fib Bulletin 14 (2001)

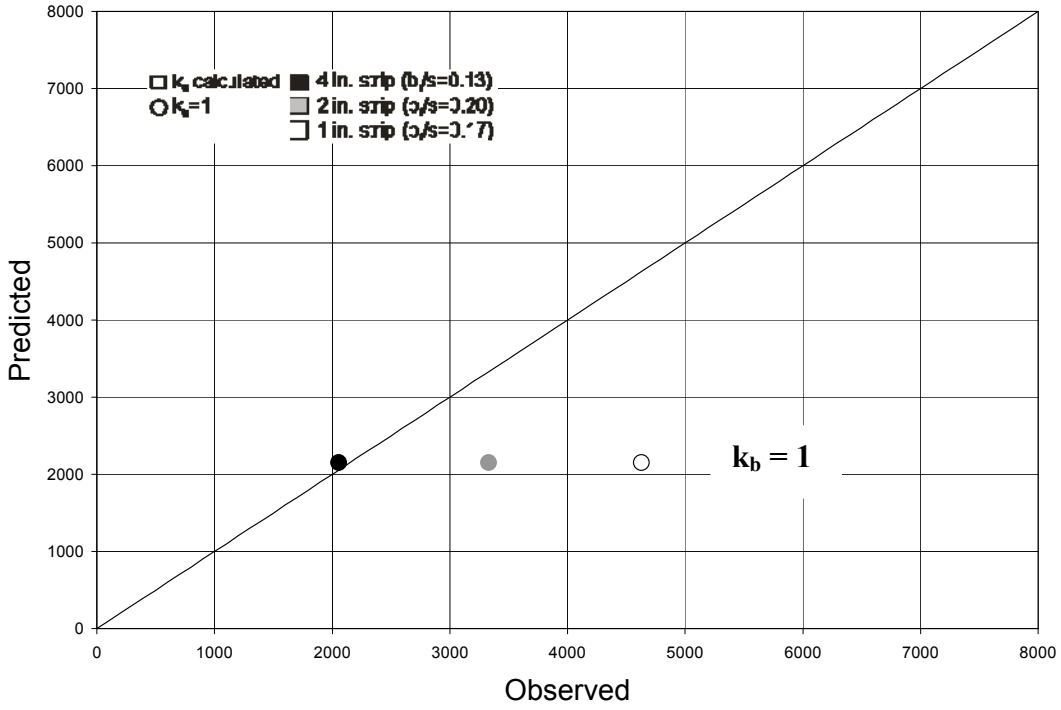

(d) Predicted vs. Observed strains based on JSCE Recommendations (2001)

Figure 6.3 Predicted vs. Observed strains based on various specifications.

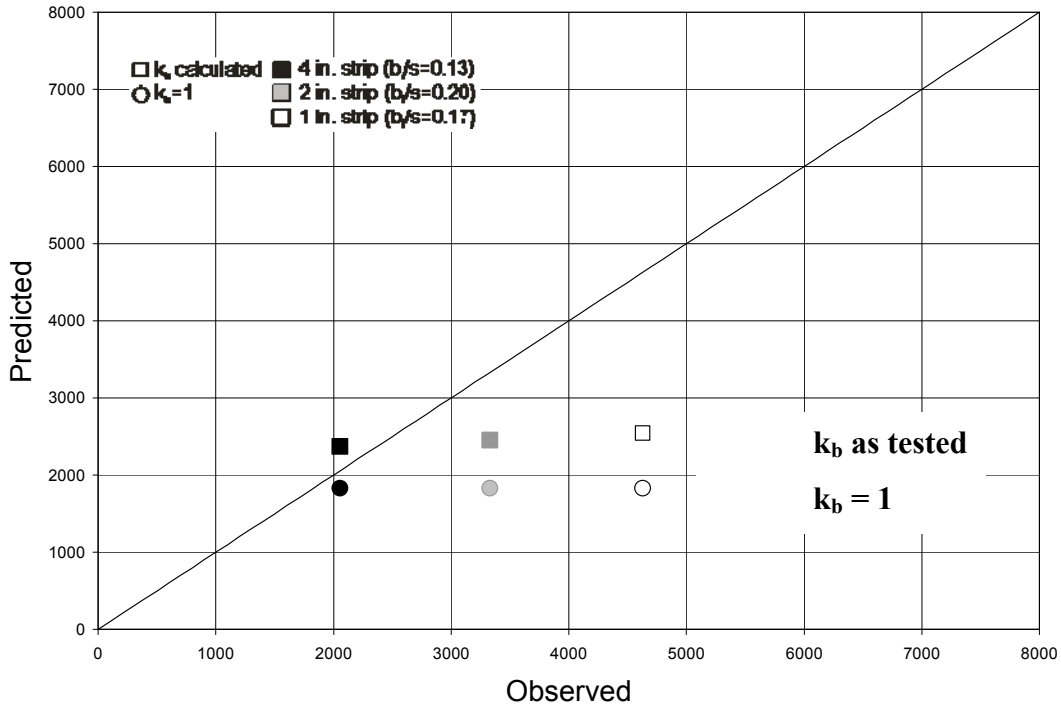

(e) Predicted vs. Observed strains based on Concrete Society TR-55 (2000)

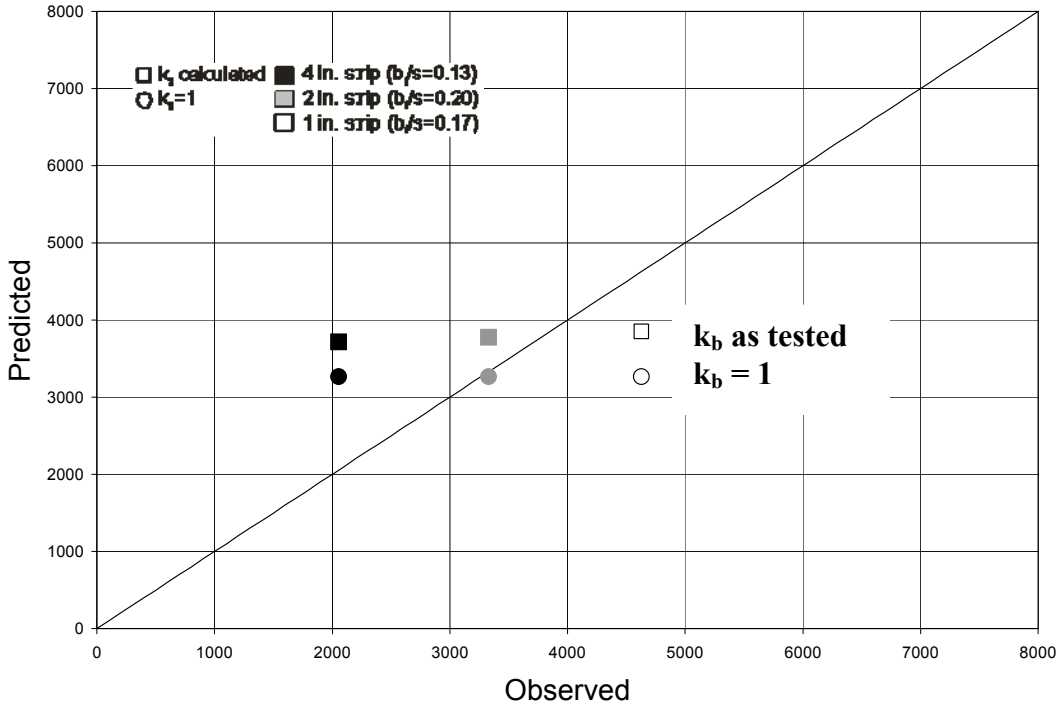

(f) Predicted vs. Observed strains based on Italian CNR DT-200 (2004)

Figure 6.3 Predicted vs. Observed strains based on various specifications.

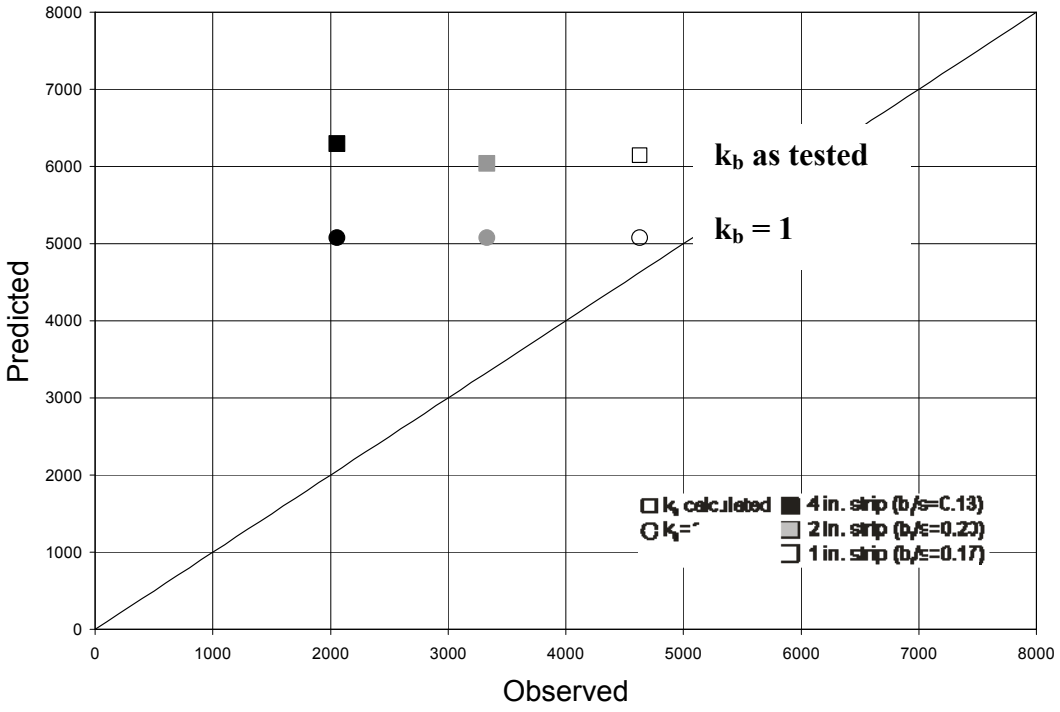

(g) Predicted vs. Observed strains based on Chinese CECS-146 (reference 2006)

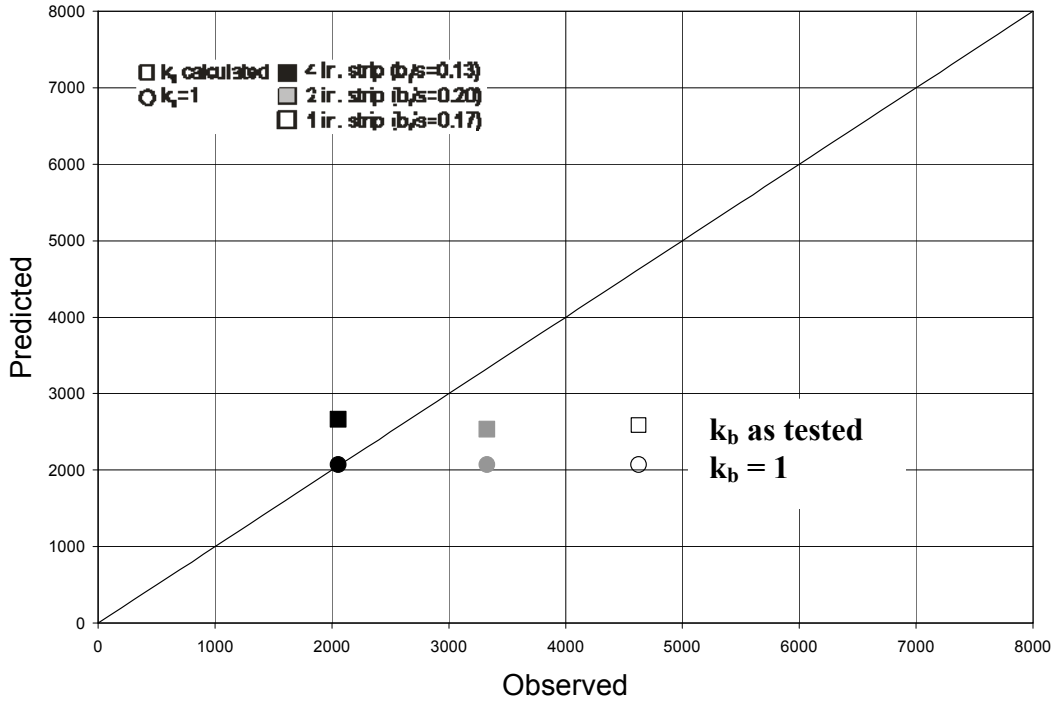

(h) Predicted vs. Observed strains based on the draft Australian Guideline (2006)

Figure 6.3 Predicted vs. Observed strains based on various specifications.

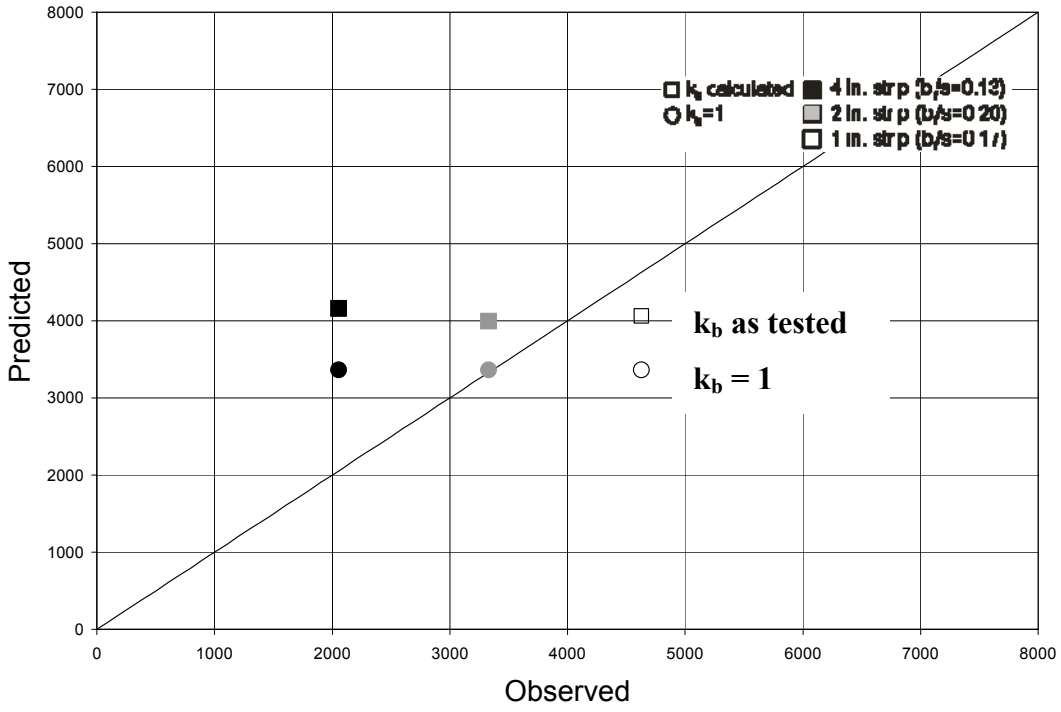

(i) Predicted vs. Observed strains based on Teng et al. (2004)

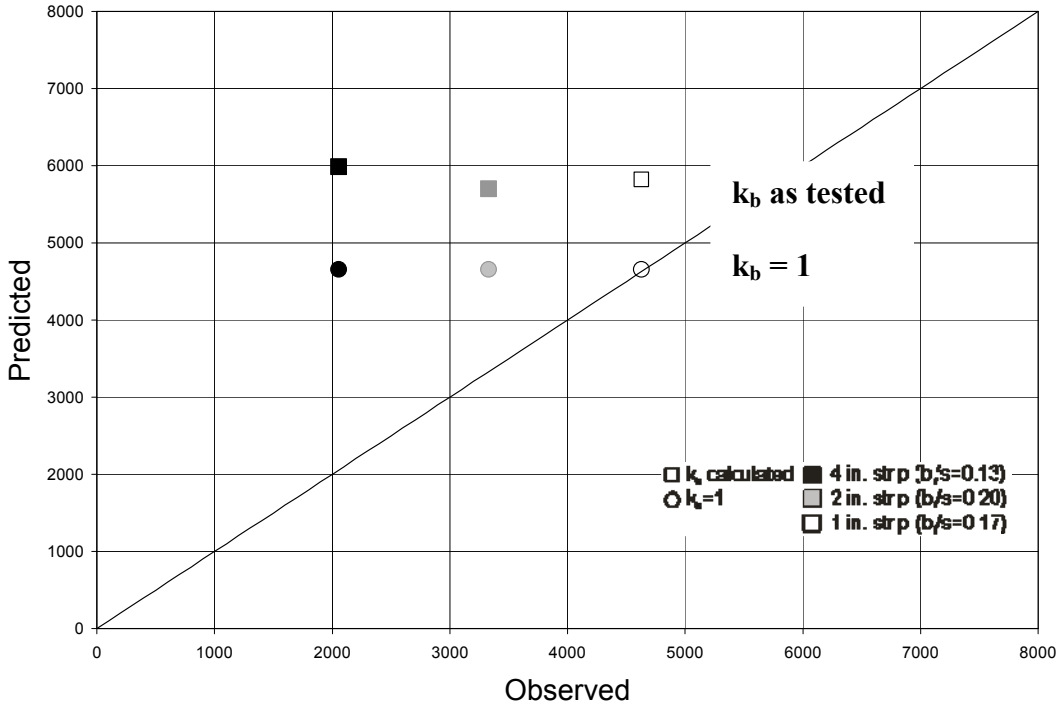

(j) Predicted vs. Observed strains based on Teng et al. (2001)

Figure 6-3 Predicted vs. Observed strains based on various specifications.

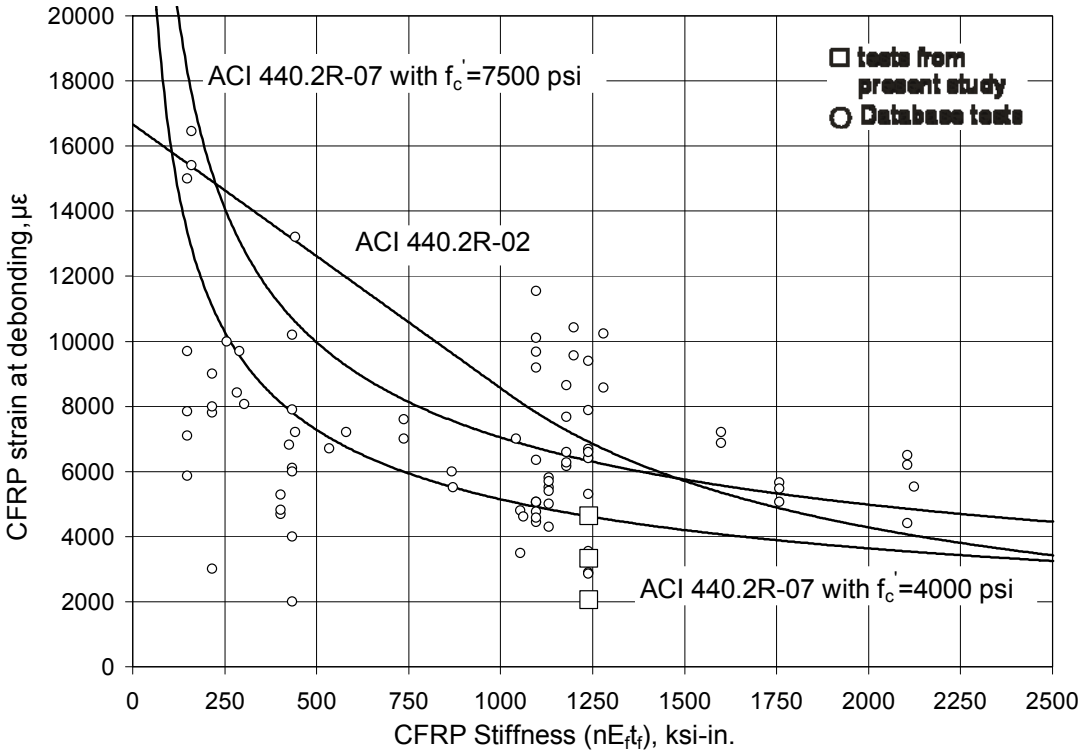

Figure 6-4 ACI 440.2R-07 and ACI 440.2R-02 provisions and extent bond data.

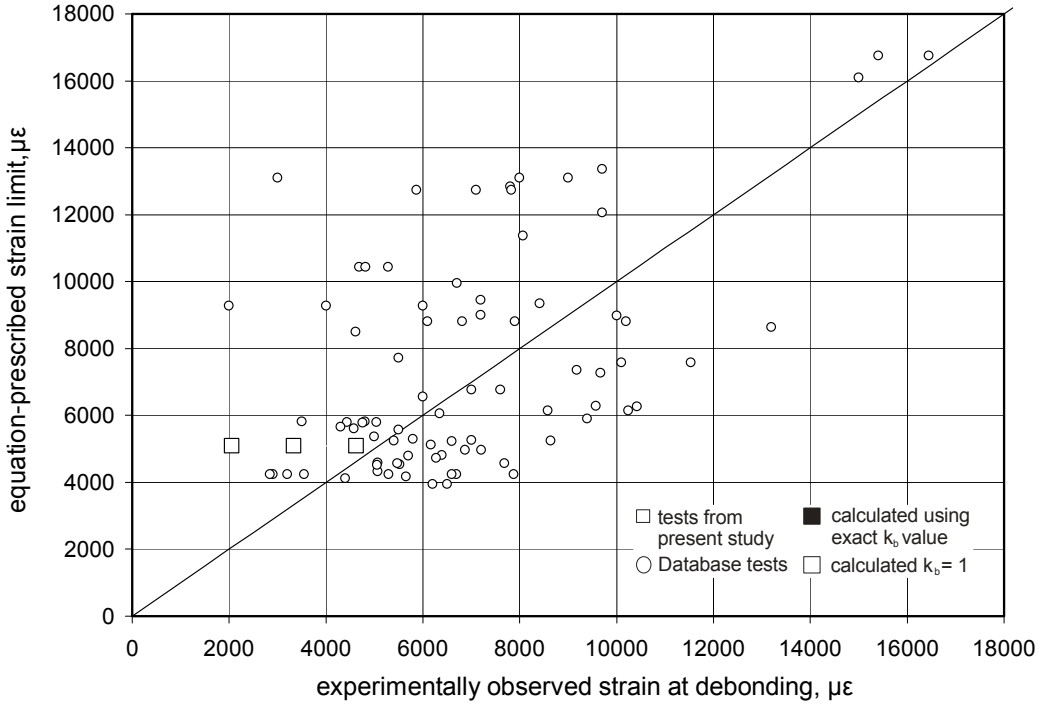

(a) Experimentally observed vs. equation prescribed strains based on ACI 440.2R-07

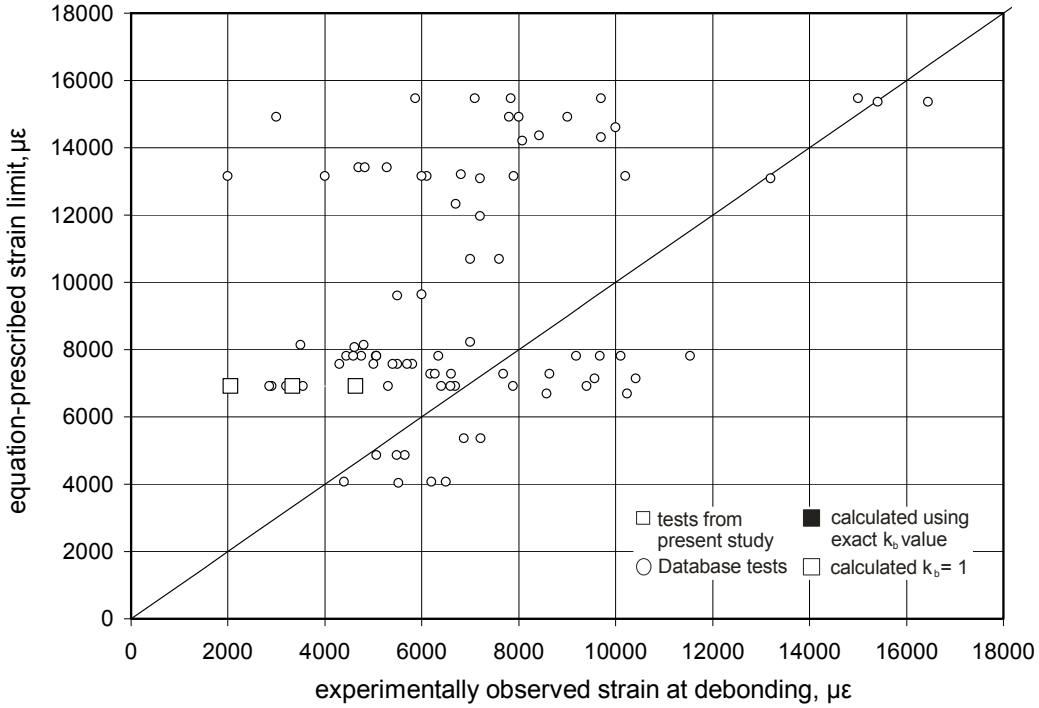

(b) Experimentally observed vs. equation prescribed strains based on ACI 440.2R-02

Figure 6.5 Experimentally observed vs. equation prescribed strains for the task group database tests.

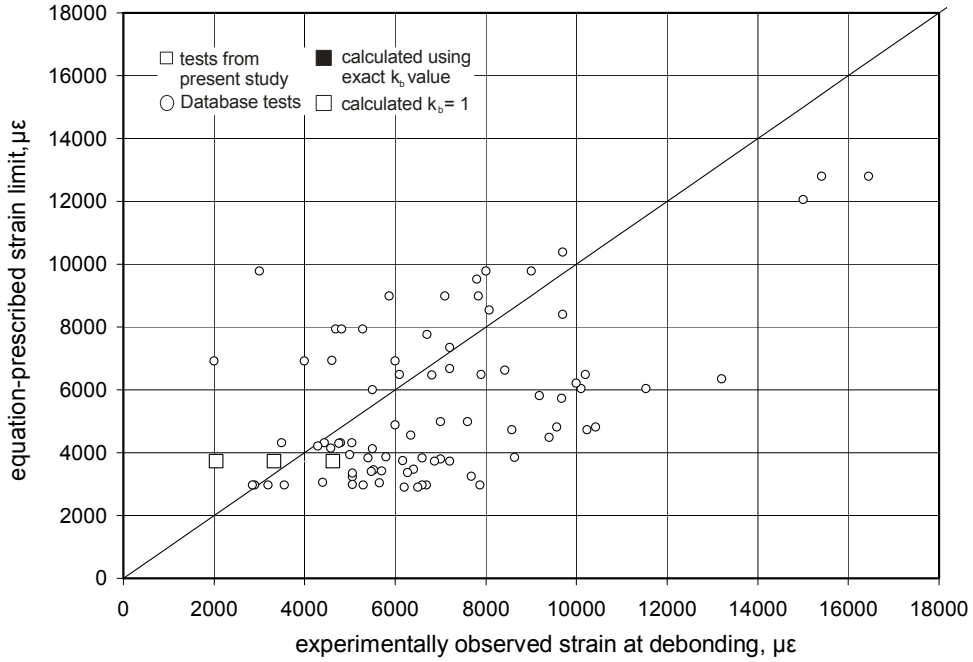

(c) Experimentally observed vs. equation prescribed strains based on fib Bulletin 14 (2001)

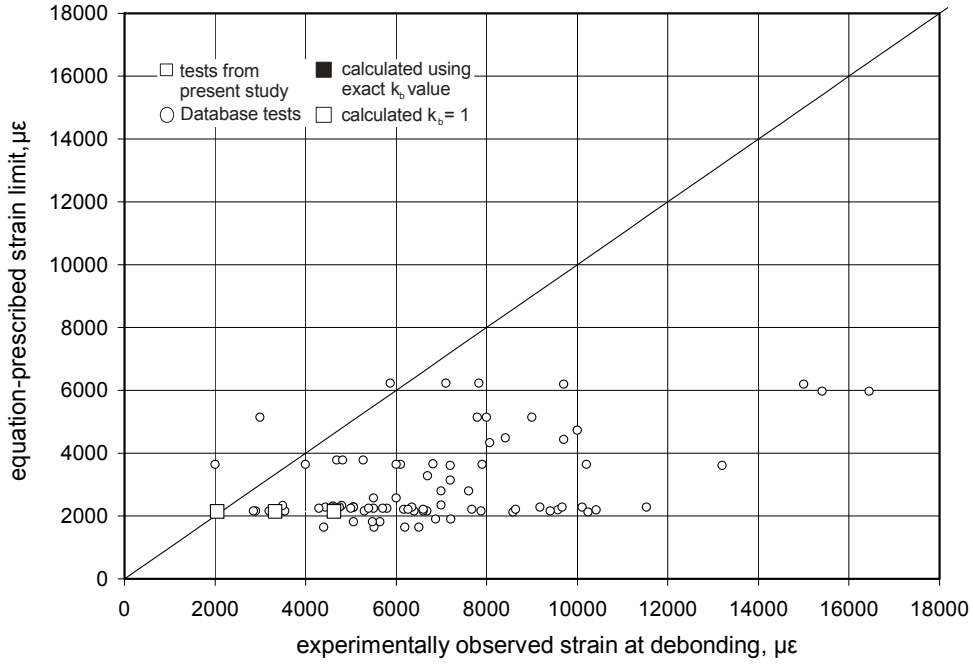

(d) Experimentally observed vs. equation prescribed strains based on JSCE Recommendations (2001)

Figure 6.5 Experimentally observed vs. equation prescribed strains for the task group database tests.

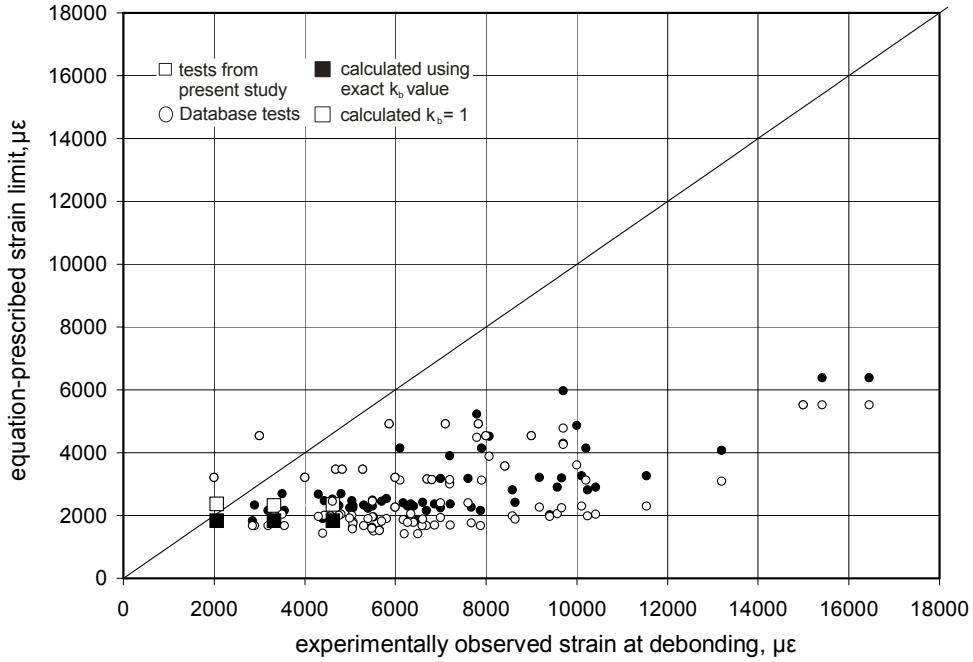

(e) Experimentally observed vs. equation prescribed strains based on Concrete Society TR-55 (2000)

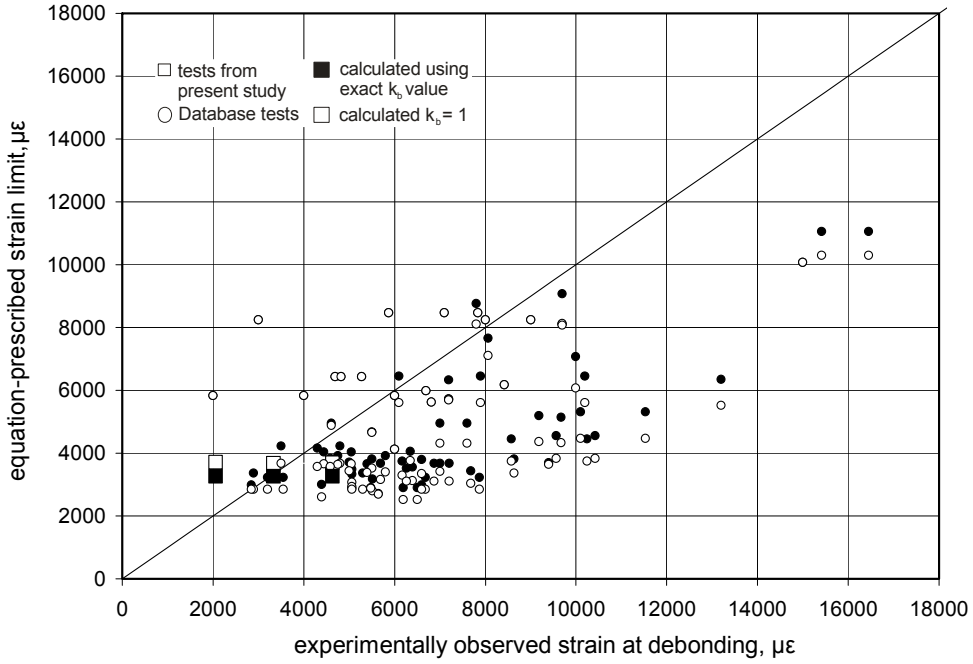

(f) Experimentally observed vs. equation prescribed strains based on Italian CNR DT-200 (2004)

Figure 6.5 Experimentally observed vs. equation prescribed strains for the task group database tests.

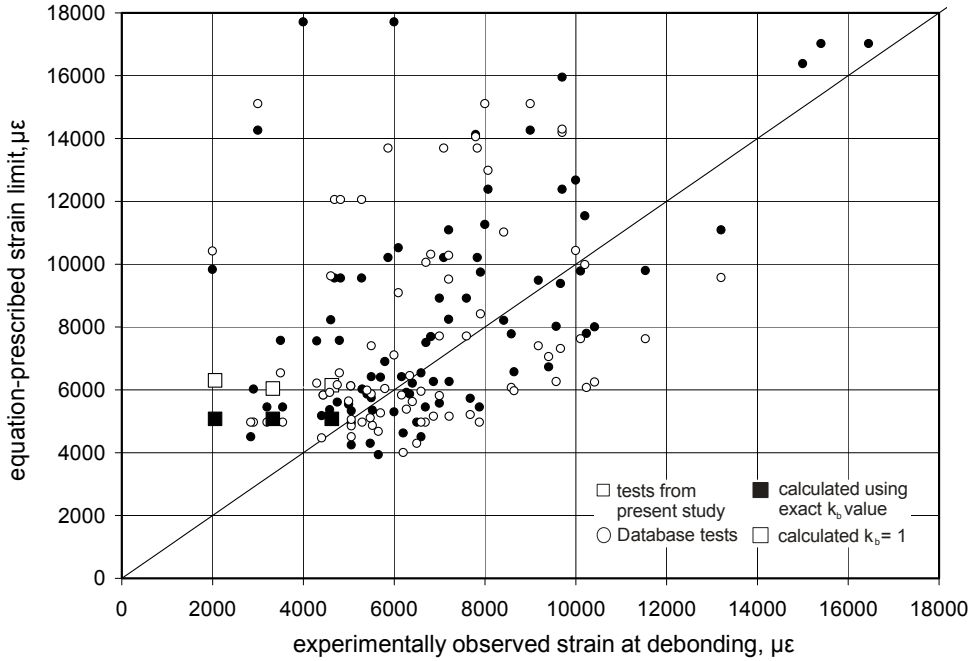

(g) Experimentally observed vs. equation prescribed strains based on Chinese CECS-146 (reference 2006)

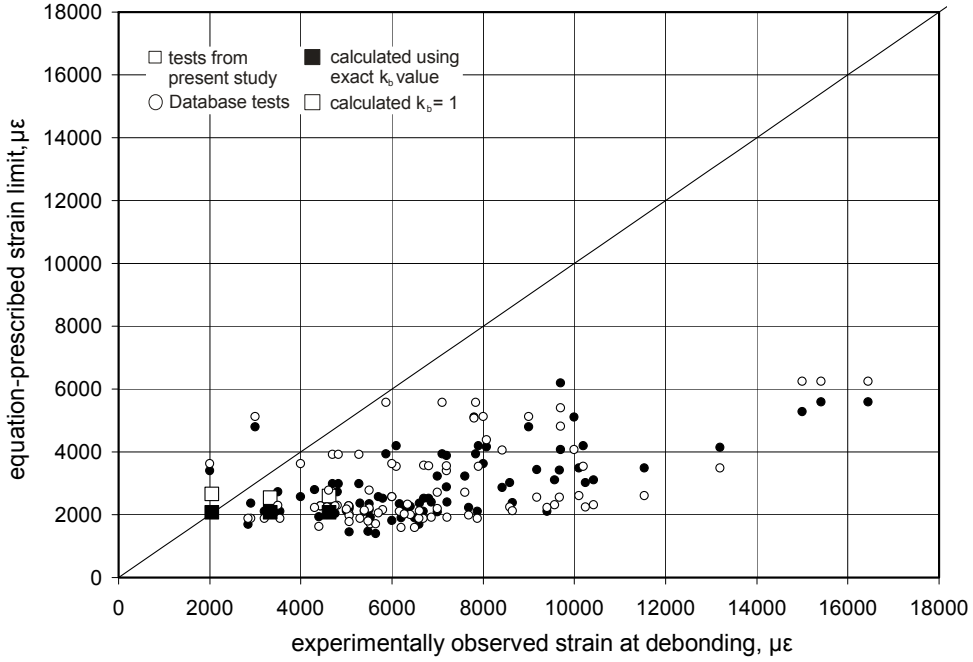

(h) Experimentally observed vs. equation prescribed strains based on the draft Australian Guideline (2006)

Figure 6.5 Experimentally observed vs. equation prescribed strains for the task group database tests.

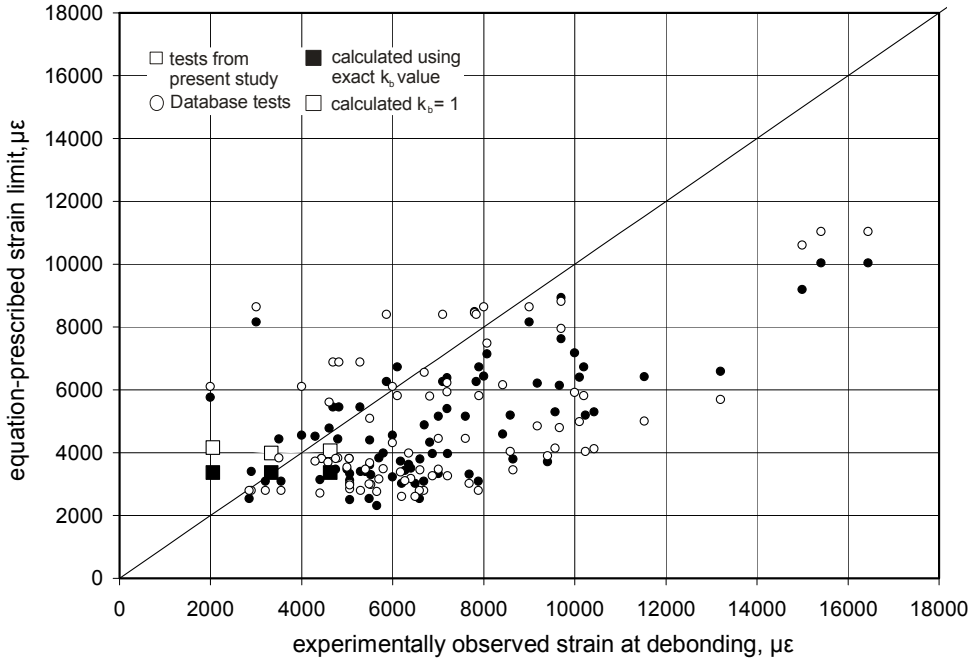

(i) Experimentally observed vs. equation prescribed strains based on Teng et al. (2004)

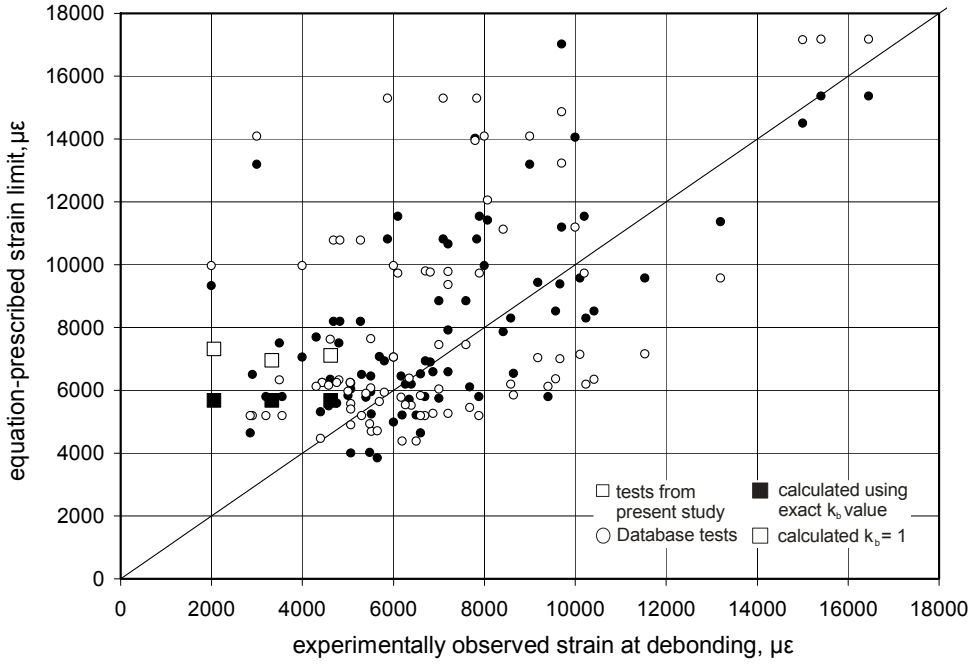

(j) Experimentally observed vs. equation prescribed strains based on Teng et al. (2001)

Figure 6-5 Experimentally observed vs. equation prescribed strains for the task group database tests.

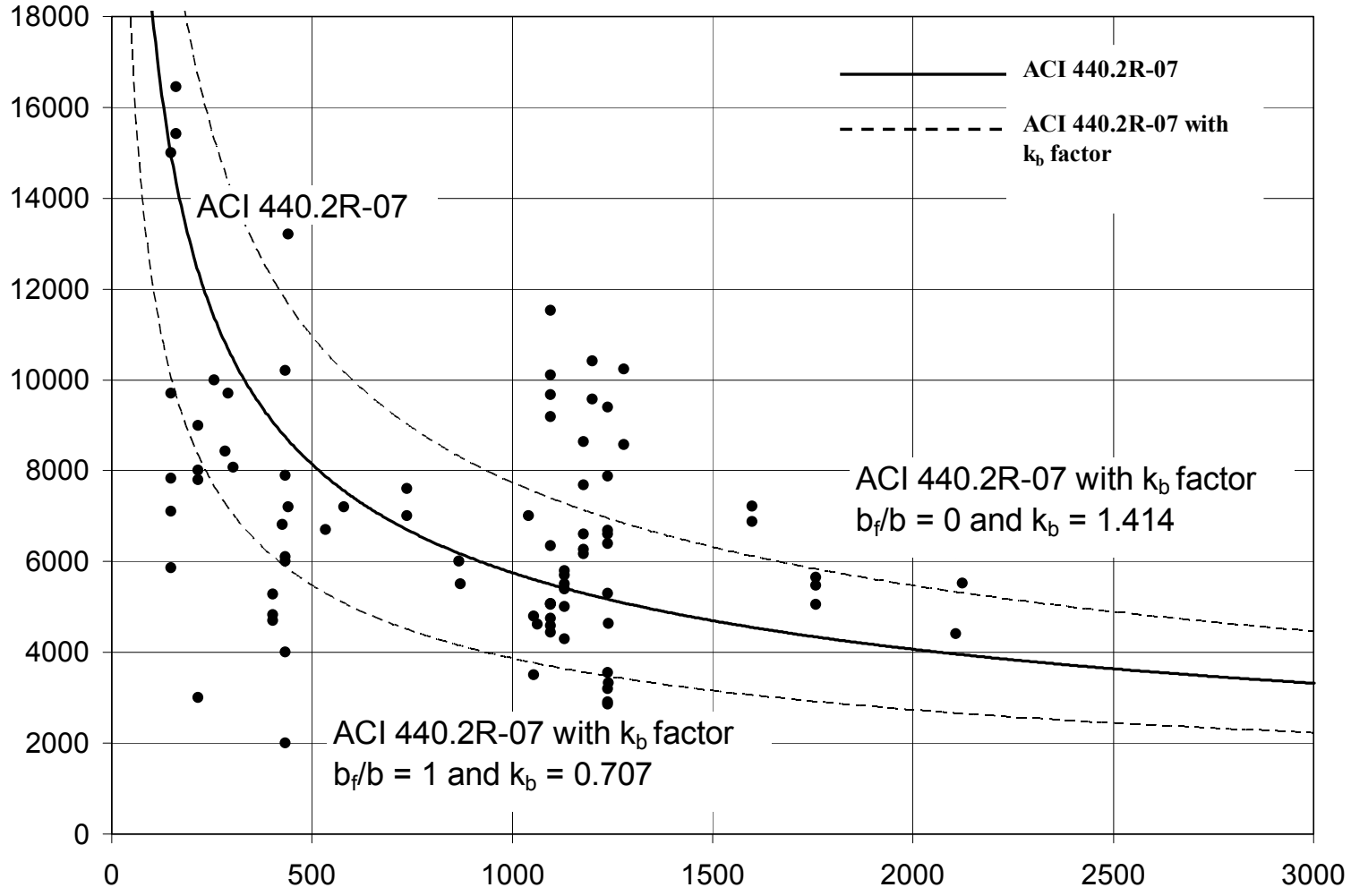

Figure 6-6 ACI 440.2R-07 provisions with and without kb factors (for two values of kb = 1.414 and 0.707) and extent bond data.

7.0 SUMMARY, CONCLUSIONS AND RECOMMENDATIONS

7.1 SUMMARY OF THE TEST PROGRAM

Ten reinforced concrete slabs were tested in the Watkins Haggart Structural Engineering laboratory at the University of Pittsburgh. The slabs were 50 in. (1270 mm) x 30 in. (762 mm) and 3 in. (76 mm) deep. Nine slabs were strengthened with various arrangements of carbon fiber reinforced polymer (CFRP) strips and one was left as an unretrofit control specimen (Control). Each slab contained seven #3 (9.5 mm diameter) longitudinal reinforcing steel bars at a spacing of 4 in. (100 mm) as primary flexural reinforcement. Nine retrofit measures were tested in order to investigate the effect of the CFRP width to spacing (b_f/s) ratio on the bond behavior. The CFRP strips were commercially available in widths of 4 in. (102 mm). These strips were cut to widths of 2 in. (51 mm) and 1 in. (25 mm) as required. The first grouping of specimens had a single 4 in. CFRP strip bonded to its soffit, a slab with two 2 in. strips and a slab with four 1 in. strips. Thus, the area of CFRP applied to each slab was constant: 0.22 in^2 (143 mm^2). The second grouping had slabs with two 4 in. strips, four 2 in. strips and eight 1 in. strips, resulting in an area of CFRP of 0.44 in^2 (286 mm^2). The third grouping had slabs with three 4 in. strips, six 2 in. strips and twelve 1 in. strips, resulting in an area of CFRP of 0.66 in^2 (428 mm^2).

All the ten specimens were tested to failure under four point bending over a clear span of 48 in. (1220 mm). The resulting shear span was 21 in. (533 mm) and the shear span-to-depth

ratio was 7. Each monotonic test was completed at failure of the specimen, defined by debonding of the CFRP strip or shear failure of the slab in the more heavily reinforced specimens.

7.2 CONCLUSIONS

The first group of specimens, having a CFRP area of 0.22 in^2 (Specimens 1x4, 2x2 and 4x1) tested in this program exhibited intermediate crack induced (IC) debonding behavior. The second (2x4, 4x2 and 8x1) and third (3x4, 6x2 and 12x1) groups failed in a shear-dominated mode. The ultimate behavior of the slabs, however, is not a critical issue in the present study. Rather the effect of the b_f/s ratio on bond performance is the focus of the work. Assessment of bond performance is easily made and compared for load levels up to that which shear became dominant. It is noted that increasing the shear capacity of a slab, rather than a beam, is difficult in practice. Thus existing shear capacity places a *de facto* limit on flexural strengthening of slab elements.

The following conclusions have been drawn from this work:

1. Increased first cracking and maximum loads (and therefore, increased flexural capacity) were observed with increasing CFRP retrofit material area.
2. Concomitantly, deflection capacity was observed to decrease with increasing CFRP retrofit area.
3. In the first group of specimens, the 2x2 and 4x1 specimens showed greater maximum load carrying capacity, greater deflection capacity and higher maximum strains when compared to 1x4 indicating that the retrofit geometry has some influence on the overall retrofit performance and that multiple thinner strips may be preferable to fewer wider

strips in terms of performance. A similar result was observed in the second and third groups of test specimens. Thus the FRP width-to-substrate width ratio, b_f/b, (in this case the FRP width-to-spacing ratio, b_f/s) is shown to affect intermediate crack induced debonding behavior.

4. The transverse strain distributions obtained for the first group of specimens indicates that the strain distribution across the CFRP strip is essentially uniform. It is believed that the instrumentation scheme used in this case was insufficiently refined to capture the expected shear lag effect.

Considering the IC-debonding dominated behavior of the first group of specimens (1x4, 2x2 and 4x1), the following conclusions with regard to modeling such behavior are made.

5. The present ACI 440.2R-07 equation is non conservative, overestimating the strain at which debonding occurs. However, this equation is an improvement over ACI 440.2R-02 which is highly non conservative. This observation is not as critical as it may seem in as far as the ACI 440.2R-07 equation represents a median response rather than a lower bound behavior. The ACI 440.2R-07 recommendation is based on the format of Teng et al. recommendations without considering the effect of b_f/b ratio; that is: k_b is taken as unity.
6. Similar predictions of the maximum allowable strain to mitigate IC debonding, ε_{fub}, were found for the recommendations made by ACI 440.2R-07, ACI 440.2R-02, Teng et al. (2007), Teng et al. (2001) and Chinese CECS-146. In all these cases the prescribed equations provided non-conservative estimates of the FRP strain to cause debonding. ACI 440.2R-02, Teng et al. (2002) and Chinese CECS-146, in particular, overestimate the

debonding strain. These recommendations must be understood to represent empirically derived median, rather than lower bound behavior.

7. The Concrete Society TR-55, Italian CNR DT 200, fib Bulletin 14 and Australian guidelines resulted in non conservative estimates of the maximum allowable strain, ε_{fub}. These equations underestimate the strain at which debonding initiates and are understood to represent expected lower bound debonding behavior; thus this observation should be expected.
8. Correlation coefficients have been calculated based on the ACI 440 Bond Task Group Database between the experimentally-observed debonding strains and the equation-prescribed strains for each of the specifications considered. It was seen that improved correlation is obtained when the retrofit geometry parameter, k_b is considered rather than neglected ($k_b = 1$). Teng et al. (2004) recommendations were fund to have the best correlation with experimental data (Section 2.5.10).
9. For cases where $k_b = 1$, the ACI 440.2R-07, fib Bulletin 14 and Teng et al. (2004) recommendations result in the best correlation with database results, however, as noted above, the correlation improves when k_b is calculated using the appropriate value of b_f/b.
10. Correlation coefficients for the experimentally-observed strains and equation-prescribed strains were obtained using the ACI 440.2R-07 recommendations modified by the k_b factors prescribed by Teng et al. (2001 and 2004). It was observed that better correlation was obtained using the k_b factor recommended by Teng et al. (2001) given in Equation 2.24.
11. Fit coefficients, α were obtained for the ACI 440.2R-07 equation with and without the k_b factor proposed by Teng et al. (2001). When k_b is neglected as in the present ACI

440.2R-07 recommendations, $\alpha = 0.41$ yields the best fit to the mean data. When k_b is considered, this value is decreased marginally to 0.39 to fit the mean data. It was observed that the correlation is improved in the latter case as represented by a reduction in the standard deviation of the ratio of observed to predicted results. It is therefore recommended that Equation 7.1 with a value of $\alpha = 0.4$ be adopted. It is noted that reducing the precision by setting $\alpha = 0.4$ does not affect predicted results in any meaningful manner and better reflects the expected precision of such calculations.

$$\varepsilon_{fub} = \alpha k_b \sqrt{\frac{f_c'}{nE_f t_f}} = 0.4 \sqrt{\frac{2-(b_f/b)}{1+(b_f/b)}} \sqrt{\frac{f_c'}{nE_f t_f}} \qquad (7.1)$$

Although not a focus of the present work, the effect of calibrating empirical design equations using an existing database is shown to be effected by the size of the specimens included in the database. Reduced correlation coefficients and increased fit coefficients result from excluding small-scale ($h < 10$ in. (250 mm)) test results from the dataset used to calculate the coefficients in this study. This observation indicates the presence of a size effect. The following conclusions are drawn in this regard:

12. Reduced correlation at larger scales is a typically observed size effect as control of specimen parameters is improved with smaller specimens.
13. The present guidance: using $\alpha = 0.4$ is conservative when applied to larger specimens having realistic dimensions. Nonetheless, caution should be practiced when using small-scale tests to calibrate such predictive equations.

7.3 RECOMMENDATIONS

The primary recommendation coming from this work is that ACI Committee 440 should adopt a k_b factor, based on the values b_f/b or b_f/s, into their present equations for debonding strain. Equation 7.1 is proposed for adoption.

The following recommendations for further research are proposed based on the outcomes of the present work:

7.3.1 Investigation of Effect of Specimen Geometry

There remain few studies that have considered specimens other than simply supported beams. Some areas that warrant further study include:

1. The effects of inflection behavior in continuous spans on FRP debonding behavior and required "development".
2. Effects of specimen size (the "size effect"); data is particularly required for large-scale applications approximating bridge structures.
3. Effects and methods of anchoring FRP at "fixed" supports.

7.3.2 Shear Lag Effects in Adhesive-Applied FRP Strips

Based on the discussion in Section 2.6.1, shear lag effects may be expected to be significant in bonded FRP applications. The higher shear at the strip edge results in higher bond stresses and thus debonding may be expected to be a progressive phenomena, propagating transversely from the edge of the strip inwards and longitudinally from a stress raiser (concrete

crack) in the direction of decreasing moment (see Section 2.2). This effect may explain the generally non-conservative estimates of debonding behavior when average bond stresses are considered. It is recommended that a study be undertaken to investigate this effect. To obtain useful data, thin strain gage widths, located at the FRP edge will be required. The use of photo-elastic methods may be appropriate to qualify the effect. Dense instrumentation patterns are required to capture this localized effect.

APPENDIX A

ACI 440 BOND TASK GROUP DATABASE

Citation	Specimen	Specimen Properties					Tension Steel		Comp. Steel		Transverse Steel		FRP Properties						Adhesive Properties			Test Results		
		h	b	L	a	f_c'	p_t	f_y	p_c	f_y	p_v	f_y	E_f	t_f	n	b_f	ε_{fu}	L_b	E_a	t_a	ε_{ua}	V	M	ε_{fub}
		in.	In.	in.	in.	psi		ksi		ksi		ksi	ksi	in.	#	in.	με	in.	ksi	in.	με	kips	k-ft	με
10	F10	9.45	6.1	110	43.3	11600	0.01	77	0.01	77	na	na	22475	0.05	1	4.72	15484	66.9	na	na	na	18.45	1830	2480
10	F5	9.45	6.1	110	43.3	11600	0.01	77	0.01	77	na	na	22475	0.05	1	4.72	15484	79.9	na	na	na	22.5	2819	3820
10	F6	9.45	6.1	110	43.3	11600	0.01	77	0.01	77	na	na	22475	0.05	1	4.72	15484	79.9	na	na	na	23.18	2915	3950
10	F7	9.45	6.1	110	43.3	11600	0.01	77	0.01	77	na	na	22475	0.05	1	4.72	15484	73.9	na	na	na	21.94	2192	2970
10	F8	9.45	6.1	110	43.3	11600	0.01	77	0.01	77	na	na	22475	0.05	1	4.72	15484	73.9	na	na	na	14.4	Na	2780
10	F9	9.45	6.1	110	43.3	11600	0.01	77	0.01	77	na	na	22475	0.05	1	4.72	15484	66.9	na	na	na	13.95	Na	2330
12	B.8	5.91	3	59.1	25.6	5220	0	72	na	72	na	na	23200	0.05	1	1.97	1940	63	1.81	0.08	4000	6.075	13	4844
12,13,14,15	B.9	5.91	3	59.1	25.6	4959	0.01	28	na	28	na	na	23200	0.05	1	1.97	1940	63	1.81	0.08	4000	11.25	24	6905
12,13,14,15	B.10 (2)	5.91	3	59.1	25.6	4959	0	72	na	72	na	na	23200	0.05	1	1.97	1940	63	1.81	0.08	4000	1.935	4	4972
12,13,14,15	B.11	5.91	3	59.1	25.6	4698	0	72	na	72	na	na	23200	0.05	1	1.97	1940	43.3	1.81	0.08	4000	3.015	6	1841
17	B-04/S	11.8	5.9	118	31.5	4132.5	0	61	0	61	na	na	23925	0.05	1	3.15	17000	100	650	na	10000	13.5	35	2500
17	B-04/S L2.1	11.8	5.9	82.7	31.5	4132.5	0	61	0	61	na	na	23925	0.05	1	3.15	17000	100	650	na	10000	10.13	27	2500
17	B-04/M	11.8	5.9	118	31.5	4306.5	0	61	0	61	na	na	23925	0.05	1	3.15	17000	100	650	na	10000	13.5	35	2680
17	B-04/M L2.1	11.8	5.9	82.7	31.5	4306.5	0	61	0	61	na	na	23925	0.05	1	3.15	17000	100	650	na	10000	13.5	35	2680
17	B-06/S	11.8	5.9	118	31.5	4683.5	0.01	71	0	61	na	na	23925	0.05	1	3.15	17000	100	650	na	10000	15.75	41	3430
17	B-06/S	11.8	5.9	118	31.5	4683.5	0.01	71	0	61	na	na	23925	0.05	1	3.15	17000	100	650	na	10000	16.31	43	3430
20	A950	3.74	na	na	9.84	4654.5	na	56	na	na	na	na	26245	0.05	1	3.15	17000	na	na	na	na	na	na	1685
20	A1100	3.74	na	na	9.84	4654.5	na	56	na	na	na	na	26245	0.05	1	3.15	17000	na	na	na	na	na	na	1848
20	A1150	3.74	na	na	9.84	4654.5	na	56	na	na	na	na	26245	0.05	1	3.15	17000	na	na	na	na	na	na	1622
20	B1	3.66	na	na	9.84	6467	na	58	na	na	na	na	26245	0.05	1	3.15	17000	na	na	na	na	na	na	2400
20	B2	3.94	na	na	9.84	6467	na	58	na	na	na	na	26245	0.05	1	3.15	17000	na	na	na	na	na	na	2250
20	C5	5.31	na	na	9.45	3639.5	na	56	na	na	na	na	26245	0.05	1	3.15	17000	na	na	na	na	na	na	2116
20	C10	4.92	na	na	9.45	3639.5	na	56	na	na	na	na	26245	0.05	1	3.15	17000	na	na	na	na	na	na	1750
20	C20	4.13	na	na	9.45	3639.5	na	56	na	na	na	na	26245	0.05	1	3.15	17000	na	na	na	na	na	na	1750
25	GS1-I	5.95	12	78.7	39.4	3271.2	0	50	na	na	na	na	2972	0.05	1	3.53	13122	70.9	na	na	na	2.25	8	9700
11	C-3	10	6	96.1	33	8004	0.01	60	0	60	na	na	7141	0.07	1	5.98	14000	58	na	na	na	31.05	43	6700
3	C1	16	8	118	48	5089.5	0	64	0	64	na	na	8990	0.04	2	1.97	12000	108	na	na	na	32.33	65	7600
3	C2	16	8	118	48	5089.5	0	64	0	64	na	na	8990	0.04	2	1.97	12000	108	na	na	na	28.33	57	7000
18	B-083m	11.8	5.9	165	55.1	4988	0.01	64	0	64	na	na	9483	0.01	3	5.91	15000	161	650	na	10000	10.35	48	6810
18	B-083mb	11.8	5.9	165	55.1	3741	0.01	64	0	64	na	na	9483	0.01	2	5.91	15000	161	650	na	10000	13.84	64	8420
22	A5	5.91	7.9	82.7	29.5	7830	0.01	83	0	83	na	na	18415	0.03	1	5.91	12063	52.4	na	na	na	14.22	18	7200

Citation	Specimen	Specimen Properties					Tension Steel		Comp. Steel		Transverse Steel		FRP Properties						Adhesive Properties			Test Results		
		h	b	L	a	f_c'	p_t	f_y	p_c	f_y	p_v	f_y	E_f	t_f	n	b_f	ε_{fu}	L_b	E_a	t_a	ε_{ua}	V	M	ε_{fub}
		in.	In.	in.	in.	psi		ksi		ksi		ksi	ksi	in.	#	in.	με	in.	ksi	in.	με	kips	k-ft	με
22	B3	5.91	7.9	82.7	29.5	7830	0.01	83	0	83	na	na	18415	0.02	1	5.91	12063	52.4	na	na	na	12.42	15	9700
22	B6	5.91	7.9	82.7	29.5	7830	0.01	83	0	83	na	na	18415	0.05	1	5.91	12063	52.4	na	na	na	15.66	19	5500
15,16,4,5	LD3BL	3.35	17	63	21.7	7134	0	83	na	48	na	na	21750	0.06	1	1.26	14000	59.1	na	na	na	3.728	7	9570
15,16,4,5	LD4BL	3.19	18	63	21.7	7105	0	83	na	48	na	na	21750	0.06	1	1.26	14000	59.1	na	na	na	3.638	7	10420
24	A3.1	11.8	5.5	0	35.4	4350	0.01	63	na	63	na	na	22040	0.05	1	3.15	15132	na	na	na	na	na	na	7000
21	CS	10	6	181	90.6	4335.5	0.01	65	na	na	na	na	22475	0.06	1	1.97	18000	173	300	na	32500	11	83	6400
1	CS	32.5	14	348	174	6525	0.03	53	na	na	na	na	22475	0.06	1	7.87	18000	336	300	na	32500	185.2	2685	9400
23	L1	9.84	5.9	179	89.3	3378.5	0.01	62	na	na	na	na	22475	0.06	1	0.98	18000	171	323	0.06	63000	8.967	67	5300
23	L2	9.84	5.9	179	89.3	3378.5	0.01	62	na	na	na	na	22475	0.06	1	1.97	18000	171	323	0.06	63000	9.968	74	6688
23	L2x1	9.84	5.9	179	89.3	3378.5	0.01	62	na	na	na	na	22475	0.06	1	1.97	18000	171	323	0.06	63000	10.24	76	7878
23	L4	9.84	5.9	179	89.3	3378.5	0.01	62	na	na	na	na	22475	0.06	1	3.94	18000	171	323	0.06	63000	11.66	87	6595
23	H1	9.84	5.9	179	89.3	3378.5	0.01	62	na	na	na	na	22475	0.06	1	0.98	18000	171	650	0.06	10000	8.477	63	2900
23	H2	9.84	5.9	179	89.3	3378.5	0.01	62	na	na	na	na	22475	0.06	1	1.97	18000	171	650	0.06	10000	9.798	73	3550
23	H2x1	9.84	5.9	179	89.3	3378.5	0.01	62	na	na	na	na	22475	0.06	1	1.97	18000	171	650	0.06	10000	10.16	76	3200
23	H4	9.84	5.9	179	89.3	3378.5	0.01	62	na	na	na	na	22475	0.06	1	3.94	18000	171	650	0.06	10000	11.08	82	2850
3	D1	16	8	118	48	5394	0	64	0	64	na	na	22475	0.05	1	1.97	14000	108	na	na	na	28.82	58	3500
3	D2	16	8	118	48	5394	0	64	0	64	na	na	22475	0.05	1	1.97	14000	108	na	na	na	30.13	60	4800
3	D3	16	8	118	48	5394	0	64	0	64	na	na	22475	0.05	2	1.97	14000	108	na	na	na	35.78	na	4400
3	D4	16	8	118	48	4973.5	0	64	0	64	na	na	22475	0.05	2	1.97	14000	108	na	na	na	42.3	na	6500
3	D5	16	8	118	48	4973.5	0	64	0	64	na	na	22475	0.05	2	1.97	14000	78	na	na	na	40.73	na	6200
10	F3	9.45	6.1	110	43.3	11600	0.01	77	0.01	77	na	na	22475	0.05	1	4.72	15484	118	na	na	na	24.95	3402	4610
26	SC	11.8	5.9	na	39.4	6612	0.02	58	na	58	na	na	22475	0.05	2	1.97	15000	0	na	na	na	na	80	5520
26	RA	11.8	5.9	na	39.4	6612	0.02	58	na	58	na	na	23200	0	4	5.31	15000	0	na	na	na	na	67	4690
26	RB	11.8	5.9	na	39.4	6612	0.02	58	na	58	na	na	23200	0	4	5.31	15000	0	na	na	na	na	70	4822
26	RC	11.8	5.9	na	39.4	6612	0.02	58	na	58	na	na	23200	0	4	5.31	15000	0	na	na	na	na	72	5281
15,16,4,5	LA4S	3.15	17	63	21.7	8743.5	0	92	na	48	na	na	23200	0.05	1	1.26	20000	59.1	na	na	na	3.443	6	9670
15,16,4,5	LB2S	3.35	17	63	21.7	8961	0	92	na	48	na	na	23200	0.05	1	1.26	20000	59.1	na	na	na	3.764	7	9180
15,16,4,5	LC1S	3.19	17	63	21.7	9512	0	92	na	48	na	na	23200	0.05	1	1.26	20000	59.1	na	na	na	3.836	7	10105
15,16,4,5	LC2S	3.35	17	63	21.7	9526.5	0	92	na	48	na	na	23200	0.05	1	1.26	20000	59.1	na	na	na	4.241	8	11534
15,16,4,5	LE3I	3.23	17	63	21.7	7279	0	81	na	48	na	na	23200	0.06	1	1.26	15000	59.1	na	na	na	3.461	6	8580
15,16,4,5	LE4I	3.07	17	63	21.7	7279	0	81	na	48	na	na	23200	0.06	1	1.26	15000	59.1	na	na	na	3.596	7	10240

Citation	Specimen	Specimen Properties					Tension Steel		Comp. Steel		Transverse Steel		FRP Properties						Adhesive Properties			Test Results		
		h	b	L	a	f_c'	p_t	f_y	p_c	f_y	p_v	f_y	E_f	t_f	n	b_f	ε_{fu}	L_b	E_a	t_a	ε_{ua}	V	M	ε_{fub}
		in.	In.	in.	in.	psi		ksi		ksi		ksi	ksi	in.	#	in.	με	in.	ksi	in.	με	kips	k-ft	με
12,13,14,15	A.3	5.91	3.9	59.1	25.6	5568	0.01	75	na	69	0.01	100	23200	0.05	1	1.97	1940	59.1	1.81	0.1	4000	5.85	12	5047
12,13,14,15	A.4	5.91	3.9	59.1	25.6	5568	0.01	75	na	69	0.01	100	23200	0.05	1	1.97	1940	46.9	1.81	0.1	4000	4.59	10	4439
12,13,14,15	B.3	5.91	3	59.1	25.6	6061	0	72	na	72	na	na	23200	0.05	1	1.97	1940	63	1.81	0.1	4000	7.211	15	6347
12,13,14,15	B.5	5.91	3	59.1	25.6	5524.5	0	72	na	72	na	na	23200	0.05	1	1.97	1940	63	1.81	0.1	4000	5.85	13	4754
12,13,14,15	B.7	5.91	3	59.1	25.6	5220	0	72	na	72	na	na	23200	0.05	1	1.97	1940	58.3	1.81	0.1	4000	5.625	12	4581
12,13,14,15	C.4	5.91	5.9	55.5	23.8	3494.5	0.02	74	na	74	na	na	23200	0.05	1	1.97	1940	59.1	1.81	0.1	4000	18.36	36	5063
12,13,14,15	C.5	5.91	5.9	55.5	23.8	3088.5	0.02	74	na	74	na	na	23200	0.05	1	1.97	1940	55.1	1.81	0.1	4000	15.3	30	5063
17	B-08/S	11.8	5.9	118	31.5	4901	0.01	71	0	61	na	na	23925	0.05	1	3.15	17000	106	650	na	10000	20.25	53	5000
17	BO-08/S	11.8	5.9	118	31.5	5292.5	0.01	71	0	61	na	na	23925	0.05	1	3.15	17000	106	650	na	10000	20.25	53	5500
17	BF-04/0.5S	11.8	5.9	118	59.1	4785	0	65	0.01	64	na	na	23925	0.05	1	1.57	17000	106	650	na	10000	10.8	53	5800
17	BF-06/S	11.8	5.9	118	59.1	4712.5	0.01	71	0	68	na	na	23925	0.05	1	3.15	17000	106	650	na	10000	19.24	95	5400
25	CP1-I	5.93	12	78.7	39.4	3920.8	0.01	50	na	Na	na	na	23925	0.05	1	1.97	16970	70.9	na	na	na	4.489	15	5700
25	CP2-I	5.98	12	78.7	39.4	5463.6	0.01	50	na	na	na	na	23925	0.05	1	1.97	16970	70.9	na	na	na	3.956	13	4300
18	B-08S	11.8	5.9	165	55.1	4683.5	0.01	72	0	76	na	na	24940	0.05	1	1.97	17000	161	650	na	10000	10.58	49	6170
18	B-08Sk	11.8	5.9	165	55.1	4901	0.01	72	0	76	na	na	24940	0.05	1	1.97	17000	161	650	na	10000	11.48	53	8640
18	B-08Sm	11.8	5.9	165	55.1	4857.5	0.01	72	0	76	na	na	24940	0.05	1	1.97	17000	161	650	na	10000	11.48	53	6600
18	B-08Smb	11.8	5.9	165	55.1	3726.5	0.01	63	0	76	na	na	24940	0.05	1	1.97	17000	161	650	na	10000	12.83	59	7680
18	BO-08Smb	11.8	5.9	165	55.1	3973	0.01	63	0	76	na	na	24940	0.05	1	1.97	17000	161	650	na	10000	12.38	59	6270
4,5	V4	7.09	4.7	70.9	29.5	5945	0	77	na	81	na	na	29000	0.06	1	0.79	11000	68.5	na	na	na	4.412	11	6870
4,5	V6	7.09	4.7	70.9	29.5	5945	0	77	na	81	na	na	29000	0.06	1	0.79	11000	68.5	na	na	na	4.592	12	7210
18	B-08M	11.8	5.9	165	55.1	5408.5	0.01	72	0	76	na	na	31900	0.06	1	4.72	12400	161	650	na	10000	15.75	72	5060
18	B-08Mk	11.8	5.9	165	55.1	4640	0.01	72	0	76	na	na	31900	0.06	1	4.72	12400	161	650	na	10000	16.88	77	5650
18	B-08Mn	11.8	5.9	165	55.1	5539	0.01	72	0	76	na	na	31900	0.06	1	4.72	12400	161	650	na	10000	17.1	79	5480
3	A1	14	8	106	41.9	5089.5	0.01	64	0	64	na	na	33350	0.01	2	1.97	15000	42	na	na	na	26.93	47	7900
3	A2	14	8	106	41.9	5089.5	0.01	64	0	64	na	na	33350	0.01	2	1.97	15000	50.1	na	na	na	28.33	50	6100
3	A3	14	8	106	41.9	5089.5	0.01	64	0	64	na	na	33350	0.01	2	1.97	15000	82	na	na	na	31.12	54	10200
3	A4	14	8	106	41.9	5394	0.01	64	0	64	na	na	33350	0.01	1	3.94	15000	52	na	na	na	29.03	51	7800
3	B1	14	8	106	41.9	5394	0.01	64	0	64	na	na	33350	0.01	2	2.95	15000	92	na	na	na	29.84	53	7200
3	B5	14	8	106	41.9	4973.5	0.01	64	0	64	na	na	33350	0.01	2	1.97	15000	70.1	na	na	na	29.25	na	13200
2	S-T2L2	9.45	59	177	59.1	5626	0.01	81	0.01	81	na	na	33350	0.03	1	59.1	15217	114	na	na	na	160.9	396	6000
2	S-T3L1	9.45	35	177	59.1	5626	0.01	81	0	81	na	na	33350	0.01	1	35.4	15217	114	na	na	na	64.13	158	8000

Citation	Specimen	Specimen Properties					Tension Steel		Comp. Steel		Transverse Steel		FRP Properties						Adhesive Properties			Test Results		
		h	b	L	a	f_c'	p_t	f_y	p_c	f_y	p_v	f_y	E_f	t_f	n	b_f	ε_{fu}	L_b	E_a	t_a	ε_{ua}	V	M	ε_{fub}
		in.	In.	in.	in.	psi		ksi		ksi		ksi	ksi	in.	#	in.	με	in.	ksi	in.	με	kips	k-ft	με
2	S-T3L2	9.45	59	177	59.1	5626	0	81	0	81	na	na	33350	0.01	1	35.4	15217	114	na	na	na	76.5	189	9000
2	S-T4L1	9.45	59	177	59.1	5626	0.02	81	0	81	na	na	33350	0.01	1	35.4	15217	114	na	na	na	146.3	360	3000
2	S-T4L2	9.45	59	177	59.1	5626	0.02	81	0	81	na	na	33350	0.01	1	35.4	15217	114	na	na	na	157.5	388	2000
2	C-T2L2	9.45	59	236	59.1	5626	0.01	81	0.01	81	na	na	33350	0.01	1	59.1	15217	114	na	na	na	56.25	369	4000
2	C-T4L2	9.45	59	236	59.1	5626	0.01	81	0	81	na	na	33350	0.01	1	59.1	15217	114	na	na	na	50.85	334	6000
27	BM0	7.87	16	148	54.3	5834.8	0.01	54	0	54	na	na	34075	0	1	11.8	15106	109	na	na	na	26.33	60	15000
9	B1	7.87	5.9	59.1	21.7	3619.2	0.01	42	0	44	na	na	34075	0	1	5.91	14894	37	na	na	na	14.63	14	7834
9	B2	7.87	5.9	59.1	21.7	3619.2	0.01	42	0	44	na	na	34075	0	1	5.91	14894	37	na	na	na	15.09	14	7100
9	B3	7.87	5.9	59.1	21.7	3619.2	0.01	42	0	44	na	na	34075	0	1	5.91	14894	37	na	na	na	14.97	14	5868
4,5	V2	7.09	4.7	70.9	29.5	5945	0	77	na	81	na	na	34800	0	2	2.76	15000	68.5	na	na	na	4.185	10	8070
6,7,8	V.B	3.94	3	35.4	17.7	6800.5	0.01	72	na	64	0.01	64	34800	0	1	1.97	1550	31.5	na	na	na	4.905	7	16450
6,7,8	V.C	3.94	3	35.4	17.7	6800.5	0.01	72	na	64	0.01	64	34800	0	1	1.97	1550	31.5	na	na	na	4.914	7	15410
25	CS1-I	5.94	12	78.7	39.4	3108.8	0	50	na	na	na	na	39295	0.01	1	1.97	13727	70.9	na	na	na	1.915	6	10000
19	GFRP-S1	23	9	228	84	4060	0	76	0	78	na	na	3785	0.05	2	9	0.022	216	4611	na	0.05	48.13	337	11200

n.a. not available

1 Aidoo et al. 2006
2 Arduini et al. 2004
3 Brena et al. 2003
4 Dias 2001
5 Dias et al. 2006
6 Dimande 2003
7 Dimande et al. 2004
8 Dimande et al. 2005
9 Fang 2002
10 Fanning and Kelly 2001
11 Grace et al. 2002
12 Juvandes et al. 1997
13 Juvandes et al. 1998
14 Juvandes 1999
15 Juvandes et al. 1999
16 Juvandes et al. 2001
17 Kaminska and Kotynia 2000
18 Kotynia and Kaminska 2003
19 Lopez
20 Ngyuen et al. 2001
21 Quattlebaum et al. 2005
22 Rahimi and Hutchinson 2001
23 Reeve et al. 2005
24 Spadea et al. 1998
25 Teng et al. 2003
26 White et al. 2001
27 Ye et al. 2001

REFERENCES

Aidoo, J. (2004) *Flexural Retrofit of Reinforced Concrete Bridge Girders Using Three CFRP Systems*, Ph.D. Dissertation, Department of Civil and Environmental Engineering, University of South Carolina, 197pp.

American Concrete Institute (ACI) 318-05 (2005) *"Building Code Requirements for Structural Concrete and Commentary",* 456pp.

American Concrete Institute (ACI) 445-99 (1999) *"Recent Approaches to Shear Design of Structural Concrete"*, 55pp.

American Concrete Institute (ACI) Committee 440 (2002) *ACI 440.2R-02 "Guide for the Design and Construction of Externally Bonded FRP Systems for Strengthening Concrete Structures"*, 45pp.

American Concrete Institute (ACI) Committee 440 Task Group on Bond of Externally Bonded FRP (2006) "*Current Recommendations and Guidelines for Mitigating Debonding Failures in Adhesively Bonded, Externally Applied FRP Applications"* (Dr. Kent A. Harries, chair), Committee Report.

Arockiasamy, M., Amer, A. and Shahawy, M. (1996) "Concrete beams and slabs retrofitted with CFRP laminates", *Proceedings of the Eleventh Conference on Engineering Mechanics*, ASCE, New York, USA, pp776-779.

Buyukozturk, O., Gunes, O. and Karaca, E. (2004) "Progress on understanding debonding problems in reinforced concrete and steel members strengthened using FRP composites", *Construction and Building Materials*, Vol. 18, pp9-19.

Carter, W.J. (1958) "Torsion and Flexure of Slender Solid Sections", *Journal of Applied Mechanics*, Vol. 25, pp.115-121.

Chen, J.F. and Pan, W.K. (2005) "Three dimensional stress distribution in FRP-to-concrete bond test specimens", *Construction and Building Materials*, Vol. 20, pp46-58.

Concrete Society (2004) *"Design Guidance for strengthening concrete structures using fibre composite materials"*, Concrete Society Technical Report 55, Second Edition, Camberley, Surrey, UK, 102pp.

Consiglio Nazionale Delle Richerche (2004) CNR-DT 200 *"Istruzioni per la Progettaazione. I'Esecuzione ed il Controllo di Interventi di Consolidamento Statico mediante I'utilizzo di Compositi Fibrorinforzati"*, Rome, Italy, 164pp.

Dias, S.J.E. (2001) *"Experimental research of strengthening with CFRP concrete structures in bending"*, MS Thesis, Faculty of Engineering, University of Porto (FEUP), 203pp (in Portuguese).

Erki, M.A. and Heffernan, P.J. (1995) "Reinforced concrete slabs externally strengthened with fibre-reinforced plastic materials", *Non-Metallic (FRP) Reinforcement for Concrete Structures, Proceedings of the Second International RILEM Symposium*, Ghent, Belgium, pp509-516.

Federation Internationale du Beton (CEB) (2001) *fib Technical Report Bulletin 14: Externally Bonded FRP Reinforcement for RC Structures*, Lausanne, Switzerland, 130pp.

Harajli, M.H. and Soudki, K.A. (2003) "Shear Strengthening of Interior Slab-Column Connections Using Carbon Fiber-Reinforced Polymer Sheets", *Journal of Composites for Construction*, ASCE, Vol. 7, No. 2, pp145-153.

Harries, K.A. and J. Aidoo (2005) "Deterioration of FRP-to-concrete bond under fatigue loading", *International Symposium on Bond Behavior of FRP in Structures (BBFS)*, Hong Kong, International Institute for FRP in Construction, 2005.

Harries, K.A. (2006) "Practical use of Pull-Off Strength Testing (ASTM 4541) for Assessing Quality of FRP-to-Concrete Bond", *Proceedings of the 3rd International Conference on FRP Composites in Civil Engineering (CICE 2005)*, Miami, Florida, USA.

Harries, K.A., Zorn, A., Aidoo, J. and Quattlebaum, J. (2006) "Deterioration of FRp-to-Concrete Bond Under Fatigue Loading", *Advances in Structural Engineering-Special Issue on Bond Behavior of FRP in Structures*, Vol. 9, No. 6, pp779-789.

Japan Society of Civil Engineers (JSCE) (2001) *"Recommendations for Upgrading of Concrete Structures with use of Continuous Fiber Sheets"*, Concrete Engineering Series 41, Tokyo, 250pp.

Juvandes, F.P.L. (1999) "*Strengthening and rehabilitation of concrete structures using CFRP composites"*, Ph.D. Dissertation, Faculty of Engineering, University of Porto (FEUP), 400pp (in Portuguese).

Karbhari, V.M., Seible, F., Seim, W. and Vasquez, A. (1999) "Post-Strengthening of concrete slabs", *Proceedings of the Fourth International Symposium on Fiber Reinforced Polymer Reinforcement for Reinforced Concrete Structures*, Baltimore, Maryland, USA, pp1163-1173.

Karbhari, V.M. and Seible, F. (2000) "Fiber reinforced composites – advanced materials for the renewal of civil infrastructure", *Applied Composite Materials*, Vol.7, pp95-124.

Kotynia, R., Harries, K. A. (2006) "Strain Efficiency and Limit States of Externally Bonded and Near-Surface Mounted CFRP-Strengthened RC Members." *Composites B* (under review)

Kotynia, R. and Kaminska, M.E. (2003) "Ductility and failure mode of RC beams strengthened for flexure with CFRP", *Technical Report 13*, Department of Concrete Structures, Technical University of Lodz, Poland, 51pp.

Limam, Q., Foret, G. and Ehrlacher, A (2003) "RC two-way slabs strengthened with CFRp strips: experimental study and a limit state analysis approach", *Composite Structures*, Vol. 60, pp467-471.

Longworth, J., Bizindavyi, L., Wight, R.G. and Erki, A. (2004) "Prestressed CFRP Sheets for Strengthening Two-Way Slabs in Flexure", *Advanced Composite Materials in Bridges and Structures*, Canadian Society for Civil Engineering, 8pp.

Marzouk, H. and Ebead, U. (2003) "Fiber-reinforced polymer strengthening of two-way slabs", *ACI Structural Journal*, Vol. 101, No. 5, pp650-659.

Minnaugh, P. (2006) "*Experimental Behavior of Steel Reinforced Polymer Retrofit Measures"*, MS Thesis, Department of Civil and Environmental Engineering, University of Pittsburgh, Pittsburgh, PA, pp97.

Mohammed Ali, M.S., Oehlers, D.J. and Sung-Moo Park (2001) "Comparison between FRP and steel plating of reinforced concrete beams", *Composites Part A: applied science and manufacturing*, Vol. 32, pp1319-1328.

Monti, G., Renzelli, M. and Luciani, P. (2003) "FRP adhesion in uncracked and cracked concrete zones", *Proceedings of the 6th International Symposium on FRP Reinforcement for Concrete Structures (FRPRCS-6)*, World Scientific Publishing Company, pp183-192.

Mosallam, A.S. and Mosalam, K.M. (2003) "Strengthening of two-way concrete slans with FRP composite laminates", *Construction and Building Materials*, Vol. 17, pp43-54.

Neale, K.W., Ebead, U.A., Adbel Baky H.M., Elsayed, W.E. and Godat A. (2005) "Modelling of Debonding Phenomena in FRP-Strengthened Concrete Beams and Slabs", *Proceedings of the International Symposium on Bond Behavior of FRP in Structures (BBFS)*, Hong Kong, International Institute for FRP in Construction, pp45-54.

Neubauer, U. and Rostasy, F.S. (1997) "Design aspects of concrete structures strengthened with externally bonded CFRP plates", *Proceedings of the International Conference on Structural Faults and Repairs*, Edinburgh, ECS Publications, pp109-118.

Oehlers, D.J. and Bradford, M.A. (1999) *"Elementary behavior of Composite Steel and Concrete Structural Members"*, Butterworth Heinemann, Oxford, 250pp.

Oehlers, D.J. and Seracino, R. (2004) *"Design of FRP and Steel Plated RC Structures"*, Elsevier, 228pp.

Oehlers, D.J. (2005) "Generic Debonding Mechanisms in FRP Plated Beams and Slabs", *Proceedings of the International Symposium on Bond Behavior of FRP in Structures (BBFS)*, Hong Kong, International Institute for FRP in Construction, pp35-44.

Oehlers, D.J. (2006) "Ductility of FRP plated flexural members", *Cement and Concrete Composites*, Vol. 28, No. 10, pp898-905.

O'Neill, A., Harries, K.A. and Minnaugh, P. (2007) "Fatigue Behavior of Adhesive Systems used for Externally-bonded FRP Applications", *Proceedings of the Third International Conference on Durability and Field Applications of Fiber Reinforced Polymer (FRP) Composites for Construction (CDCC 2007)*, Quebec City, Canada, pp41-48.

Quattlebaum, J.B., (2003) "*Comparison of Three CFRP Flexural Retrofit Systems under Monotonic and Fatigue Loads"*, Ph.D. Dissertation, Department of Civil and Environmental Engineering, University of South Carolina, Columbia, SC, 134pp.

Quattlebaum, J., Harries, K.A. and Petrou, M.F., (2005) "Comparison of Three CFRP Flexural Retrofit Systems Under Monotonic and Fatigue Loads.", *ASCE Journal of Bridge Engineering*, Vol. 10, No. 6, pp731-740.

Reeve, B.Z. (2005) "*Effect of adhesive stiffness and CFRP geometry on the behavior of externally bonded CFRP retrofit measures subject to monotonic loads"*, MS Thesis, Department of Civil and Environmental Engineering, University of Pittsburgh, Pittsburgh, PA, 98 pp.

Reissner, E. and Thomas, G.B. (1946) "Note on the Shear Stresses in a Bent Cantilever Beam of Rectangular Cross Section", *Journal of Mathematics and Physics*, Vol. 25, pp.241-243.

Seim, W., Horman, M. and Karbhari, V. (2001) "External FRP Post-strengthening of Scaled Concrete Slabs", *Journal of Composites for Construction*, Vol. 5, No. 2, pp67-75.

Shahawy, M.A., Beitelman, T., Arockiasamy, M. and Sowrirajan, R. (1996) "Experimental investigation on structural repair and strengthening of damaged prestressed concrete slabs utilizing externally bonded carbon laminates", *Composites: Part B*, Vol. 27B, pp217-224.

Tan, Z., Lu, X.Z., Ye, L.P. and Jiang, J.J. (2003) "Finite element analysis of debonding at the interface between FRP sheet and concrete", *Engineering Mechanics*, Vol. 21, No. 6, pp45-50.

Tann, D.B. (2003) "A semi-empirical approach for the prediction of deflections of FRP strengthened RC slabs", *Proceedings of the Sixth International Symposium on FRP Reinforcement for Concrete Structures (FRPRCS-6)*, Singapore, pp357-366.

Teng, J.G., Lam, L., Chan, W. and Wang, J. (2000) "Retrofitting of Deficient RC Cantilever Slabs using GFRP Strips", *Journal of Composites for Construction*, Vol. 4, No. 2, pp75-84.

Teng, J.G., Cao, S.Y. and Lam, L. (2001) "Behavior of GFRP-strengthened RC cantilever slabs", *Construction and Building Materials*, Vol. 15, pp. 339-349.

Teng, J.G., Smith, S.T., Yao, J. and Chen, J.F. (2001) "Intermediate Crack Induced Debonding in RC Beams and Slabs", *Construction and Building Materials*, Vol. 17, No. 6-7, pp447-462.

Teng, J.G., Chen, J.F., Smith, S.T. and Lam, L. (2002) *"FRP Strengthened RC Structures"*, John Wiley and Sons Ltd., Chichester, England, 245pp.

Teng, J.G., Chen, J.F., Smith S.T. and Lam, L. (2003) "Behaviour and strength of FRP strengthened RC structures: a state-of-the-art review", *Proceedings of the Institution of Civil Engineers-Struct Build*, pp51-62.

Teng, J.G., Lu, X.Z., Ye, L.P. and Jiang, J.J. (2004) "Recent Research on Intermediate Crack Induced Debonding in FRP Strengthened Beams", *Proceedings of the 4th International Conference on Advanced Composite Materials for Bridges and Structures*, Calgary, Alberta, pp1-12.

Thomsen, H., Spacone, E., Limkatanyu, S. and Camata, G. (2004) "Failure Mode Analyses of Reinforced Concrete Beams Strengthened in Flexure with Externally Bonded Fiber-Reinforced Polymers", *Journal of Composites for Construction*, Vol. 8, No. 2, pp-123-131.

Timoshenko, S.P. and Goodier, J.N. (1970) *"Theory of Elasticity"*, McGraw-Hill Book Company, 567pp.

Wan, B., Sutton, M., Petrou, M.F., Harries, K.A. and Li, N. (2004) "Investigation of Bond between FRP and Concrete Undergoing Global Mixed Mode I/II Loading", *ASCE Journal of Engineering Mechanics*, Vol. 130, No. 12, pp1467-1475.

Ye, L.P., Lu, X.Z. and Chen, J.F. (2005) "Design Proposals for the Debonding Strengths of FRP Strengthened RC Beams in the Chinese Design Code", *Proceedings of the International Symposium on Bond Behavior of FRP in Structures*, Hong Kong, pp55-62.

Zhang, J.W., Teng, J.G., Wong, Y.L. and Lu, Z.T. (2001) "Behavior of Two-Way RC Slabs Externally Bonded with Steel Plate", *Journal of Structural Engineering*, Vol. 127, No. 4, pp390-397.

Zorn, A.V. (2006) *"Effect of adhesive stiffness and CFRP geometry on the behavior of externally bonded CFRP retrofit measures subject to fatigue loads"*, MS Thesis, Department of Civil and Environmental Engineering, University of Pittsburgh, Pittsburgh, PA, 93 pp.